การพัฒนาเทคนิคการเก็บข้อมูลสำหรับคำนวณสร้างภาพโทโมกราฟีของแบบจำลองหอกลั่นที่ใช้ในโรงงานปิโตรเลียมและปิโตรเคมี

นายธนรรจน์ แสงจันทร์

วิทยานิพนธ์นี้เป็นส่วนหนึ่งของการศึกษาตามหลักสูตรปริญญาวิศวกรรมศาสตรดุษฎีบัณฑิต
สาขาวิชาวิศวกรรมนิวเคลียร์ ภาควิชาวิศวกรรมนิวเคลียร์
คณะวิศวกรรมศาสตร์ จุฬาลงกรณ์มหาวิทยาลัย
ปีการศึกษา 2560

DEVELOPMENT OF DATA ACQUISITION TECHNIQUE FOR COMPUTED TOMOGRAPHY OF SIMPLIFIED DISTILLATION COLUMN MODEL AS USED IN PETROLEUM AND PETROCHEMICAL PLANTS

Mr. Dhanaj Saengchantr

A Dissertation Submitted in Partial Fulfillment of the Requirements
for the Degree of Doctor of Engineering Program in Nuclear Engineering
Department of Nuclear Engineering
Faculty of Engineering
Chulalongkorn University
Academic Year 2017

Thesis Title	DEVELOPMENT OF DATA ACQUISITION TECHNIQUE FOR COMPUTED TOMOGRAPHY OF SIMPLIFIED DISTILLATION COLUMN MODEL AS USED IN PETROLEUM AND PETROCHEMICAL PLANTS
By	Mr. Dhanaj Saengchantr
Field of Study	Nuclear Engineering
Thesis Advisor	Associate Professor Somyot Srisatit
Thesis Co-Advisor	Associate Professor Nares Chankow

Accepted by the Faculty of Engineering, Chulalongkorn University in Partial Fulfillment of the Requirements for the Doctoral Degree

.....Dean of the Faculty of Engineering
(Associate Professor Supot Teachavorasinskun, Ph.D.)

THESIS COMMITTEE

.....Chairman
(Associate Professor Sunchai Nilsuwankosit, Ph. D.)

.....Thesis Advisor
(Associate Professor Somyot Srisatit)

.....Thesis Co-Advisor
(Associate Professor Nares Chankow)

.....Examiner
(Assistant Professor Somboon Rassame, Ph.D.)

.....Examiner
(Assistant Professor Phongphaeth Pengvanich, Ph.D.)

.....External Examiner
(Chanatip Tippayakul, Ph.D.)

ธนรรจน์ แสงจันทร์ : การพัฒนาเทคนิคการเก็บข้อมูลสำหรับคำนวณสร้างภาพโทโมกราฟีของแบบจำลองหอกลั่นที่ใช้ในโรงงานปิโตรเลียมและปิโตรเคมี (DEVELOPMENT OF DATA ACQUISITION TECHNIQUE FOR COMPUTED TOMOGRAPHY OF SIMPLIFIED DISTILLATION COLUMN MODEL AS USED IN PETROLEUM AND PETROCHEMICAL PLANTS) อ.ที่ปรึกษาวิทยานิพนธ์หลัก: รศ. สมยศ ศรีสถิตย์, อ.ที่ปรึกษาวิทยานิพนธ์ร่วม: รศ. นเรศร์ จันทน์ขาว, หน้า.

งานวิจัยนี้นำเสนอเทคนิคการเก็บข้อมูลสำหรับการคำนวณสร้างภาพโทโมกราฟีของแบบจำลองหอกลั่นที่ใช้ในโรงงานปิโตรเลียมและปิโตรเคมี โดยมีวัตถุประสงค์เพื่อประยุกต์ใช้งานเทคนิคการสร้างภาพโทโมกราฟีกับงานตรวจสอบหอกลั่นในโรงงานอุตสาหกรรมซึ่งเทคนิคที่พัฒนานี้ไม่จำเป็นต้องใช้ระบบขับเคลื่อนหัววัดและต้นกำเนิดรังสีที่ซับซ้อน จะอาศัยการเคลื่อนย้ายหัววัดและต้นกำเนิดรังสีแบบอิสระตามรูปแบบที่ออกแบบขึ้น ข้อมูลที่ได้จะถูกนำมาสร้างภาพด้วยเทคนิคฟิลเตอร์แบคโปรเจกชัน ทำให้ได้ภาพตัดขวางในส่วนที่ต้องการสแกน ในการวิจัยเริ่มจากการจำลองการแผ่รังสีผ่านตัวกลางด้วยโปรแกรม MCNP เพื่อจำลองผลจากการวัดรังสีและทดลองสร้างภาพโทโมกราฟีเพื่อดูลักษณะภาพตัดขวางที่จะเกิดขึ้น จากนั้นจึงได้ออกแบบวิธีการย้ายตำแหน่งหัววัดรังสีและต้นกำเนิดรังสีให้มีรูปแบบต่าง ๆ 3 รูปแบบ เพื่อเป็นทางเลือกในการนำไปใช้งานโดยทำการทดลองกับวัตถุตัวกลางเดียวกับที่ใช้ในการจำลอง ผลการทดลองที่ได้พบว่ารูปแบบทั้ง 3 ที่ออกแบบมา สามารถสร้างภาพโทโมกราฟีของวัตถุที่จำลองเป็นท่อได้อย่างชัดเจน โดยสามารถระบุขนาดของท่อได้ มีความคลาดเคลื่อนไม่เกิน 15% อย่างไรก็ตามผลการจำลองและผลการทดลองไม่สามารถระบุความหนาของท่อได้ นอกจากนี้ยังได้ทำการทดลองกับวัตถุตัวกลางที่ต่างกันออกไป พบว่าเทคนิคการเก็บข้อมูลที่พัฒนาขึ้นสามารถประยุกต์ใช้ในการตรวจสอบความผิดปกติของโครงสร้างภายในได้อย่างมีประสิทธิภาพ ซึ่งสามารถนำไปประยุกต์ใช้กับงานด้านอุตสาหกรรมปิโตรเลียมและปิโตรเคมีได้ต่อไปในอนาคต

ภาควิชา	วิศวกรรมนิวเคลียร์	ลายมือชื่อนิสิต .....
สาขาวิชา	วิศวกรรมนิวเคลียร์	ลายมือชื่อ อ.ที่ปรึกษาหลัก .....
ปีการศึกษา	2560	ลายมือชื่อ อ.ที่ปรึกษาร่วม .....

5671414821 : MAJOR NUCLEAR ENGINEERING
KEYWORDS: INDUSTRIAL COMPUTED TOMOGRAPHY / DISTILLATION COLUMN INSPECTION / PIPE ARRAY INSPECTION / GAMMA RAY TRANSMISSION

DHANAJ SAENGCHANTR: DEVELOPMENT OF DATA ACQUISITION TECHNIQUE FOR COMPUTED TOMOGRAPHY OF SIMPLIFIED DISTILLATION COLUMN MODEL AS USED IN PETROLEUM AND PETROCHEMICAL PLANTS. ADVISOR: ASSOC. PROF. SOMYOT SRISATIT, CO-ADVISOR: ASSOC. PROF. NARES CHANKOW, pp.

This dissertation propose the development of data acquisition technique for computed tomography of simplified distillation column model as used in petroleum and petrochemical industries. The aim of this dissertation is to apply the computed tomography technique to inspect the internal structure of distillation column regardless of complex system to move radiation detectors and source. The developed data acquisition technique allows the operator to move radiation detectors and radiation source by follow designed algorithm. The scanning data are reconstructed using filtered back projection algorithm to evaluate internal structure at the region of interest from cross sectional reconstructed image. In this dissertation, simulation using MCNP was assisted in order to obtain the transmitted gamma radiation profiles through different size pipe objects and use them as prior knowledge information. Three data acquisition techniques were designed afterward using same diameter and thickness of pipes which lead to results that all three data acquisition techniques had similar results which maximum error less than 15% when measuring the pipe diameter. However, the reconstructed image could not display a thickness of pipe objects. Moreover, the designed data acquisition algorithms were extended to other experiments which successfully provided consistency results compared to the real situation in model. This developed data acquisition technique is useful and can be applied to scanning of large object in industries..

Department:	Nuclear Engineering	Student's Signature	.....
Field of Study:	Nuclear Engineering	Advisor's Signature	.....
Academic Year:	2017	Co-Advisor's Signature	.....

ACKNOWLEDGEMENTS

I would like to express my deepest gratitude to Assoc. Prof. Somyot Srisatit, my advisor, for his valuable advice, supervision and comments. I am equally greateful to Assoc. Prof. Nares Chankow, my co-advisor, for his guidance during research implementation. I am also gratefully thanks to Dr. Saensuk Wetchagarun and Dr. Chanatip Tippayakul for their kind advice to my research and my study throughout the study course.

I would also like to extend my appreciation to Thailand Institute of Nuclear Technology for supporting on all equipment that had been used in the experiment as well as all funding from institute since beginning until the end. My sincere appreciation goes to all of my colleagues at Radiation Application for Industrial Services team for their kind support in all experiment preparations.

Last but not least, I am grateful to my family for their encouragement, entirely care and understanding during the course of study.

CONTENTS

Page

Page

LIST OF TABLES

LIST OF FIGURES

CHAPTER 1

INTRODUCTION

1.1 Background and rationale

In petroleum and petrochemical plants, the distillation column is one of the most important equipment installed in the process [1]. The distillation column is used in separation process in the chemical plans especially in the petroleum and petrochemical plants. Normally, the phase of raw materials inside distillation column can be vapor, liquid or liquid-vapor mixture and the separation process occurs when phase of feeds are separated in each equilibrium stages. Less volatile element which mostly contain liquid phase more than vapor phase is regarding as heavy or high boiling elements and its flow direction is always downward to the bottom of distillation column in one hand. On the other hand, a high volatile element mainly composed of vapor phase is regarding as light element and its flow direction is always upward to the top of column. During normal operation, the operating condition and all important parameters are monitoring on process control panels. The displaying parameters are the value measured at the important location where all sensors and transduced are installed. In the problem cases, process conditions and operating parameters are deviated from the design or deviated from the normal operation (process is upset), the indicator on control panels will be activated and prompt or alarm to warn the operators and request them to take an action. In case of the problem is persisting and situation seems to be propagated or cannot be recovered, the operators must consider the safety criteria and keep all parameters under that accepted criteria. Finally, root causes must be investigated to find out what could probably be main reasons and the most important is the location where problem is initiated. The persisting abnormality is directly affecting to the distillation efficiency and could degrade the specification of final products at the end of production line. In such a case, process engineers and maintenance engineers are in charged to investigate what could be the problems and shall cooperate to relevant department to recover the production process in function as soon as possible to prevent the propagation of

abnormality to the other stages that would cause the “plant shutdown”. Non-destructive testing or evaluation (well known as NDT/E) plays an important role to inspect or investigate and reveal the location of problem [2]. There are several techniques such as radiographic testing (RT) which deal with the radiation or non-radiation concern such as ultrasonic testing (UT), acoustic testing (AT), gamma scanning, etc. The results from NDT/E can be used for maintenance guidance and enable engineers to solve the problem in the precise way.

One investigation technique among others, called “Gamma-scanning”, is a technique which is radiation concern technique likewise the RT technique. The technique applies gamma radiation to the inspection process and use the gamma detector to receive and translate signal into recordable electrical signal. The technique is useful in inspection of the distillation column, but not limited to, based on principles of the gamma radiation transmission passing through the interesting medium and uses the receiver or sensor, for instant film or gamma rays detector, to obtain the transmitted gamma intensity. The transmitted gamma intensity measured at the detector is ideally a function of gamma ray energy, build-up factor, thickness and density of medium (very well known in terms of Lambert’s law)**. Generally, regardless of build-up factor, if the energy of gamma is fixed as well as the thickness of medium is constant, the gamma intensity transmitted through the medium is inversely proportional to the density of medium, i.e. the high density of medium resulting in lower gamma intensity transmitted to the sensor whereas the low density of medium resulting in higher gamma intensity measured at the detectors. By the principle, differentiated density in different location can be plotted as density distribution. It can be applied to the distillation column since inside the distillation column, the density at each location in different elevation are varied and depends on the design and operating condition during online. Thus, plotted of density profile of distillation column reflects to the condition inside the distillation column and it is possible to locate the problem by Gamma-scanning technique.

Though the gamma scanning technique has its principle similar to the RT, the recording of output is completely different. RT uses the image recording and it record the image as the super imposed to the film or other image recorder. Gamma

scanning record the data in terms of transmitted radiation in a point, thus x-y plots were conducted. The scanning results are plotted in the line-graph between gamma intensity (in x-axis) versus the elevation height of the distillation column (y-axis). In many cases the line-graph cannot clearly explain the problem behavior and it still be in doubt when the density profile does not communicate to the on-site engineer because their experience are not in the field of radiation application. For example the polymerization is occurring when the operating condition is unbalanced, the exchanging between liquid and gas are not in the equilibrium and it could lead to liquid changing phase to solid in some local places (solidify). The polymerization is randomly formed and obstruct flow path of liquid inside column and reduce the distillation efficiency, finally, the product is out of specification. This problem is regarding as a channeling and it is interesting to the process engineer for problem solving. The other example, normally, inside the distillation column composed of many nozzle pipes as function designed by manufacturing company. During normal operation or abnormality, the pipes could be accidentally broken by some means and leads to malfunction due to internal structure integrity in this case scanning technique might not sufficient to cope with the problem investigation. The cross-section of distillation column where the problem is initiated gives more information. Therefore, the conventional gamma scanning technique couples with the developing technique in this paper will emphasize on the computed tomography technique for better understanding when the conventional technique specify the suspecting problem location and then apply the developing technique to explain the behavior inside the distillation column or even in the normal operation this technique can also be applied to explain the characteristic of distillation column.

The complication of this dissertation is to design the scanning method for gathering information at the location where it is suspected to be a problem. Since the size of column is large and external structures obstruct the operation, the data acquisition system and technique is needed to be developed. The fan beam projection technique is applied and image reconstruction algorithm is incorporated in the software. The simulation software is also developed to provide the comprehensive view of problem especially the projection profiles from simulation can be used to compare with experiment results. Monte Carlo computer code (MCNP) is also used in

this dissertation to estimate the appropriate radioactive source activity for implement the scanning.

1.2 Research Objectives

To develop the data acquisition technique for computed tomography of the simplified distillation column model as used in the petroleum and petrochemical plants.

1.3 Scope of dissertation

1.3.1 Develop the inspection technique for process distillation column based on computed tomography method

1.3.2 Develop data acquisition system and accessories

1.3.3 Develop software for image reconstruction

1.3.4 Apply developed technique to the simplified distillation column model as used in the petroleum and petrochemical plants

1.4 Anticipated Outcomes

1.4.1 Obtain the applicable data acquisition technique to enhance the quality of result interpretation in inspection of distillation column in petroleum and petrochemical plants

1.4.2 Improve the precision of process distillation column scanning technique

CHAPTER 2

THEORY AND LITERATURES REVIEW

This chapter provides necessary theories to support this dissertation. It composed of 6 important sections. Section 2.1 describes “Fundamental of gamma-ray interaction with matters”,as well as its attenuation behavior of gamma rays [3, 4]. Section 2.2 describes fundamental of gamma ray detection and measurement system used in this dissertation. Section 2.3 describe the principle of computed tomographic technique, including the image projection using single beam, fan beam and cone beam technique as well as image back projection algorithms. Section 2.4 briefly explains a relevant internal structure of various types of distillation column and their inspection technique “Conventional column scanning technique for distillation column”. The technique was developed since ’80s but it still useful to explain the characteristic of distillation column. This section also raised some encountered problem of distillation column which is a state of motivation to conduct this dissertation. In section 2.5 describes the advantages of using Monte Carlo for N-Particle (MCNP) computer code for “Simulation of industrial fan-beam CT using MCNP computer code”. It is a powerful tool to simulate the phenomena of photons behavior when passed through the medium. The simulated results can be used in design and algorithm testing. Section 2.6 the previous works that has been done by other authors was presented.

2.1 Fundamental of gamma-ray interaction with matters

Three major gamma rays interactions are (2.1.1) photoelectric absorption, (2.1.2) Compton scattering and (2.1.3) pair production. These interactions completely describe the process how gamma ray energy reduces by transferring energy to the matters that they passed through. The last topic in this section (2.1.4) describes the gamma-ray attenuation fundamental which is a principle of gamma scanning of distillation column [5].

2.1.1 Photoelectric absorption

This interaction occurs when low energy of gamma-rays photon enters to the atom of matter and the gamma-rays photon transfer its energy to atom disappears. Once the gamma-rays photon transfers its energy to the atom, excess energy consequent to the atom ejects "photoelectron" (E_{e^-}) from tightly bound shell (K-shell is the most likely possibility to be an origin of ejected photoelectron). The ejected photoelectron carry the energy of excess gamma rays energy (E_γ) over the energy of electron bound and is given by

$$E_{e^-} = E_\gamma - E_b$$

$$E_{e^-} = h\nu - E_b \quad \text{Eq. 2.1}$$

$$\nu = \frac{c}{\lambda} \quad \text{Eq. 2.2}$$

where *h* is a Planck's constant ($h = 6.6 \times 10^{-34}$ J.s in SI unit), E_b is a binding energy at the origin of photoelectron and v is the frequency in unit of hertz of the gamma-rays energy at speed of light *c* (m/s). The frequency can be represented by the ratio of speed of light per wavelength λ (m).

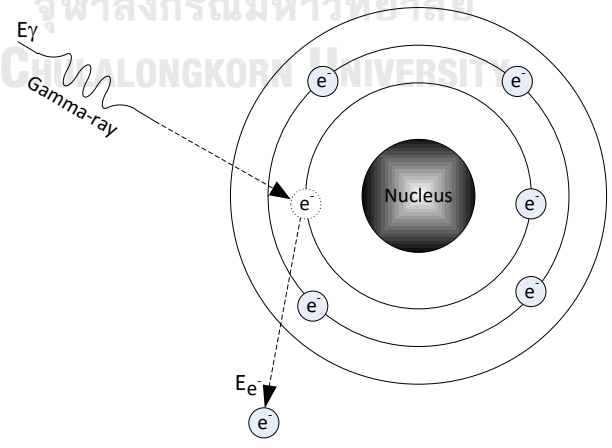

Figure 2.1 Photoelectric absorption of gamma-ray

The photoelectric absorption mostly occurs with low-energy photons interact with high atomic mass number *Z* materials. The possibility of photoelectric absorption

per atom ever all range of energy E is explained by terms of cross section τ and can be approximated by

$$\tau = constant \times \frac{Z^n}{E_\gamma^{3.5}} \qquad \text{Eq. 2.3}$$

The power n of Z^n varies between 4 and 5 over gamma-rays energy region of interest. From the relationship in Eq. 2.3, cross-section τ is increase when energy of gamma-rays is small and *Z* is high. It means the gamma-rays have high possibility to be absorbed when it exposes to the high *Z* materials and this is one of reason that high *Z* materials are selected and used as a radiation shielding. Lead is the most popular material for shielding by the appropriate reason in terms of economic and radiation safety.

2.1.2 Compton scattering

In case of the gamma-rays energy is large enough, the photoelectric absorption does not effective to absorb all energy of gamma-rays. Hence, after gamma-rays transfer its energy to atom, for more specific it transfers the energy to the electron in the atom. The energy is still remaining in the gamma-rays while the electron strikes out from its orbital, namely, recoiled electron. The collision angle between gamma-rays photon and electron can be possible at all angles (it is assumed that the electron is at the rest mass); the energy transferred can vary from zero to large fraction of the gamma-ray energy.

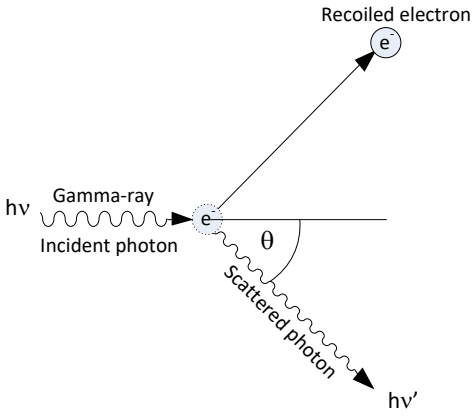

Figure 2.2 Scattering angle of gamma-ray in Compton scattering

By energy conservation of collision and sketch in Figure 2.2, the remaining energy of gamma-rays after collision can be expressed by Eq. 2.4

$$hv' = \frac{hv}{1 + \frac{hv}{m_0c^2}(1 - cos\ \theta)} \qquad \text{Eq. 2.4}$$

where m_0c^2 is the rest-mass energy of electron (0.511 MeV). The gamma-rays energy transferred is scattering angular θ dependent. If scattering angular is small, little energy is transferred to the electron. At some angle, the original energy is still retained in the incident photon, for example, at $\theta = 0$ or even in extreme condition when $\theta = 180^{o}$ then Eq. 2.4 becomes

$$hv' = \frac{hv}{1 + \frac{2hv}{m_0c^2}}$$

The gamma-rays incident is backscattered toward its direction of origin whereas the electron recoils along the direction of incident. Eq. 2.4 explains the remaining energy is not only depending on the scattering angular, but also depends on the rest-mass energy of electron. The probabilities of Compton scattering, σ, can be described by Nishina-Klein formula in Eq. 2.5

$$\frac{d\sigma}{d\Omega} = \frac{r_0^2}{2}\left(\frac{hv'}{hv}\right)\left(\frac{hv}{hv'} + \frac{hv'}{hv} - sin^2\theta\right) \qquad \text{Eq. 2.5}$$

The solid angle Ω is projects the travelling trajectory the direction of interaction between gamma-rays and electron. Solving Eq. 2.5, the solution can be approximated as following:

$$\sigma = \frac{8\pi}{3}r_0^2 \qquad hv \ll m_0c^2 \quad \text{Eq. 2.6}$$

$$\sigma = r_0^2\pi\frac{m_0c^2}{hv}\left[ln\left(\frac{2hv}{m_0c^2}\right) + \frac{1}{2}\right]hv \qquad hv \gg m_0c^2 \quad \text{Eq. 2.7}$$

The r_0 is a classical radius of electron (2.81810×10^{-15} m). The Compton scattering plays important roles to reduce the energy of gamma-rays photon and if the photon still travel in the geometry of material (not escape from the geometry) it will be eventually absorbed by photoelectric absorption as described in 2.1.1

2.1.3 Pair production

Pair production interaction can only occur when gamma-rays energy is higher than 2 times of rest mass energy of electron ($2m_0c^2 = 2 \times 0.511\text{MeV} = 1.022\text{MeV}$). The gamma-ray photon travels in to the atom and must travel in to the coulomb field of nucleus, and then gamma-ray photon disappears and transformed to electron and positron pair. The energy and momentum conservation is only possible when the gamma-ray photon has entered into the high electric filed. After the positron is absorbed in the material, it then annihilates and produce two annihilate photons as secondary product of interaction. This interaction is important when the event is dealing with the gamma detection.

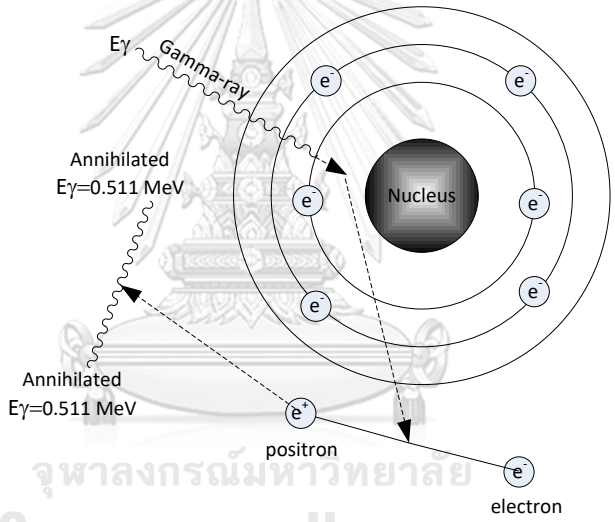

Figure 2.3 Process of pair production interaction

To quantify the probability of this interaction is difficult, there is no simple expression but the main criteria should be kept in mind that the pair production interaction can occur only if the gamma-rays energy is larger than 1.022 MeV, in terms of energy, Eq. 2.8 describe the pair production scheme

$$E_{e^+} + E_{e^-} = hv - 1.022\ MeV \qquad \text{Eq. 2.8}$$

Probability of pair production (κ) can be expressed by (Bethe-Heitler)

$$\kappa \approx \alpha Z^2 r_0^2 ln(E_\gamma) \qquad \text{Eq. 2.9}$$

2.1.4 Gamma-ray attenuation

Section 2.1.1 - 2.1.3 explained three important interactions of gamma-ray with the matters which describe also a possibility of each interaction as τ (photoelectric), σ (Compton scattering) and κ (pair production). The combination of these three parameters create a simply probability per unit path length, namely "linear attenuation coefficient: μ".

$$\mu = \tau \text{ (photoelectric)} + \sigma \text{ (Compton scattering)} + \kappa \text{ (pair production)} \quad \text{Eq. 2.10}$$

Since each interaction, the gamma-rays are removed from the origin gamma-rays incident (I_0) when the original incident pass through and interact with medium with the thickness of x. The mathematical explanation is expressed as follow

$$\frac{dI}{dx} = -\mu I$$

$$\frac{dI}{I} = -\mu dx$$

$$\int \frac{dI}{I} = -\mu \int dx$$

$$ln\, I = -\mu x + I_0$$

$$I = I_0 e^{-\mu x} \quad \text{Eq. 2.11}$$

Eq. 2.11 can be regarded as ideal gamma-rays attenuation equation or in some text book called "good geometry" [3]. In fact, the Compton scattering plays dominant roles when the gamma-ray photon energy is high and hence it is possible that scattered photon leak out from the geometry of medium before completely absorbed. This escaped photon depends on the atomic mass number of medium, thickness of medium and energy of gamma-ray photon. The parameters called Build-up factor (B) and defined, by relation in Eq. 2.12, at and interesting position

$$\mathrm{B} = \frac{\text{primary incident} + \text{secondary incident}}{\text{primary incident}} \quad \text{Eq. 2.12}$$

Then Eq. 2.11 and Eq. 2.12 can be re-arranged to Eq. 2.13 and called as "poor geometry" [3]

$$I = B \times I_0 e^{-\mu x} \quad \text{Eq. 2.13}$$

The linear attenuation coefficient is change when the density of medium has changed therefore the new parameter is introduced i.e. mass attenuation coefficient (μ_ρ). Using this parameter, the attenuation coefficient will not depends on a density (ρ) of matter and defined in Eq. 2.14

$$\mu_\rho = \frac{\mu_a}{\rho} \qquad \text{Eq. 2.14}$$

$$I = B \times I_0 e^{-\mu_\rho \rho x} \qquad \text{Eq. 2.15}$$

2.2 Gamma ray detection and measurement system

The gamma ray detection system used in this dissertation composed of scintillation detectors that made up of Sodium Iodine (NaI (Tl)) and connected to radiation counter. The counter is commercialized by LUDLUM Co., Ltd with model 4612.

Sodium iodine is one type of inorganics detector, in Alkali Halides, which has advantage of its excellent light yield. The emission spectra of light that illuminate from sodium iodine compared to other common inorganic scintillator are shown in Figure 2.4. The wavelength of maximum emission of NaI (Tl) is 415 nm, decay time of 0.23 μs, absolute light yield is 38,000 photon/MeV, approximately. The light emits from scintillator are multiplied and convert to electric signals using photo multiplier tube (PMT) and then feed to preamplifier, linear amplifier, discriminator and finally counter and display, the diagram is shown in Figure 2.5.

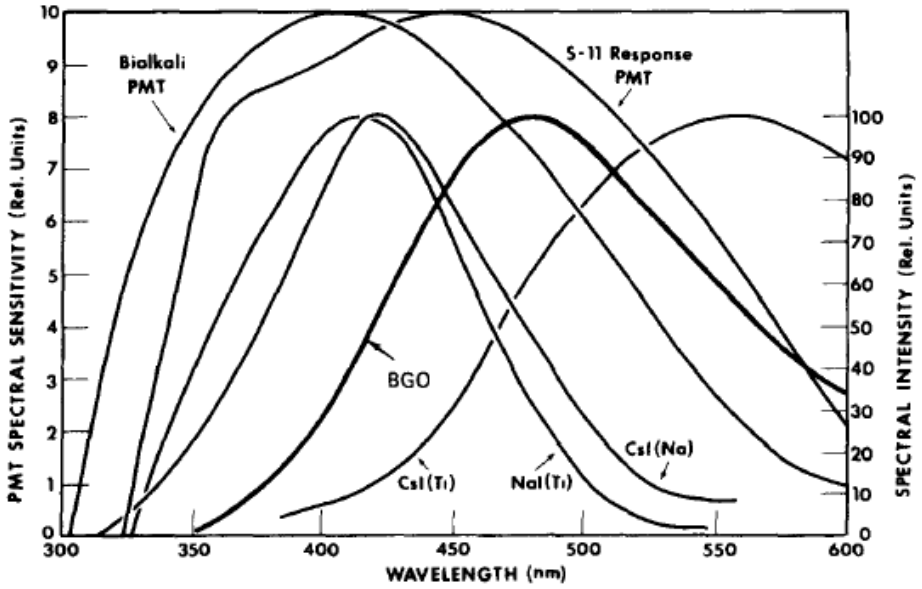

Figure 2.4 Comparison of emission spectra from several inorganic scintillators

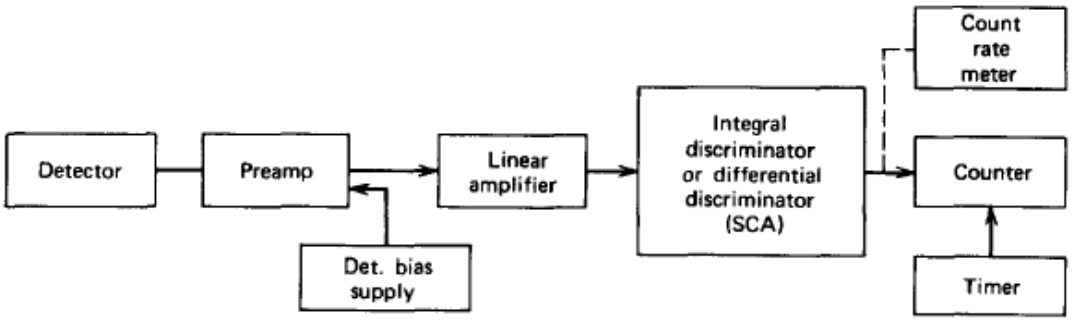

Figure 2.5 Signal chain diagram

Basically, the radiation counter counts the pulses that occur by interaction between photon and scintillator detectors. Hence, the shaping of linear pulses must be converted into logic pulse, to increase the counting reliability. This conversion can be done by using algorithm called “differential discriminator” or known in name of “Single-Channel Analyzer (SCA). Discriminator has function to justify the level of signal which will be count or will be eliminate. Differential discriminator provides two justification levels namely, “*lower-level discriminator*” (LLD) and “*upper level discriminator*” (ULD) [4]. This SCA generates logic output pulse only if the input linear pulse amplitude lies between ULD and LLD as indicated in Figure 2.6. The figure shows three signals generated from detector and fed to SCA with statistically different amplitude. In the SCA treated all signals and select only middle amplitude

because middle signal lies between ULD and LLD, hence output pulse signal can be generated.

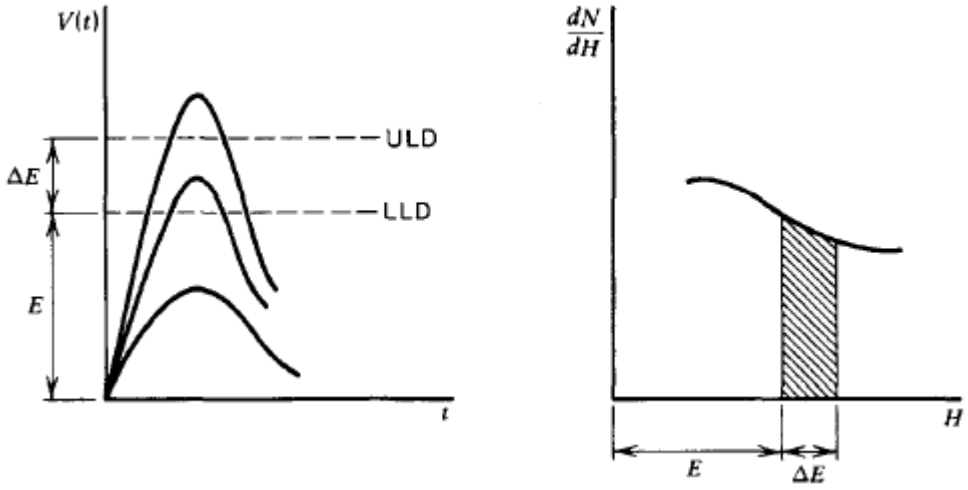

Figure 2.6 Function of differential discriminator or single channel analyzer (SCA)

Arrangement of system used in this dissertation is indicated in

Figure 2.7 Ludlum Model 4612 is connected to NaI (Tl) 11 detectors with size of 25.4 mm (1”). The system allows user to set High voltage, ULD and LLD through software. System calibration is the most important since all detectors must have very close efficiency which mean statistically identical output must be generate from all detectors until the display shows same count from all detectors.

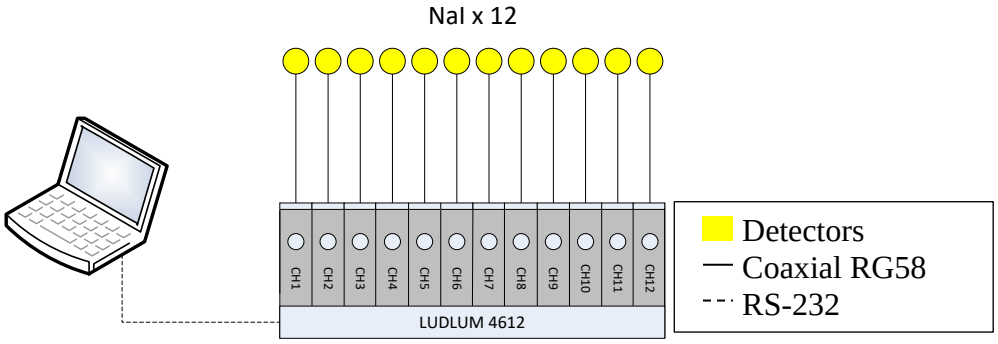

Figure 2.7 System arrangement, connection of LUDLUM 4612 to detectors and computer

2.3 Principle of Computed Tomographic Technique

The principle of Computed Tomography (CT) [6, 7] is the technique to obtain or to calculate an image from the projected information measured by the system, either in 2-D or 3D of the medium using the radiation from X-ray machine or from gamma rays radioactive source. In each projection, the ray-sum collects the data along the straight trajectories of source. Let's consider the 1-D projection as indicated in Figure 2.8 below

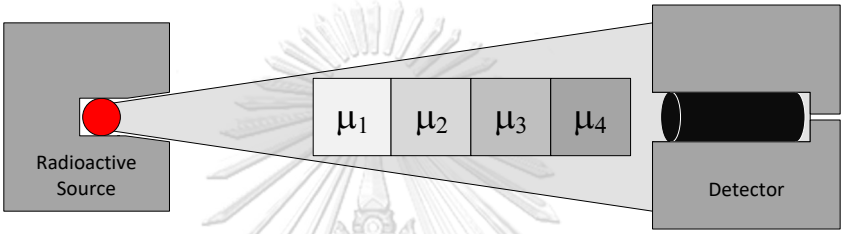

Figure 2.8 Gamma attenuation with cascade different medium

The transmitted radiation passed through 4 different materials which has 4 different linear attenuation coefficients (μ). The measured incident is expressed in Eq. 2.16

$$I = I_0 e^{-\sum_i \mu_i x_i} \qquad \text{Eq. 2.16}$$

In this case, the exact distribution of linear attenuation coefficient (μ_i) of each block cannot be identified. From this problem, the reconstruction of tomographic is the inversion of information or transmitted radiation seems to be a critical process. The choice of process is trading of between the number measurements, noises interference during measurement and the calculation time for image reconstruction. Thus, the main objective of computed tomography is to inverse the set of equations relating to the measurements of transmitted data in to the image. Finally, the reconstructed image is information represents the linear attenuation coefficients distributed in the medium. In the petroleum and petrochemical process, the linear attenuation is, ideally, converted to chemical parameters, mainly gas – liquid – solid

fractions including steels. In 2-D, the problem in Figure 2.8 and Eq. 2.16 are now modified

$$I = I_0 e^{-\int_L \mu(x,y)dl} \qquad \text{Eq. 2.17}$$

Where $\mu(x,y)$ is the linear attenuation coefficient of the image at point (*x*,*y*), thus the equation will be simplified to the only interesting part

$$g = \int_L \mu(x,y)dl \qquad \text{Eq. 2.18}$$

Generally, g implied the measured data from projection and can be calculated as Eq. 2.19

$$g = ln\left(\frac{I_0}{I}\right) \qquad \text{Eq. 2.19}$$

In two dimensions, CT system collect the transmitted data passed through the medium and projected onto the detector. Each single projection line at angle is represented by $L(\rho,\theta)$ where ρ is distance from center slides to interesting location at angle θ. Sketch in Figure 2.9 and Figure 2.10 illustrates a parallel beam projection system that shall be used in first generation CT scanning.

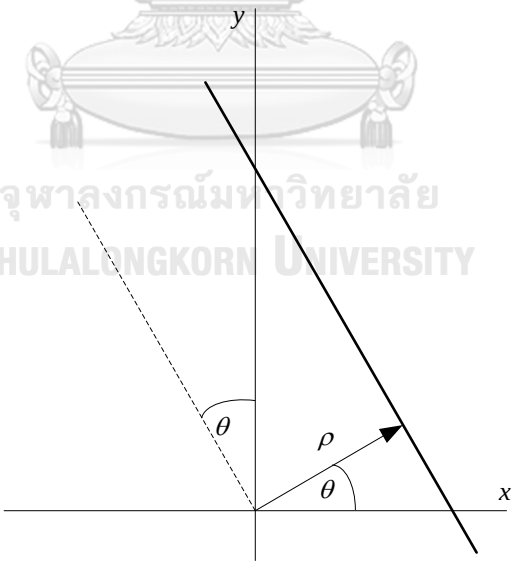

Figure 2.9 Cartesian coordinate represents axis transformation

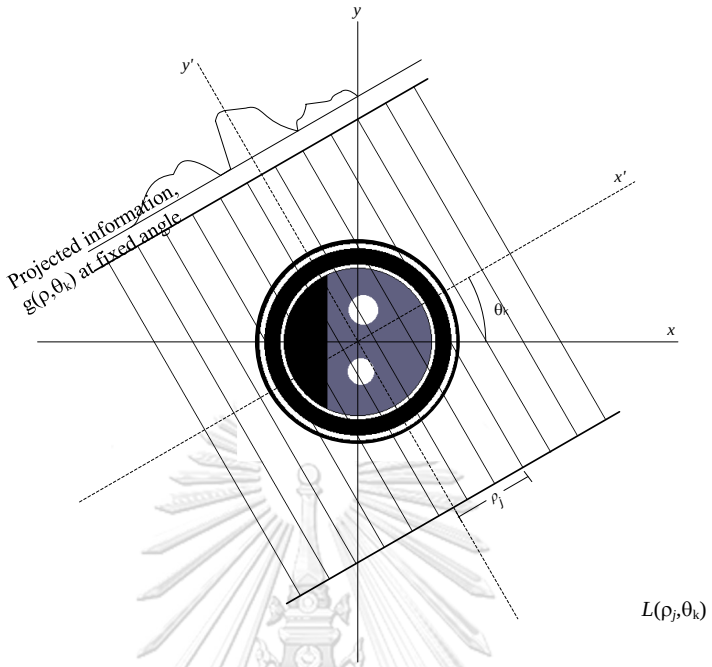

Figure 2.10 Geometry of a parallel-ray beam

From Figure 2.9, the Cartesian transformation is considered and the relationship of *x*, *y*, ρ and θ can be expressed by Eq. 2.20

$$\rho = x\cos\theta + y\sin\theta \qquad \text{Eq. 2.20}$$

The projection of parallel-ray beam may be modeled by a set of such lines, as shown Figure 2.10. An arbitrary point in the projection signal is given by rays-sum along the line $\rho_j = x\cos\theta_k + y\sin\theta_k$. The raysum is line integral, given by

$$g(\rho_j, \theta_k) = \int_{-\infty}^{\infty}\int_{-\infty}^{\infty} f(x,y)\delta\left(x\cos\theta_k + y\sin\theta_k - \rho_j\right)dxdy \qquad \text{Eq. 2.21}$$

Where δ is an impulse operator. The $g(\rho_j, \theta_k)$ in equation called Radon transform and has a notation as $\Re\{f(x,y)\}$ or $\Re\{f\}$

In discrete form, Eq. 2.22 is represented by

$$g(\rho,\theta) = \sum_{x=0}^{M-1}\sum_{y=0}^{N-1} f(x,y)\delta(x\cos\theta + y\sin\theta - \rho) \qquad \text{Eq. 2.22}$$

2.3.1 Image reconstruction from parallel beam

An image reconstruction is a process to recover the pattern of medium from projected ray sums. In parallel beam, the Cartesian coordinate is taken into account since the computer screen arrange the coordinate in x and y pixels. Combination of pixels will construct the image whose the color of each pixel is quantified in Gray-scale.

The following algorithm explains the method to reconstruct the parallel beam image using back projection algorithm.

(a) The (*x*, *y*) coordinate in computer screen is defined as show in Figure 2.11. The top- left corner of screen is defined (0, 0) and bottom-right (MAX_X, MAX_Y). These parameters defined a boundary of reconstructing image. In general, a boundary depends on the availability of screen, however, the image processing may assist the programming to extend the boundary larger than the screen but it is out of scope of this paper.

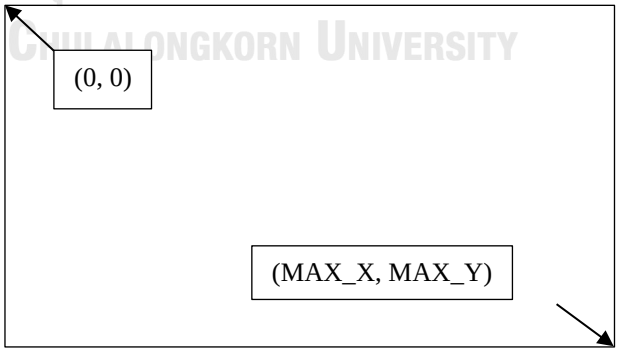

Figure 2.11 Computer screen coordinate

(b) The coordinate conversion is needed to convert the computer screen coordinate to calculation Cartesian coordinate as show in Figure 2.12 where the (0, 0) is in the middle of the system space.

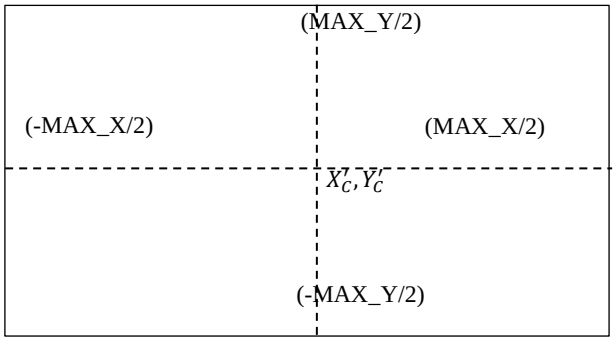

Figure 2.12 The Cartesian coordinate

For computerize, the center of Cartesian coordinate will be represented by, X'_C and Y'_C, respectively. Moreover, the *X'* and *Y'* in Cartesian coordinate will represent the *x* and *y* value in computer screen coordinate.

For any x and y in computer screen coordinate, the equivalent *X'* and *Y'* coordinate will be calculated by

$$X' = x - X'_C$$

$$Y' = Y'_C - y$$

(c) The ray-sum at a distance from center in Cartesian coordinate will be represented by parameter ρ and since there are j parallel beams in each angle, the subscript, ρ_j, represents ray-sum at jth position.

(d) The angle of each exposure will be called projection and represented the angle by θ.

(e) Starting at angle $\theta = 0^o$, sweep x and y in computer coordinate from the most left and to until the most right bottom. At each pixel, calculate Cartesian coordinate from -X', -Y' at most left to +X', +Y' at most right and check if (X'2 + Y'2) is bounded by

(f) Only if the condition (X'2 + Y'2) ≤ (MAX_X/2)2 is true, the calculation will be continued. Otherwise increases the value of pixel to be considered.

(g) Calculate the value of position bin (P_b) in the ray-sum from

$$P_b = X' \cos\theta + Y' \sin\theta$$

(h) If P_b is not integer, the interpolation of data in position bin of θ projection and jth ray-sum ρ_j is mandatory.

(i) Summation each pixel by the value in bin calculated from (g)

(j) Increase θ and repeat step (e) until last projection and thus the image is back projected

(k) Example of image reconstruction from parallel beam

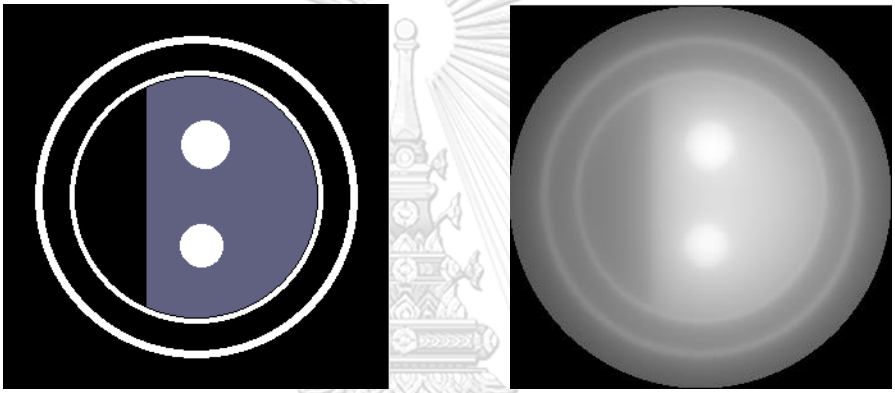

(a) original image (b) reconstructed image

Figure 2.13 Parallel beam image reconstruction using "back projection algorithm"

2.3.2 Image reconstruction from fan beam

The image reconstruction for fan beam can be considered in the same manner of parallel beam image reconstruction. The difference is only the transformation from Cartesian coordinate into the polar coordinates. Figure 2.14 shows the coordinate system of fan beam.

Though the coordinate system has been transformed to polar system, the transformation of computer screen coordinate into polar system is still valid.

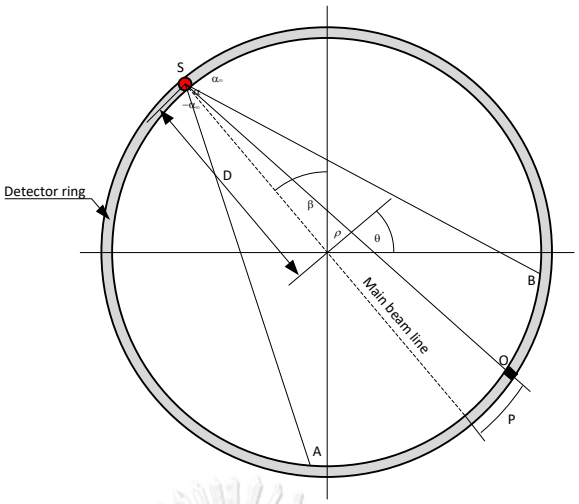

Figure 2.14 Fan beam projection system

Let the shape $A\hat{S}B$ represent the fan beam rays from the radioactive source (*S*) which is installed with a distance *D* measured from center of the system. The interested information will be acquired from the detector installed between arcs *AB* with the equiangular installation of α. Assume that the main beam line represents the reference angle from y-axis when source is rotated by the angle of β.

The calculation example will be explain with the point of interest is at the *O* position in Figure 2.14. The detector installed at point O has angle of α deviated from the main beam line and has angle of β from the reference y-axis. At this point, if ρ is an orthogonal vector to the main beam line with a distance from main beam line to the beam line of $\overline{SO}$, the following Eq. 2.23 and Eq. 2.24 are the angular transformation

$$\theta = \beta + \alpha \qquad \text{Eq. 2.23}$$

$$\rho = D \sin \alpha \qquad \text{Eq. 2.24}$$

Moreover, the transformation from Cartesian coordinate to polar coordinate system or (*x*, *y*) to (*r*, ϕ) will be explained by $x = r\cos\emptyset$ and $y = r\sin\emptyset$ then Eq. 2.20 can be re-written as

$$x\cos\theta + y\sin\theta = (r\cos\emptyset\cos\theta) + (r\sin\emptyset\sin\theta) \qquad \text{Eq. 2.25}$$
$$= r\cos(\theta - \emptyset)$$

Since the information is considered when the fan beam is covered the detector installed between arcs *AB* then the information at other location by other detectors will be force to zero that is the consideration ray-sums has value only when $|\rho| < T$ and the source considered to be moved around the object. The interesting projection angle is 2π degree. Eq. to describe function *f*(*x*, *y*) can be express in Eq. 2.26

$$f(x,y) = \frac{1}{2}\int_0^{2\pi}\int_{-T}^{T} g(\rho,\theta)\delta(x\cos\theta + y\sin\theta - \rho)\, d\rho d\theta$$

$$f(x,y) = \frac{1}{2}\int_0^{2\pi}\int_{-T}^{T} g(\rho,\theta)\delta(r\cos(\theta - \emptyset) - \rho)\, d\rho d\theta \qquad \text{Eq. 2.26}$$

Apply Eq. 2.23, Eq. 2.24 into Eq. 2.26, we get

$$f(x,y) = \frac{1}{2}\int_0^{2\pi}\int_{-T}^{T} g(D\sin\alpha, \beta+\alpha)\delta(r\cos(\beta+\alpha-\emptyset) - D\sin\alpha)\, D\cos\alpha\, d\alpha d\theta \qquad \text{Eq. 2.27}$$

If the interested angle of detectors in fan beam are bounded by $-\alpha_m$ to α_m, Eq. 2.27 can be rewritten

$$f(x,y) = \frac{1}{2}\int_0^{2\pi}\int_{-\alpha_m}^{\alpha_m} g(D\sin\alpha, \beta+\alpha)\delta(r\cos(\beta+\alpha-\emptyset) - D\sin\alpha)\, D\cos\alpha\, d\alpha d\theta \qquad \text{Eq. 2.28}$$

Following steps describe the algorithm to implement the fan-beam image reconstruction in computer programming

(a) The fan beam projected to each detector is considered as single ray-sum. It means that one ray-sum information is the data acquired from measurement of a detector at angle α between fan boundary $-\alpha_m$ to α_m

(b) The projections occur when source has moved around the object. Each step angle moving with β degree. Then one projection will composed of the ray-sums with the amount number of ray-sums will be the same as the number of detectors bounded by angle described in (a)

(c) At each ray-sum in each projection, determine X' and Y' of source (in poly coordinate system). The first source position is locating at reference angle (normally at +Y' axis).

(d) Setup the first ray-sum path to determine the path vector by starting from $-\alpha_m$ angle

(e) Increase the path length of point in fan beam. At each position, determine the corresponding "x" and "y" in computer screen coordinate and start to make a back projection in each pixel.

(f) Varies the value of α until the angle reach α_m

(g) Change the β angle (outer integral in Eq. 2.27) and repeat step (c) until β reaches 2π radian

(h) Plot the pixels

(i) Example of image reconstruction from fan beam

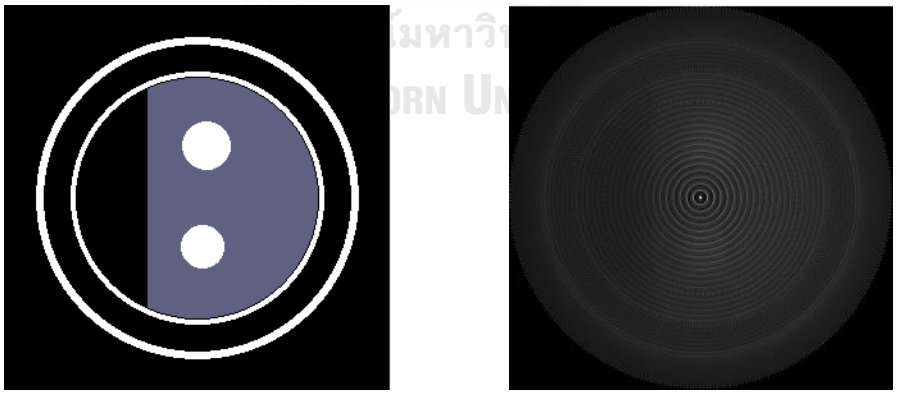

(a) original image (b) reconstructed image

Figure 2.15 Fan beam image reconstruction using "back projection algorithm"

2.3.3 Discrete Fourier Transformation

Fourier transformation is a mathematic method to transform functions from time domain into frequency domain which represent all frequency distribution in functions. The transformation results are easier to understand system behaviour and allows designer to manipulate such a complicate system, especially important to this dissertation is its usefulness of filtering.

In the CT algorithm, each single projection represents by Fourier slice theorem as explain in earlier section. Recalling all measured data in pattern of fan beam are finite sets of discrete values, every single projection to detectors are regarding as a single period, i.e. this system composed of 21 detectors, hence single projection produces 21 measured data and can be regarding as period N of measurement. The data points are specified at n = 0, 1, 2, … , N – 1. A discrete Fourier transform can be written as [numerical methods for engineers]

$$F_k = \sum_{n=0}^{N-1} f_n e^{-i\omega_0 nk} \qquad \text{for } k = 0 \text{ to } N-1 \qquad \text{Eq. 2.29}$$

and the inverse Fourier transform as

$$f_n = \frac{1}{N}\sum_{k=0}^{N-1} F_k e^{i\omega_0 nk} \qquad \text{for } n = 0 \text{ to } N-1 \qquad \text{Eq. 2.30}$$

where $\omega_0 = 2\pi/N$

Since $e^{\pm ia} = \cos a \pm i \sin a$ and factor 1/N is merely a scaling factor which can be placed in either Eq. 2.29 and Eq. 2.30 such that both equations can be rewritten as

$$F_k = \frac{1}{N}\sum_{n=0}^{N-1} [f_n \cos(k\omega_0 n) \pm i f_n \sin(k\omega_0 n)] \qquad \text{Eq. 2.31}$$

$$f_n = \sum_{k=0}^{N-1} [F_k \cos(k\omega_0 n) \pm i F_k \sin(k\omega_0 n)] \qquad \text{Eq. 2.32}$$

2.3.4 Filtering

From Figure 2.13 and Figure 2.15, the image from back projection displayed with artifacts which is a noise from the back projection algorithm. Obviously, quality of reconstructed images is very poor. The ways to improve the reconstructed image quality is introducing the mathematic convolution or in another name “filter”. The convolution will enhance the important information at the middle and suppress the information at the periphery of data in each ray-sum of projections.

For parallel beam image reconstruction, the equation is modified to Eq. 2.33

$$f(x,y) = \frac{1}{2}\int_{0}^{2\pi}\int_{-T}^{T} g(\rho,\theta) * h(m)\delta(x\cos\theta + y\sin\theta - \rho)\, d\rho d\theta \qquad \text{Eq. 2.33}$$

For fan beam image reconstruction, the equation is modified to Eq. 2.34

$$f(x,y) = \tfrac{1}{2}\int_{0}^{2\pi}\int_{-T}^{T} g(\rho,\theta) * h(m)\delta(r\cos(\theta - \emptyset) - \rho)\, d\rho d\theta \qquad \text{Eq. 2.34}$$

After applying the Shepp-Logan filter, the reconstructed image for parallel beam and fan beam are improved as show in Figure 2.16 and Figure 2.17, respectively.

In frequency domain, the convolution of $g(\rho,\theta) * h(m)$ becomes more simple just multiply corresponding $G(\rho,\theta) \times H(k)$ where $G(\rho,\theta)$ and $H(k)$ are Fourier transform of $g(\rho,\theta)$ and $h(m)$, respectively.

(a) Shepp-Logan filter is the mathematics function that used in this paper. The function of Shepp-Logan is expressed in Eq. 2.35

$$h_s(m) = \frac{4}{\pi^2 d(1-4m^2)} \qquad \text{Eq. 2.35}$$

where d is the value of pixel size (generally constant ~ 0.2). Eq. of back projection is then added the term of filter and become “Filtered Back Projection”.

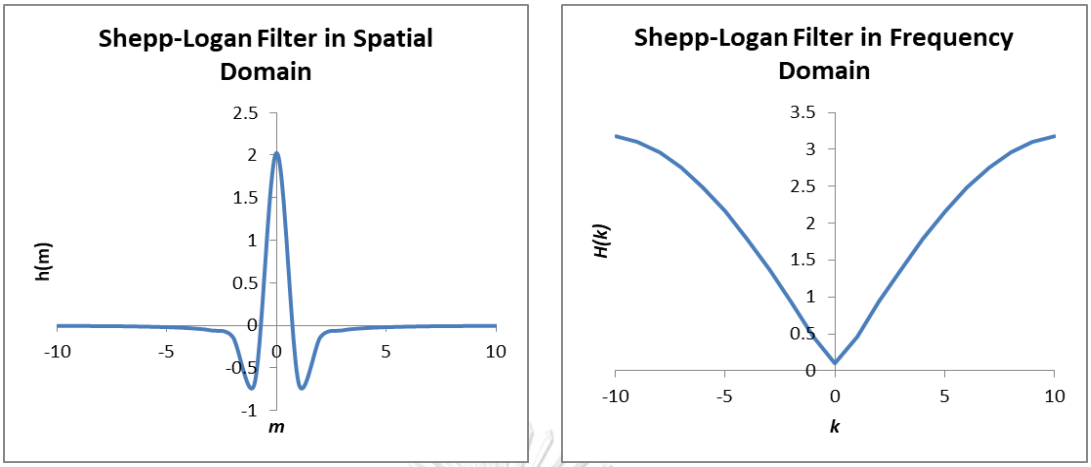

(a) (b)

Figure 2.16 A plot of Shepp and Logan Filter in (a) spatial domain ($h(m)$) and (b) frequency domain ($H(k)$)

(b) Ram-Lak filter function

$$h_r(m) = \begin{cases} \frac{1}{4\tau^2} & \text{for } m = 0 \\ 0 & \text{for } m = even \\ -\frac{1}{k^2\pi^2\tau^2} & \text{for } m = odd \end{cases} \qquad \text{Eq. 2.36}$$

in this dissertation, $\tau = 1$, $m = -(N\text{-}1)/2, \ldots, -2, -1, 0, 1, 2 \ldots (N\text{-}1)/2$

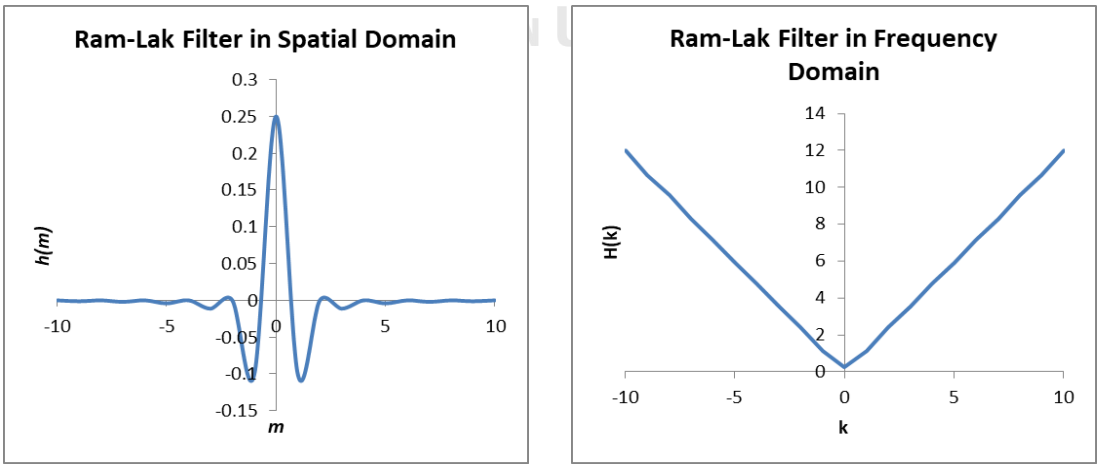

(a) (b)

Figure 2.17 A plot of Ram-Lak (Ramachandran and Lakshminarayanan, 1971) Filter in (a) spatial domain ($h(m)$) and (b) frequency domain ($H(k)$)

2.3.5 Example of image reconstruction from parallel beam after filtering

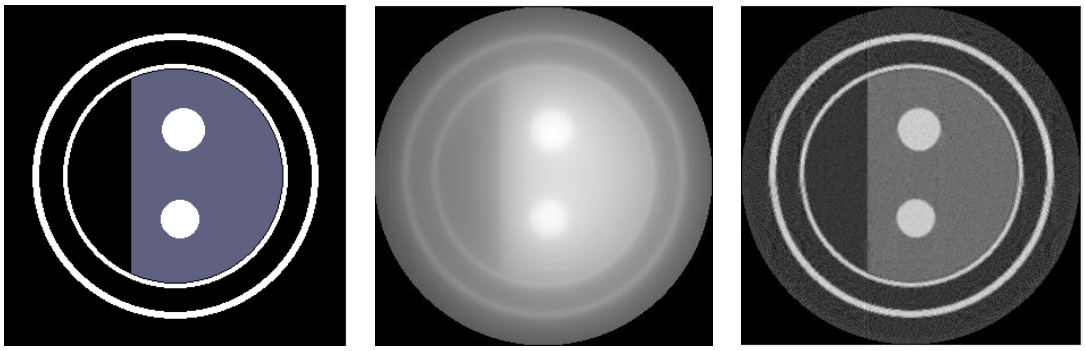

(a) original image (b) reconstructed image without filter (c) reconstructed image with filter

Figure 2.18 Parallel beam image reconstruction using “filtered back projection algorithm

2.3.6 Example of image reconstruction from fan beam after filtering

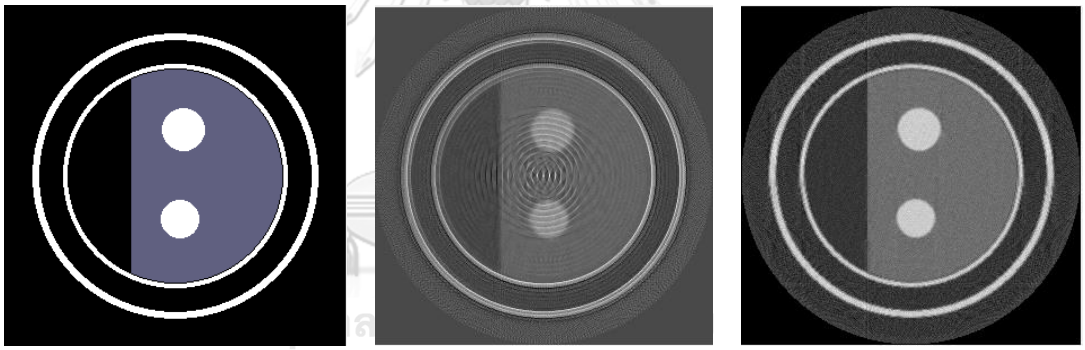

(a) original image (b) reconstructed image without filter (c) reconstructed image with filter

Figure 2.19 Fan beam image reconstruction using “filtered back projection algorithm”

2.3.7 Image reconstruction using algebraic reconstruction technique (ART)

The algebraic reconstruction technique (ART) is the iterative calculation algorithm which was introduced by Gordon R., R. Bender and G.T. Herman in 1970 to solve the linear equation by implementing Kaczmarz algorithm. The first iteration results were guess and projected the value onto the hyper-plane of each equation in linear equations until convergence of results are determined. This algorithm has superimposed a N’s square grid on the image with constant matrix of $f(x, y)$.

Figure 2.20 illustrated the square grid that superimposed onto the image. Assume that each cell represents each square grid has constant value, at cell jth, f_j. The projected data is denoted by p_i represents i^{th} raysum, the relationship between $f_j's$ and $p_i's$ can be expressed by Eq. 2.37. w_{ij} represents the weighting factor that cell j^{th} contributed to the raysum i^{th} [6] .

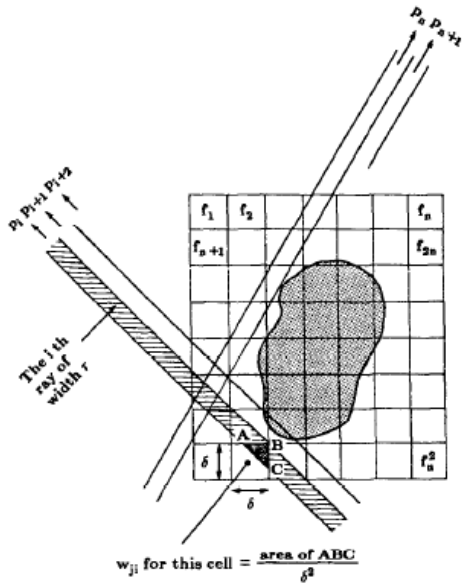

Figure 2.20 Square grid that superimposed on the image usd in ART algorithm

$$\begin{aligned} p_1 &= w_{11}f_1 + w_{12}f_2 + \cdots + w_{1N}f_N \\ p_2 &= w_{21}f_1 + w_{22}f_2 + \cdots + w_{2N}f_N \\ &\vdots \\ p_M &= w_{M1}f_1 + w_{M2}f_2 + \cdots + w_{MN}f_N \end{aligned} \qquad \text{Eq. 2.37}$$

$$\vec{p} = \vec{w}.\vec{f}$$

Using Kaczmarz algorithm, Eq. 2.37 can be iteratively solved by Eq. 2.38

$$\vec{f}^{(i)} = \vec{f}^{(i-1)} - \left(\frac{\vec{f}^{(i-1)}\overrightarrow{w_i} - p_i}{\overrightarrow{w_i}.\overrightarrow{w_i}}\right)\overrightarrow{w_i} \qquad \text{Eq. 2.38}$$

2.4 Conventional gamma scanning technique for distillation column

2.4.1 Introduction

The gamma scanning technique is based on the absorption of gamma radiation in the medium and measure the transmitted radiation which has not been absorbed in the medium [8]. The interactions with matter of gamma radiation play dominant mechanism of gamma ray energy reduction and this mechanism is proportional to the density in terms of absorption. A high density of matter is a higher absorption of gamma rays energy in one hand; on the other hand, a lower density of matter would be lower absorbed gamma rays energy. Using this principal the gamma-ray scanning technique is capable to reveal a change of density inside the distillation column during it is operating. The terms "on-stream gamma-ray transmission scanning technique" is used in some paper to illustrate the application of technique when the plant is on-line.

To perform the scanning, radioactive source such as ^{60}Co or ^{137}Cs is installed at one side of distillation column while the radiation detector is installed in the opposite side of the source (the setting up orientation of radioactive source and radiation detector will be discussed in section 2.2.2). Transmitted gamma-ray after absorbed in medium is measured. It can be approximated, theoretically, by Eq. 2.11 and using the mass attenuation coefficient instead of linear attenuation coefficient as in Eq. 2.14. Thus the measured gamma-ray intensity is expressed by

$$I = I_0 e^{-\mu_\rho \rho x}$$

where μ_ρ is mass attenuation coefficient (cm^2/g), ρ is density of the medium (g/cm^3) and x is a diameter of column or distance from source to detector (cm).

It is not necessary that column diameter will be equal along the column height and also the wall thickness of column could probably be not a constant. This information can be found in the engineering drawing of that column. Physically, if the column diameter and wall thickness does not change along the height of column, transmitted gamma intensity is directly reflecting the internal feature of the structures and phase density of production inside the column.

The transmitted gamma-ray profile is plotted by recording the measured transmitted gamma-ray at each elevation. After recording the information at that elevation, the radiation source and detector are simultaneously lifting in vertical at specified elevation step (normally 25 mm – 50 mm) data recording is then repeated over and over until it reaches the interesting elevation. The profile is plotted as gamma-intensity vs. elevation.

The information obtaining from recorded profiles are compared with the engineering drawing. It also induces to the interesting internal information such as the integrity of trays, liquid distributor, froth on trays and vapor gap between froth on tray and tray to tray, etc. Not only the physical structure can be identified, the process operating condition such as flooding, weeping, foaming etc. can also be obtained.

Setting Radiation Source - Detector

In general, the types of distillation column are categorized into two types.

(a) Trays type distillation column

A tray type distillation column is composed of trays to hold the froth. On a tray, it has holes to allow the gas flowing from bottom of column upward to the top of column. These holes might be covered by valves or without valves depend on the design of the company. The distillation occurs when the gas and froth is exchanging in physical properties. The trays may have down comer or may not have down comer depend on the design of the company as well.

(b) Packed bed type distillation column

A packed bed type distillation column composed by either structure pack or random pack. The structure pack is something like trays but it is folding in a volume, cylindrical shape and put into the column. The random pack is made up of small piece of rings size is more or less like a bracelet and fills into the column randomly until it reach the volume as design.

In order to set up the scanning equipment, radioactive source and detector, the internal structure of column must be studied through engineering drawing. Since the column generally comprises of two types as explained earlier, we will first

describe the operation of gamma-ray scanning with tray type and follow by packed bed type later on.

2.4.2 Orientation for scanning of tray type distillation column

The idea of scanning the tray type column is the ability to distinguish and identify the normal tray or abnormal one. Generally, the tray itself is a very thin metal and it is not possible to be scanned. Thus the information reflects the integrity of tray come from the gamma transmitted through and absorbed in liquid on the tray (term liquid refers to multi-phase liquid). Therefore, the scanning equipment setting up must avoid the directions which pass through the down comer of tray. The frequently found down comer designs are illustrated in figure aaa1 below. It comprises of "single down comer", "double down comer" and "multi down comer".

Equipment setting up of each type of down comer trays column is indicated in Figure 2.21 (a) – (c) below.

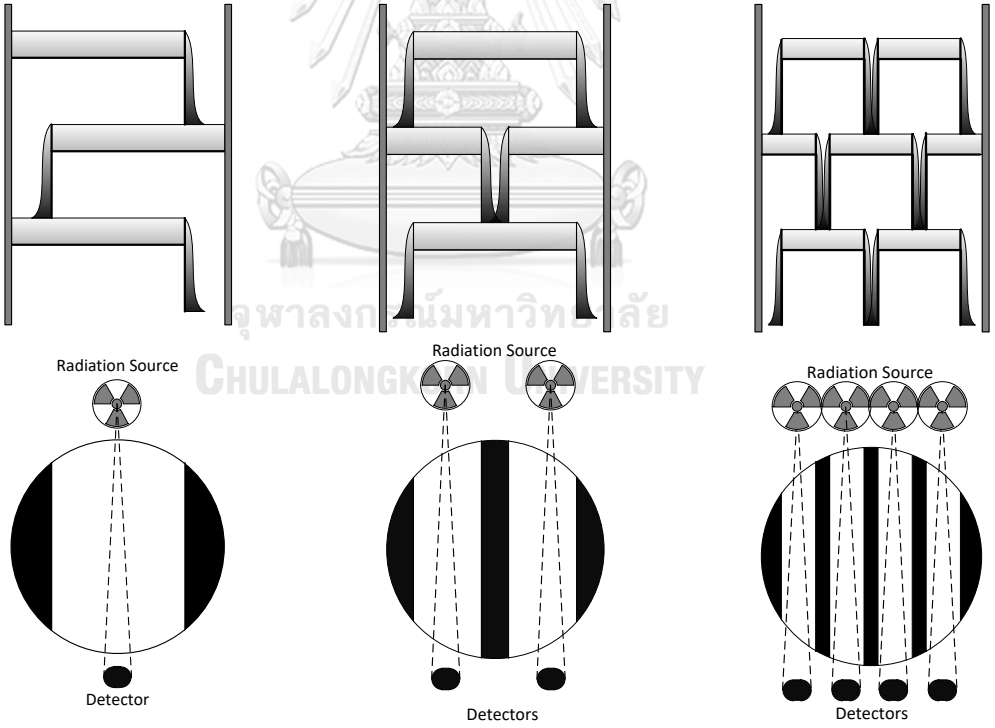

(a) (b) (c)

Single down comer trays Double down comer trays Multi-down comer trays

Figure 2.21 Trays with down comer with source and detector setting up

2.4.3 Orientation for scanning of packed bed distillation column

The scanning of packed bed distillation column can be performed by grid scanning in order to see the distribution inside the pack. Uniformly distribution is expected in every quadrant of cross-section. In general, the interesting parameters to be observed are pack bed length, blockage or fouling and flooding. The non-uniform distribution affects to the distillation performance and efficiency, when liquid and gas has not well mixed, the channeling occurs and it seems to be persist as long as the column is operating. Cleaning of column is one option to solve the channeling problem; however, in some case cleaning is not enough.

Equipment setting up of grid scanning for packed bed column is illustrated in Figure 2.22. If column is large, more scanning lines are needed.

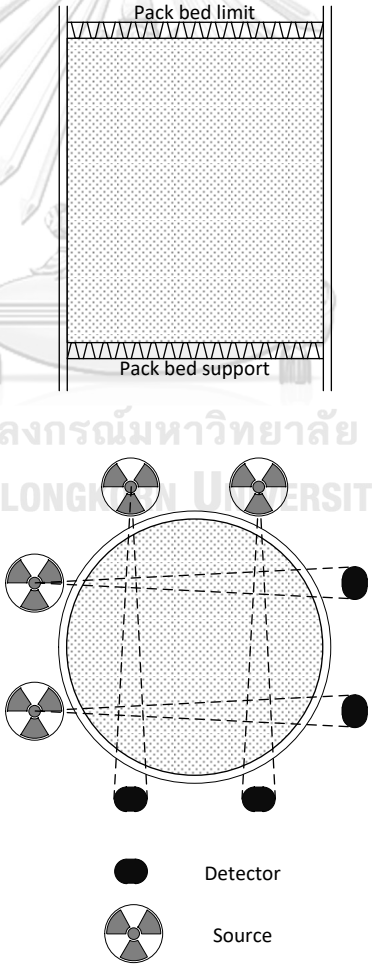

Figure 2.22 Source and detector setting up for packed bed column

2.4.4 Mechanism to construct the gamma scanning profile

Gamma scanning profile provides a clear picture of the column internals, giving the internal structure, defects and column process state without interrupting the process. Basic data interpretation is described as the following:

When the radiation beam crosses a liquid zone the weakest transmitted gamma intensity is obtained.

When the radiation beam crosses a tray which is normally filled up with froth, most of the intensity is absorbed and a narrow peak is recorded. Negative peak means lowest intensity corresponding to the froth or liquid base line.

When the radiation beam crosses a vapor zone, the intensity is the maximum (vapor base line), but the shape is not peak but rather large due to the fact that the vapor zone is larger than liquid zone or tray size.

2.4.5 Gamma scanning profiles interpretation

The gamma scanning result of normal trays type column is illustrated in Figure 2.23. The pattern indicates clearly separation between froth on trays and vapor gap between froth and upper tray.

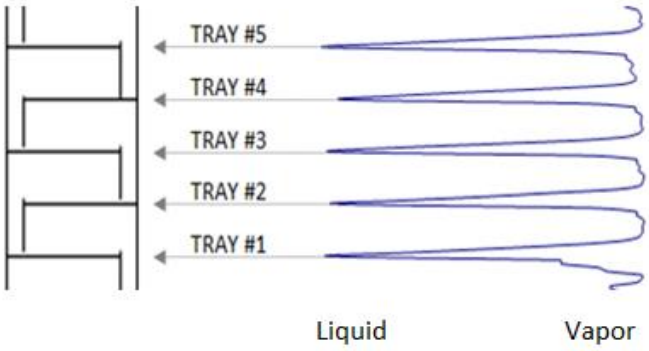

Figure 2.23 Profile of normal trays type column

The gamma scanning result of abnormal trays type column due to emulsification or foaming is illustrated in Figure 2.24. The foaming is the situation when the liquid on trays has heavy turbulent and agitated. Consequently, the liquid escape into vapor and forming deferent types of emulsions. It is comparable to the bubbles on the top of glass of beer.

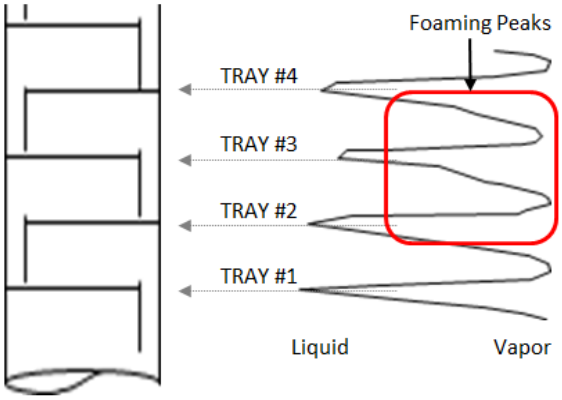

Figure 2.24 Profile of emulsification or foaming trays type column

The gamma scanning result of abnormal trays type column due to weeping is illustrated in Figure 2.25. The weeping is the situation when the liquid on trays goes downward underneath the tray. It look like condensation phenomena and produces a massive droplet, consequently, the density of vapor underneath the trays is replaced by density of droplets. The profile pattern is an inverse of emulsification phenomena.

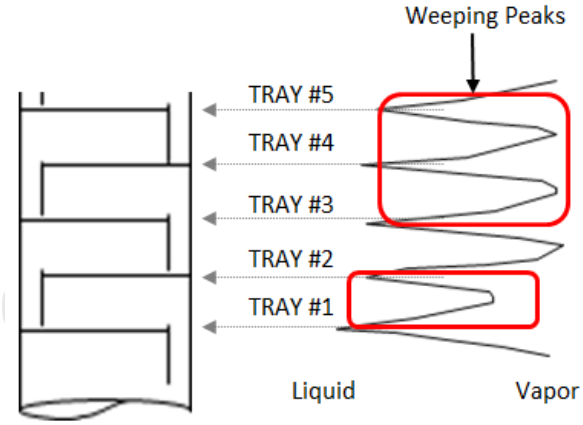

Figure 2.25 Profile of weeping phenomena in trays type column

The gamma scanning result of abnormal trays type column due to trays are missing from the position is illustrated in Figure 2.26. The trays missing situation is one of the most severe situations because the column lose the capability to distillate. The production will off its specification and can propagate the problem to other stages downstream.

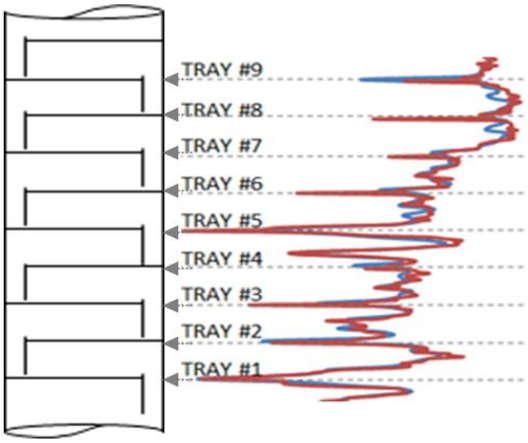

Figure 2.26 Profile of missing position of trays in trays type column

The gamma scanning result of abnormal trays type column due to obstruction or flooding is illustrated in Figure 2.27. The flooding situation is one of the most severe situations because the flooding zone will block the flow and hence the column loses the capability to distillate. In this case, the high pressure drop at the location of flooding is suspected and can be read out from the different pressure instrumentation, if they are installed. The production will off its specification and can propagate the problem to other stages downstream.

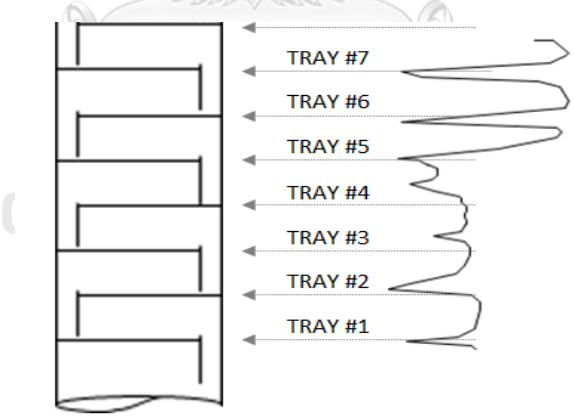

Figure 2.27 Profile of missing position of trays in trays type column

The gamma scanning result of normal packed bed type column is illustrated in Figure 2.28. The results show uniform distribution in 4 scanning lines. Some interference signals came from the external structures such as a pipe, structure support, etc. From this case, the pack length was observed with the length of 6,800 mm.

The gamma scanning result of abnormal packed bed type column is illustrated in Figure 2.29. The non-uniform distribution was observed along the pack length. However, the pack length of 6,350 mm was observed and it is good agreement when compare with engineering drawing. One more abnormal observed from the scanning result is a missing liquid distributor above the packed bed.

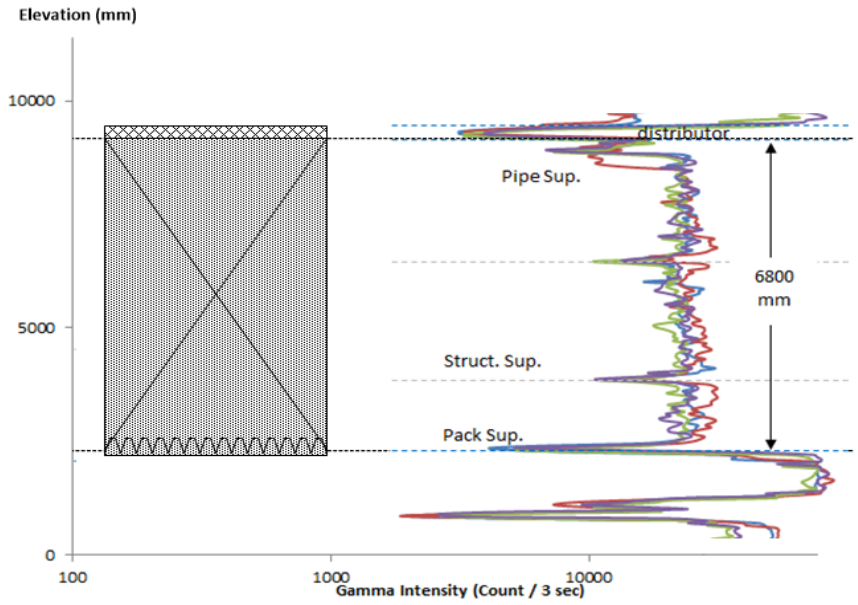

Figure 2.28 Profile of normal and uniform liquid distribution in packed bed type column

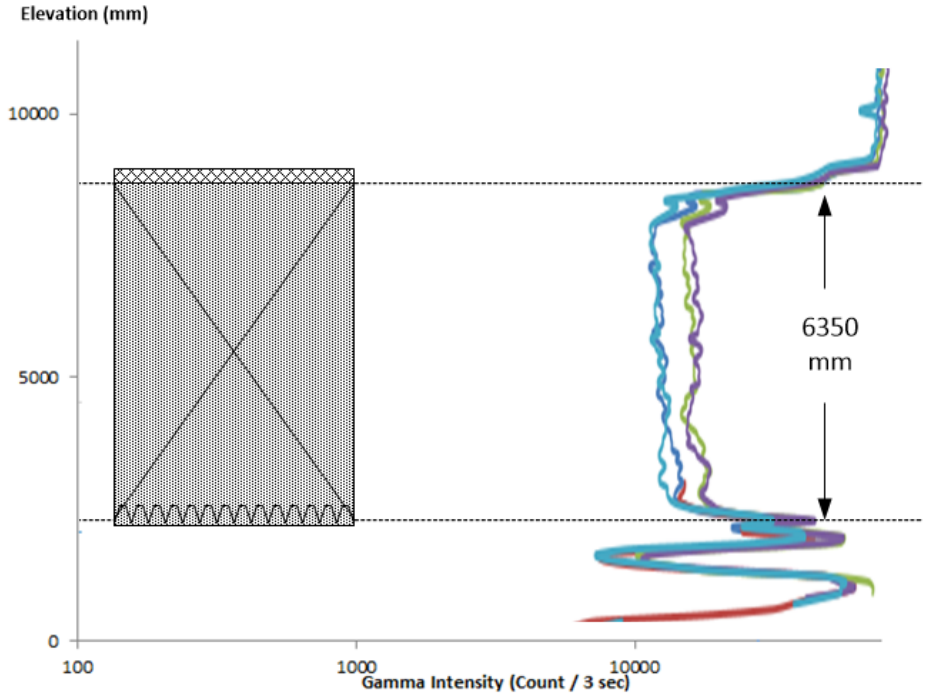

Figure 2.29 Profile of abnormal, non-uniform liquid distribution in packed bed and missing of liquid distributor at the top of packed bed

2.4.6 Example of normal trays type column gamma scanning result

The result indicates in Figure 2.30 shows a clear separation between froth on trays and vapor gap. The gamma intensity represents froth on trays is approximately 5,000 count / 6 seconds while the gamma intensity represent vapor is approximately 80,000 count/6 seconds. This pattern is interpret as normal structures and well defined operating condition.

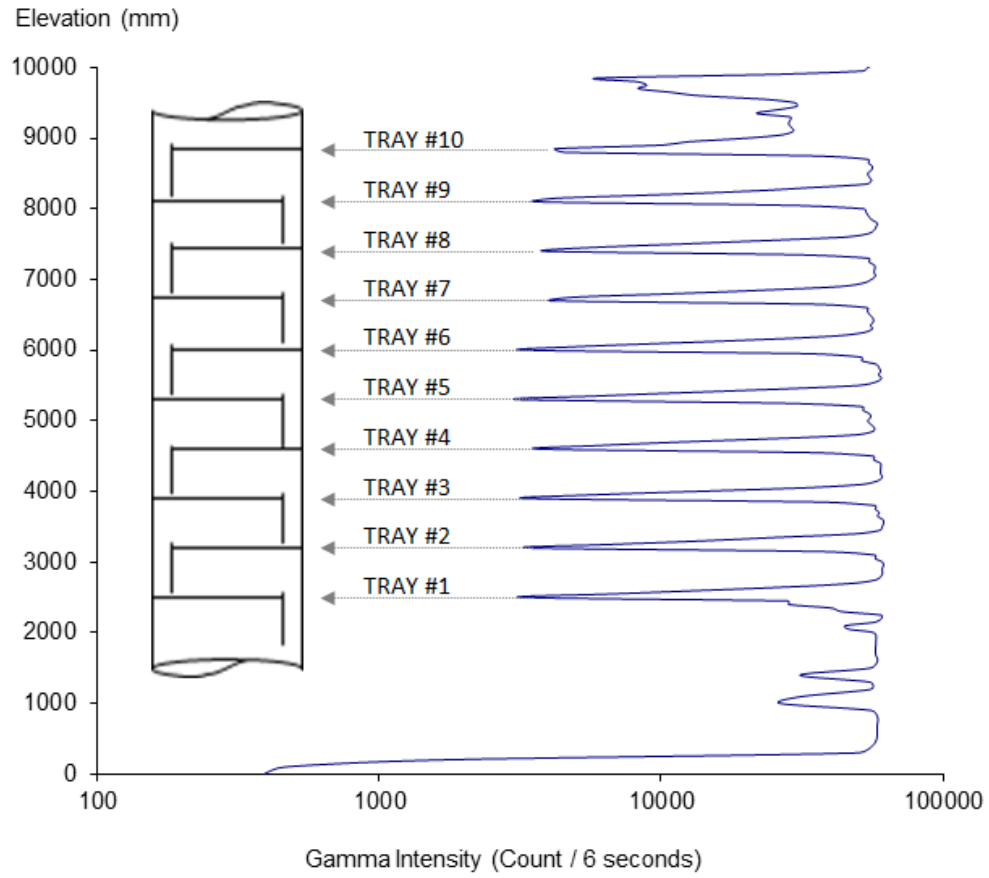

Figure 2.30 Gamma scanning profile of normal column

2.4.7 Radioactive source preparation.

The radioactive source, generally Co-60 is used in this application, can be obtained by recommended Eq. 2.39 [9]

$$Activity\ (mCi) = \frac{Dd^2 2^{e/X_{1/2}}}{T} \qquad \text{Eq. 2.39}$$

where

D is dose rate required at the detector (mR/h) (nominal value is 1 mR/h),

d is internal diameter of the column (m),

e is double wall thickness of the column (mm),

$X_{1/2}$ is half-value thickness (mm) for steel and the source (22 mm for steel and ^{60}Co)

T is gamma constant for the gamma source (e.g. 1.332 R/h in 1 distance for the source of 1 Ci)

2.5 Simulation of industrial fan-beam CT using MCNP computer code

The MCNP is standing for Monte Carlo N-Particle computer code. The code has been developed since at least 1947 at Los Alamos National Laboratory (LANL) [10, 11] in United State of America (U.S.A.). It is based on statistic phenomena of particle transportation which is capable to calculate the neutron, photon and electron transportation. It also has been widely used in calculation of the eigenvalues problem where the system criticality is needed such as nuclear research reactor and nuclear power reactor. The code treated a fundamental calculate in terms of particle tracking started from the origin of source; interact with the medium until it die out from the system. MCNP consider the trajectory of particle in three-dimension aspect toward interacted geometries. It is possible to model complicate cells using a simple surfaces combination, for instant cylindrical, rectangular, sphere and plane. The complicate cells are then modeled by arithmetic logic combination, i.e. union, intersection and complementary of simple geometry surfaces.

The point-wise ENDF material data library is coupled to the MCNP code to generate the particular cross-section in each interaction (in photon case, the major possibility interactions are explained in 2.1.1 – 2.1.3)

The structure of MCNP input file is described in three major cards (blocks) a cell card, a surface card and a data card. This composition of three cards can create a complicate geometry with specific materials and simulate much type of problems.

(a) Cell card

The cell cards are explained by logically combination (intersection, union, complementary, etc.) of surfaces provided in surface card. This combination can create complex structures such as nuclear reactor, particle acceleration, etc.

(b) Surface card

The surface cards contain a general geometric surface such as cylindrical, sphere, rectangle, hexagon, etc.

(c) Data card

The data card contains information of materials composed in each cell. This information is extracted from nuclear data library (ENDF). Composition material such as NaI, CsO, Stainless Steel, etc. can also be specified in this data card.

2.5.1 Example of MCNP input

Consider the Cesium 137 (Cs-137) radiation source that has geometry as illustrated in Figure 2.31. It is considered as a volumetric radiation source composed by Cesium Oxide powder compressed into cylindrical shape with diameter of 6 mm and height of 7 mm and then sealed with stainless steel (S.S.) such that total diameter and height become 7.5 mm and 10 mm, respectively.

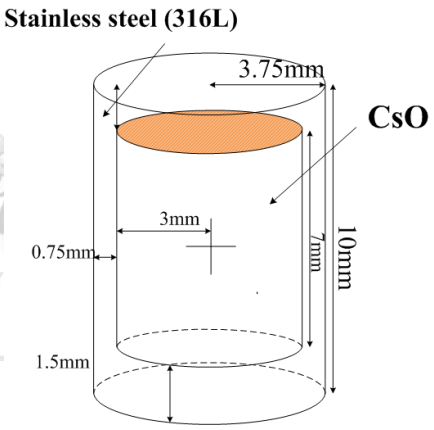

Figure 2.31 Gamma scanning profile of normal column

Input deck for MCNP to describe this radiation source is as follow (each line is explained by comment after symbol "//"):

```
Volume source                                   // title card
1  1  -1.47   -1          imp:p=1     // Cell Card 1 CsO in Surface 1
2  2  -7.9    -2     1    imp:p=1     // Cell Card 2 Stainless Steel in Surface 2
3  0  -3      2           imp:p=1     // Cell Card 3 Sphere container
```

```
4   0   3                    imp:p=0        // Cell Card 4 Excluded universe

1   RCC    0       0       -0.35     0  0  0.7   0.3     // Surface 1 cylindrical 6 x 7 mm CsO
2   RCC    0       0       -0.5      0  0  1.0  0.375 // Surface 2 cylindrical 7.5 x 10 mm Sus
3   SO     5

MODE P                                                  // Set calculation mode to Photon
SDEF  ERG=0.662  POS=0 0 0 RAD=D1                       // Set energy of Cs-137 place at origin
SI1  H   0   0.3
SP1 -21  1
SI2 H -0.35 0.35
SP2 -21  0
M1              55000   1               // Material 1 Card 1 Cesium (Cs) element
                6000    1               // Material 1 Card 2 Oxygen (O) element
M2              26000   -0.71           // Material 2 Card 1 Iron (Fe) element
                24000   -0.17           // Material 2 Card 2 Chromium (Cr) element
                28000   -0.12           // Material 2 Card 3 Nickel (Ni) element
F2:P    3                               // Tally photons with F2 in cell #3
E2              0   99I   1
PRDMP  2J  1
NPS 1000000                             // Number of particles to be run =  1,000,000
```


2.5.2 Role of MCNP in radiation application for industries.

In general, the MCNP consumes a big computing environment when the problem is setting as a large scale size since the photon transport theorem has been taken into account. A usefulness of MCNP enables the operator to prepare the desired radioactive source (Gamma source) for using with the experiment. For instant, to do the column scanning, Eq. 2.16 may be used. However, in some cases the result calculated from Eq. 2.16 is too over estimated and sometime working with high activity source is difficult. The MCNP can provide the calculation results for source activity versus the prospective gamma intensity which might be measured by detector if the geometry is setting with good enough information as close as the real plants.

2.5.3 How to use MCNP with this dissertation

The design of column with simple internal structure will be modeled. The model will be incorporated with the measurement system which comprised of 21 detectors and 1 source. The detectors are fixed in position and the radiation source ^{137}Cs is positioned specified in the problem. Consider when moving source, the new location of source will be specified in the model of MCNP input file and re-calculate. So it is not difficult to image if the problem stated that the source will move each step with 1 degree, 360 files would be generated and would be calculated.

The advantage of using MCNP is the capability to increase or decrease the equipment such as we can simulate the number of detector as much as we need. This is not possible with the real experiment; the limited of environment confines the idea of development in theoretical point of view.

2.6 Literatures Review

Kim, Jongbum presented "Development of gamma-ray tomographic system for industrial plant inspection" by using the generation 4^{th} computed tomographic technique [12, 13]. The aim of research was trying to verify the calculation of Computed Fluid Dynamics software (CFD). He presented the simulation using Monte Carlo computer code and apply the tomographic image reconstruction algorithms of algebraic algorithm such as Algebraic Reconstruction Technique (ART), and Simultaneous Iterative Reconstruction Technique (SIRT), etc. A statistic algorithm image reconstruction technique such as Expectation Maximization Technique (EM) and Diagonally Scaled Gradient Ascent Technique (DSGA) were also studied. It seems that, the statistic algorithm reconstructed a better quality of image compared to the algebraic algorithm. He has also setup the on-site system to study the catalyst distribution in the Regenerated Fluidized Catalytic Cracking Unit (RFCCU). The system comprised of 24 detectors installed at the plant around the RFCCU body. The cross-section at installed equipment was presented.

Christian W. Green, John Farone, Julie K. Briley, R. Bruce Eldridge, Richard A. Ketcham, and Ben Nightingale [14] presented the application of X-ray tomography to characterize the liquid-air behavior in the structure packing through

“Novel Application of X-ray Computed Tomography: Determination of Gas/Liquid Contact Area and Liquid Holdup in Structured Packing”. A small scaled column was simulated and contained the structured packing. The diameter of object is approximately 6 inches and operated by air and water passing through the scaled column. The result will be used to improve the structured packing design for a better distillation performance.

Zongcheng Wang, Artin Afacan, K. Nandakumar, Karl T. Chung [15] presented a research on “Porosity distribution in random packed columns by gamma ray tomography” to a simulated random packing column. The column is filled with Pall Ring packing type with various sizes; 16, 25 and 38 mm. The objective is to determine the porosity and its spatial distribution in packed column. The results presented there are always non-uniform distribution of porosity in the packed column but the variation of porosity can be described by normal distribution function in the bulk region of the packed beds. At the circumference of column or nearby column’s wall, always the radial porosity is higher than average value of porosity at bulk region.

D. Toye, P. Marchot, M. Crine, A.-M. Pelsser, G. L’Homme [16] presented the X-ray computed tomography for “Local measurements of void fraction and liquid holdup in packed columns using X-ray computed tomography” the objective is to determine the gas, liquid and solid phase’s distribution in the packed bed column. The column is 60 cm in diameter and randomly filled with Cascade Mini-Ring 1A packing elements. The column was operating with a various liquid flow rate between 0 – 6000 liters per hour. X-ray machine was setting with line detector to measure the cross-section data of column. A liquid hold-up value have been measured and evaluated and obviously found a good agreement with literature.

CHAPTER 3

METHODOLOGY

This chapter describes details of materials and equipment used in dissertation as well as the methodology of simulations, system calibrations and experiments. The materials and equipment are explained in section 3.1. Simulation using MCNP code is presenting in section 3.2 as well as its assumption and studied cases. Section 3.3 explains developed software “Simplified” which composed of three modules i.e. data acquisition module, data processing module and image reconstruction module and its example for using software. Section 3.4 proposes data acquisition technique that can be used the scanning which composed of three techniques i.e. simple scanning technique, one to end single half scanning technique and one to end double half scanning technique. The data acquired form acquisition shall be manipulated for example, how to shuffle acquired data and how to interpolate. Each technique shall be compared to the simulation as a reference result.

3.1 Materials

3.1.1 Radiation Detectors and Counting System

The equipment use in this study comprises of 12 channels benchtop radiation counter (Ludlum Model 4612) and Sodium Iodine (NaI(Tl)) uncollimated detectors, connected to the data acquisition software.

Figure 3.1 Radiation counter system with 12 NaI detectors.

3.1.2 Radioactive Source Cs-137

Uncollimated gamma radiation source Cesium – 137 (^{137}Cs), 10 mCi was used in this experiment. Radiation source and detectors were vertically aligned until the position of radiation source pellet located at the middle of active area of detectors. The radioactive source ^{137}Cs was loaded in uncollimated source holder. The size of holder is approximately 47 mm in diameter which can be loaded into the PVC detector blocks.

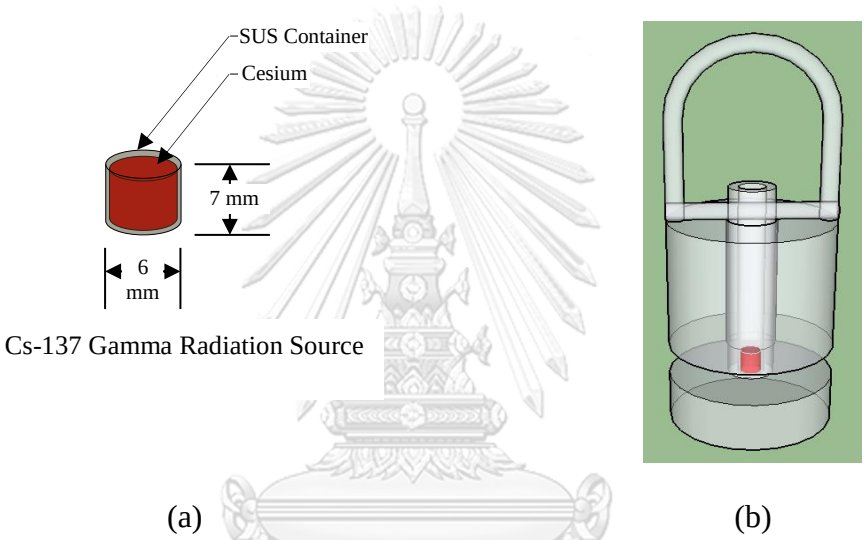

Figure 3.2 (a) ^{137}Cs Gamma radiation source pellet size and (b) Source holder

3.2 Calibrations

The calibration was done by adjusting available parameters, i.e. High Voltage (HV), Lower Level Discrimination (LLD) and Upper Level Discrimination (ULD). The LLD was setting until the measured signal had overcome the background radiation (noise and Compton scattering). Setting up ULD was opened since the radiation of higher energy played less dominant influence to the measurement data. Lowest count from one detector was selected as a reference detector and adjusted others detector's HV until the radiation count became closed to reference detector. This is the most important process since all detectors must be able to measure as a compatible to each other. If the system was not well calibrated, mess up reconstructed image would come.

Procedures to calibrate the system are displayed as diagram in Figure 3.3. Two distance positions from source to detectors were selected as “near field” and “far field” in order to compare and to adjust HV and LLD. Near field refers to position where the detector is placing close to the radiation source. Far filed refers to the position where the detector is placing far from the radiation source. Both reference detector and calibrating detector are placing at the same time in either far or near field in order to compare and adjust the value of calibrating detector to have value as close to the reference detector as possible. All detectors must be calibrated until it has almost the same efficiency as closed to each other in both near field and far field. The calibration procedures are as follow:

(a) Place reference detector at position called “near field” and place calibrating detector at another side of near field

(b) Measure the radiation count from gamma radiation source, adjust the HV or LLD until the radiation count of calibrating detector has the same value compared to the reference detector

(c) Move both reference detector and calibrating detector to position called “far field” and observe the radiation counting value, adjust the parameters if there is a big deviation

(d) Change the calibrating detector and repeat step (a) until all detectors are calibrated

It is necessary to use two positions “near and far field” instead of single point in order to observe the efficiency of detector when it detects high and low radiation since some detector has poor efficiency but it becomes over sensitive when receive high radiation. All detectors must be compromised to provide the good image. Mostly LLD are fixed at the same

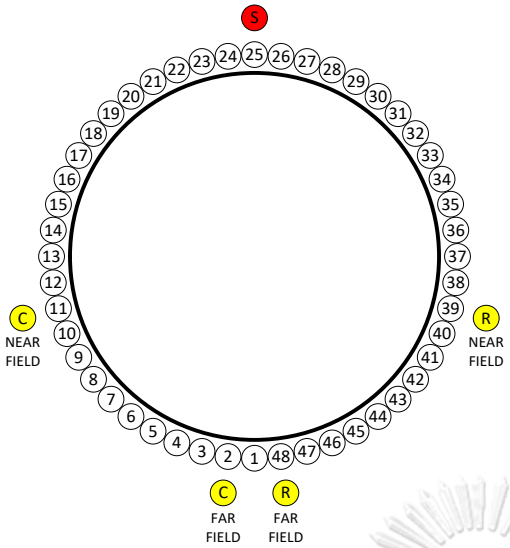

Figure 3.3 Calibration positioning of reference detector and calibrating detector.

3.3 Laboratory model

The laboratory model is top opened tank, as illustrated in Figure 3.4, which represent the distillation column, with a diameter of 800 mm Inside the tank, four steel pipes with different diameter were installed i.e. 152.4 mm (6”), 101.6 mm (4”), 76.2 mm (3”) and 114.3 mm (4.5”) located at a certain position. This model was used both in simulation and experiment in order to compare the different between simulation and experiment. The results from simulation was regarding as theoretical results while experiment might have some deviation from theoretical. It is expected that the results from experiment would be consistent to the simulation such that the simulation will be further used for planning when dealing with the field work.

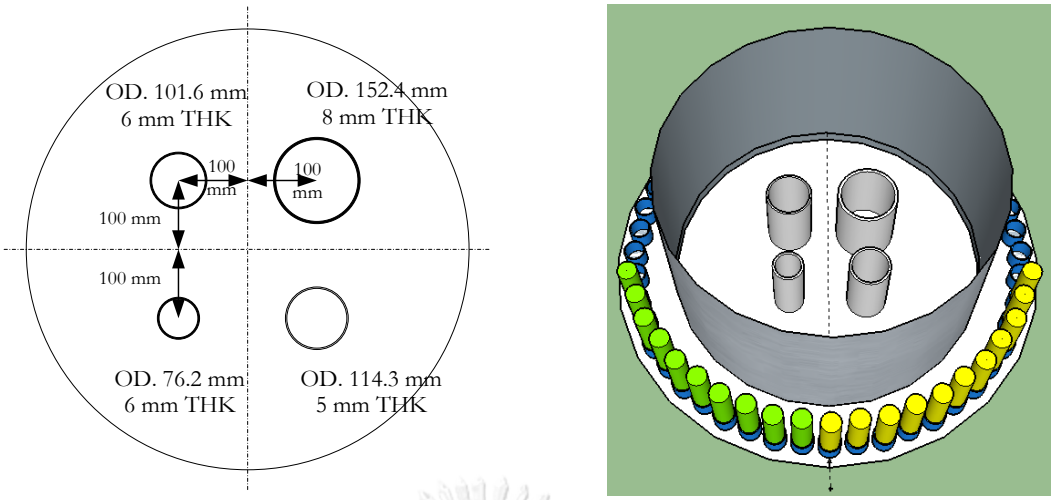

Figure 3.4 Pipes arrangement inside the top open tank 800 mm in Dia.

3.4 MCNP Simulation studied case

3.4.1 Simulation of system

The MCNPx is computer code used in both neutrons transportation and photon transportation. In this study, photon transportation is considere. The pulse height tally function F8 was used to collect information of interacted photons to detectors which can be regarded as a physical energy deposition to detectors. Simulation was arranged such that the structure of system is form in fan beam. The detectors are placed against the radiation source in the pattern of fan beam projection. In simulation the computer code generated 10^8 photons to simulate the transportation from radiation source to the detectors. The photon emitted from source interacts with the medium and finally either absorbed in the medium or absorbed in detectors. The interested results are the value of photons reached the detectors.

3.4.2 MCNP modeling of source and detector

The modelling of gamma radiation source, Cs-137 and radiation detector, NaI are displayed in Figure 3.5 below. The radiation source, exclude stainless steel container is size of 6 mm in diameter and 7 mm in height. With its container, the diameter is approximately 10 mm in diameter and 7.5 in height. In practical, the radiation source is installed inside the source holder for safe operation.

The radiation detector is a composition of Sodium-Iodine (NaI). It composed in a form of scintillation crystal with size of 25.4 mm in diameter and 25.4 mm in

height. The crystal is covered by aluminum cladding, approximately 200 mm in length, with electronics components such as a photo multiplying tube, anodes, etc. installed inside the aluminum cladding as indicate in Figure 3.5. Photon energy is set to 0.662 MeV and its photon spectrum distribution is displayed in Figure 3.6 below. The bins selected from 0.5 MeV up to 1.0 MeV are taken into account in the calculation results.

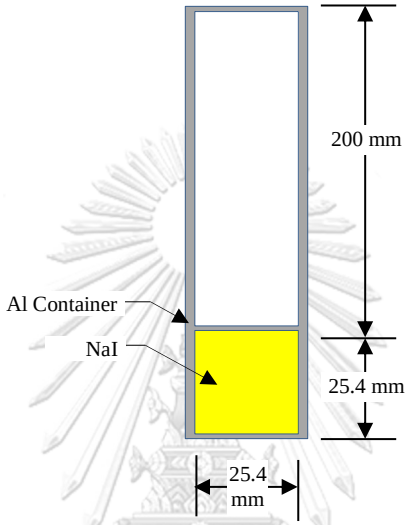

Figure 3.5 Modelling of Gamma Radiation Source and Detector

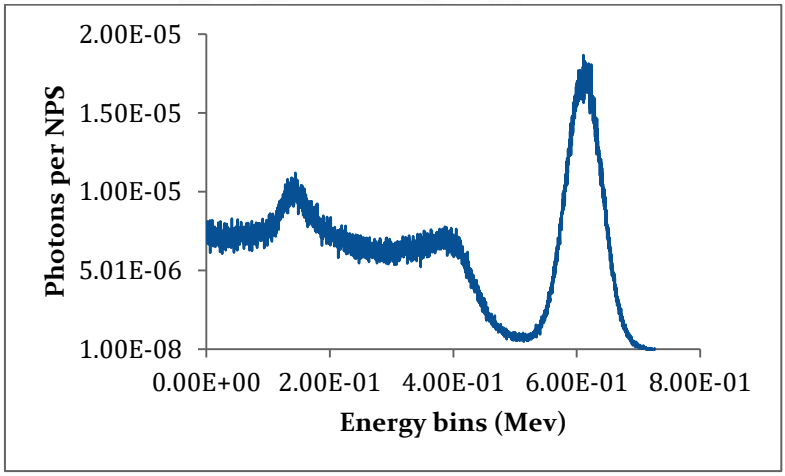

Figure 3.6 Simulated Photon Energy Spectrum Distribution by MCNPx

3.4.3 MCNP Modelling of four pipes

The input of MCNP were prepared and used “VISE” visualizer to check if the input is function. Note that red dot represent radiation source in Figure 3.7 was magnified since the true size of source could not be seen easily by figure. Sample input of projection #1 is illustrated in Appendix II

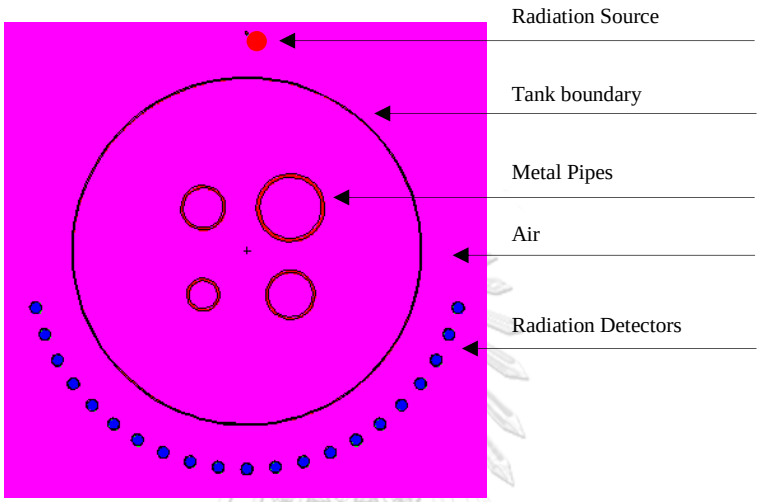

Figure 3.7 System configuration generated by MCNP computer code

3.5 Development of data acquisition, resorting and image reconstruction software

The developed software called “Simplified” composed of 4 modules i.e. Data acquisition module, Data post processing module, Image reconstruction module and Simulation module (user’s manual is attached in Appendix II). The software was developed based on the Microsoft platform through Visual Studio 2015 with C# language. Default startup module of software is Data acquisition which designed for interfacing with the radiation counter (Ludlum Model 4612) through serial communication (see user manual for details). Following section describes the detail in each module:

3.5.1 Data acquisition module

The software startup with this module which composed of information setting up, plot a raw data from all detectors, plot a sorting data from individual detector as profile projection and data table. The software connected to the radiation

counter through “Control Panel” menu. Communication port must be correctly selected until all setting up data such as HV, LLD and ULD are displayed in all channels. Figure 3.8 and Figure 3.9 show the page of Data acquisition startup page and Control panel page, respectively.

Two modes are available for data logging, i.e. continuous logging and accumulate logging. If checkbox “Accumulate Data” is uncheck, the logging is operating under the continuous logging mode, on the other hand, if checkbox “Accumulate Data” is checked the logging is operating under accumulation logging mode. The accumulation logging mode allows user to specify the data set to be accumulated since the maximum allowed counting time of radiation counter is only 2 seconds and can be set via “Control panel” (normally, it has been set to 1 second).

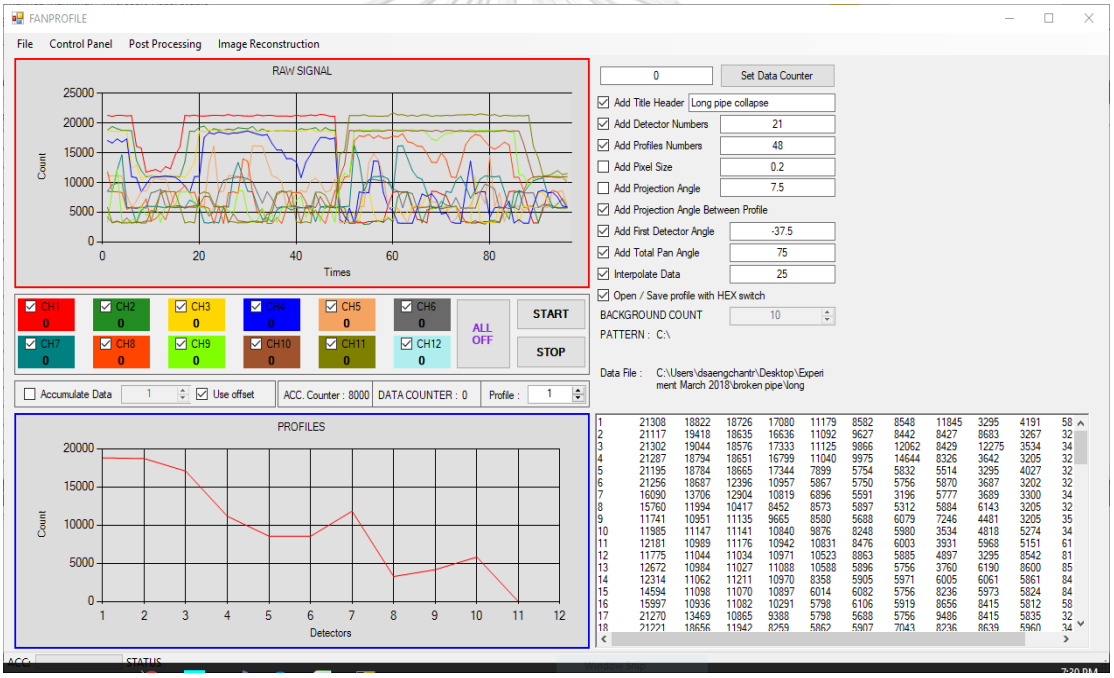

Figure 3.8 Data acquisition module

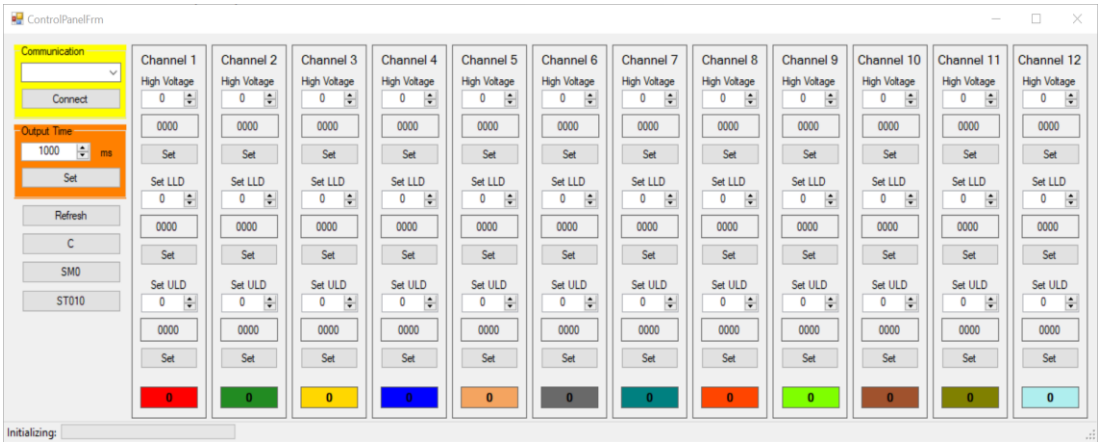

Figure 3.9 Control panel

3.5.2 Data post processing or data resorting module

The data processing was done by rearrange the detector as input pattern file. For example, if the number of detectors used in experiment is 5 detectors and 4 projections were done, using pattern by folding 2 last projections up to 2 top projections as indicated in Table 3.1 and Table 3.2.

Original Data

Projection 1: P_{11}, P_{12}, P_{13}, P_{14}, P_{15}

Projection 2: P_{21}, P_{22}, P_{23}, P_{24}, P_{25}

Projection 3: P_{31}, P_{32}, P_{33}, P_{34}, P_{35}

Projection 4: P_{41}, P_{42}, P_{43}, P_{44}, P_{45}

Where Pmn is measured data which from projection m by detector n

Table 3.1 Setting ID of each data

Projection	D_1	D_2	D_3	D_4	D_5
1	1	2	3	4	5
2	6	7	8	9	10
3	11	12	13	14	15
4	16	17	18	19	20

Dn is detector number n

Refolding Data

Rearranged Projection 1: P11, P12, P13, P14, P15, P21, P22, P23, P24, P25

Rearranged Projection 2: P31, P32, P33, P34, P35, P41, P42, P43, P44, P45

Table 3.2 The pattern file would be generated as

Projection	D_1	D_2	D_3	D_4	D_5	D_6	D_7	D_8	D_9	D_{10}
1	1	2	3	4	5	11	12	13	14	15
2	6	7	8	9	10	16	17	18	19	20

PATTERN.TXT

1 1 2 3 4 5 11 12 13 14 15

2 6 7 8 9 10 16 17 18 19 20

(For full data reshuffling pattern, see Appendix III)

3.5.3 Image reconstruction module

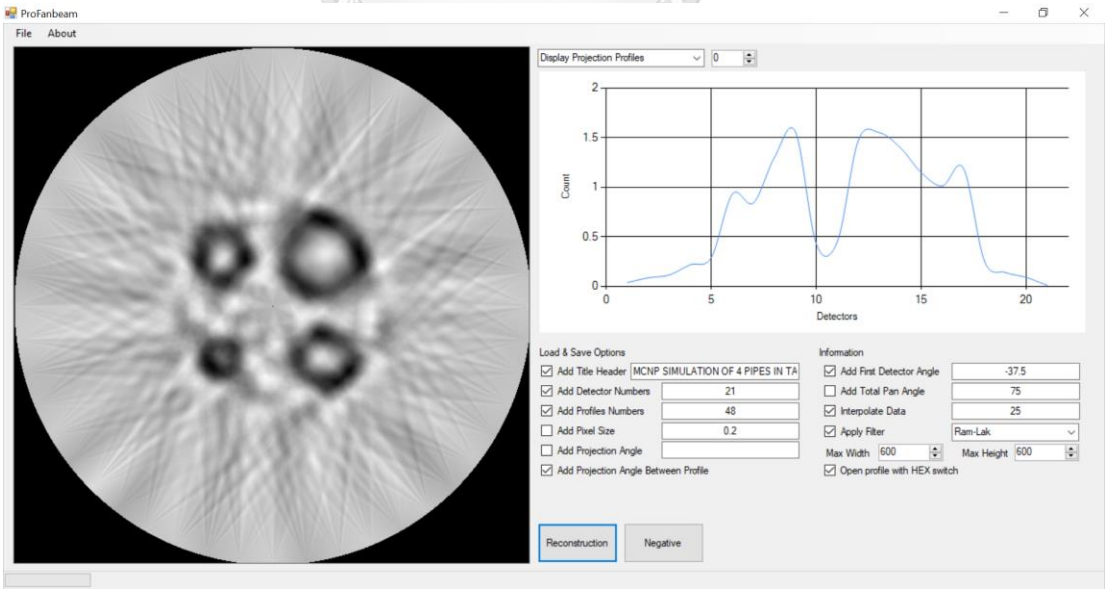

Figure 3.10 Reconstruction Module

Figure 3.10 shows invented reconstruction module based on filtered back projection algorithm as explained in Chapter 2. In this module, Ram-Lak, Shepp-Logan and Modified Ram-Lak filters were included in the module.

The plots in reconstruction module displayed projected data from all detectors used in the input file. It is possible to display projection profiles, projection profiles of I0/I, horizontal profile of reconstructed image and vertical profile of reconstructed image. Opening file must be arranged in proper format to accommodate with all required parameters.

The input file should begin at the first line with a “header switch” in order to control the sequence of data reading, this can be turned on or turned off by using checkboxes. The header switch is a converted into hexadecimal number as following details:

***Header Switch*:**

Bit 11	Bit 10	Bit 9	Bit 8
-	-	-	Title Header

Bit 7	Bit 6	Bit 5	Bit 4
Detector Numbers	Profiles Numbers	Pixel Size	Projection Angle

MSB 3	Bit 2	Bit 1	Bit 0
Proj^{n} Angle BTW	First Detector Angle	Total Pan Angle	Interpolation

For example, if the input composed of following parameters:

Title Header : Bit 8 = 1

Detector Numbers : Bit 7 = 1

Profiles Numbers : Bit 6 = 1

Proj^{n} Angle BTW : Bit 3 = 1

First Detector Angle : Bit 2 = 1

Total Pan Angle : Bit 1 = 1

Interpolation : Bit 0 = 1

Bit11	Bit10	Bit 9	Bit 8	Bit 7	Bit 6	Bit 5	Bit 4	Bit 3	Bit 2	Bit 1	Bit 0
0	0	0	1	1	1	0	0	1	1	1	1

Convert into hexadecimal = 1CF is the first line of input data as a switch value. This value is automatically generated if profile was generated by data acquisition module, otherwise text editor can be used for manually generate the projection data and header switch. Appendix IV shows the example of input data and its preparation.

Size of display image can be assigned as well by specify values in *"Max. Width"* and *"Max. Height"*. Negative button is function to invert a reconstructed image in to negative or positive image.

3.5.4 Simulation module

A simulation module is a simulator which simulates the projection of cross sectional drawing. Image of cross sectional drawing is loaded into the module with size of 601 x 601 pixels and with grayscale value of 8 bits (256 gray value level). Simulator will generate the projected profiles using fan beam which the number of detectors, number of projections, starting angle of first detector and panned angle can be specified to the input of module. Figure 3.11 displays simulation module window.

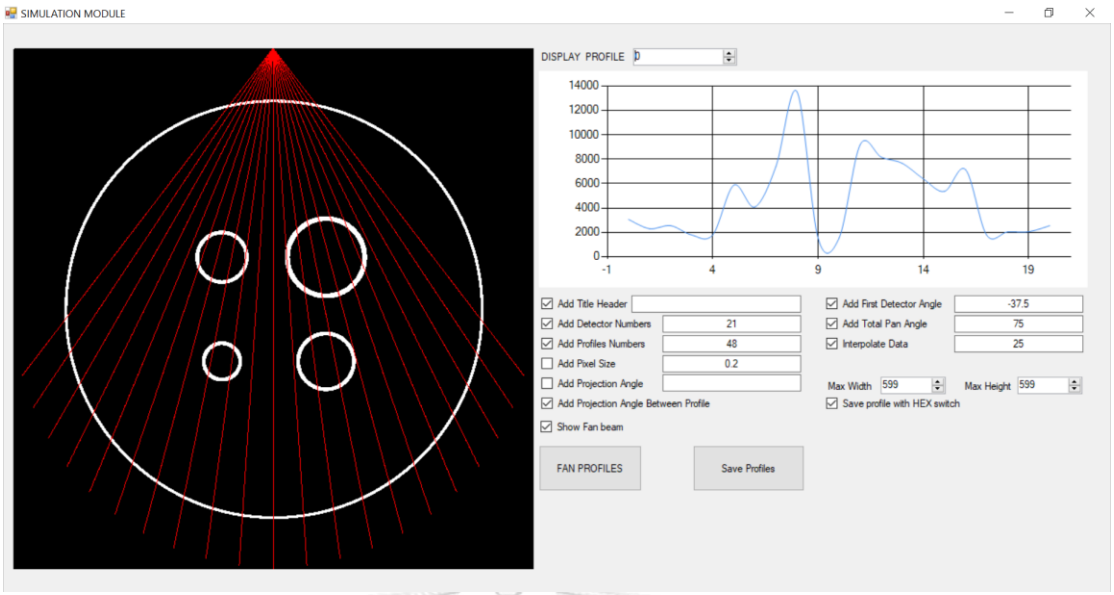

Figure 3.11 The projected data from a “Simulation Module”

3.6 Data acquisition techniques

Three scanning pattern were created in this study. The option of each pattern may vary in the real situation where the external structure of distillation column may obstruct the location of equipment. Overall projection required two half scanning set, each set required 48 projections and hence 96 projections were implemented. Each position has 7.5 degree pitch and ordering with 1 to 48 clockwise sequential. Position 1 and position 25 are regarding as a dimeter line of the system which located at 270 degree for position 1 and 90 degree for position 25 in circular system.

3.6.1 Simple scanning (Algorithm Pattern 1)

A straight forward acquisition is presented. This pattern provides a moving of all equipment as stated in theoretical of fan beam image projection by means of source and detectors clockwise or counter clockwise rotation. In each rotation step used 7.5 degree pitch movement and 360 degree rotation was assigned and fulfill whole projection by 48 projections per single half. Second half profile can be obtained by rotated remaining position to complete one scanning for 21 detectors; in total projections are 96 moving steps. Table 3.3 shows example of pattern 1 sequences (see appendix 3, A3.1, for full positioning of source and detector). The first half is starting from step 1 to step 48 while second half is starting from step 49 to step 96.

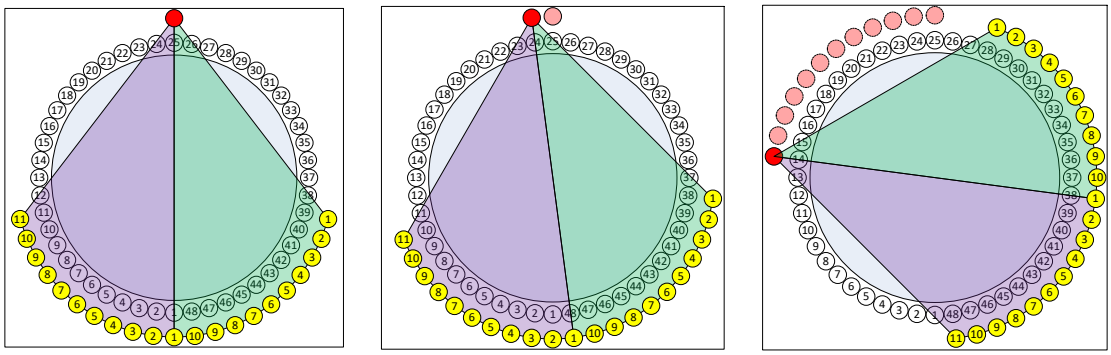

First half arrangement Counter clockwise rotation Counter clockwise rotation

Figure 3.12 Arrangement of source and detectors in algorithm pattern 1

Table 3.3 Example of detectors and source moving sequences of algorithm pattern 1

Step	S	D1	D2	D3	D4	D5	D6	D7	D8	D9	D10	D11
1	25	1	2	3	4	5	6	7	8	9	10	11
2	24	48	1	2	3	4	5	6	7	8	9	10
3	23	47	48	1	2	3	4	5	6	7	8	9
4	22	46	47	48	1	2	3	4	5	6	7	8
5	21	45	46	47	48	1	2	3	4	5	6	7
.	.	.	.	.	.	.	.	.	.	.	.	.
.	.	.	.	.	.	.	.	.	.	.	.	.
.	.	.	.	.	.	.	.	.	.	.	.	.
94	37	5	6	7	8	9	10	11	12	13	3	4
95	26	5	6	7	8	9	10	11	12	2	3	4
96	36	5	6	7	8	9	10	11	12	2	3	4

S : referred Radiation Source

Dx : referred Radiation Detector Number 1-11

3.6.2 One detector moved to end for each single half measurement (Algorithm Pattern 2)

First detector moves to end detector pattern. This pattern provides a movement of single detector from the first position to the end position while source also move in a single step. Such a case, the second detector data shall be tallied to be the first data and so on Figure 3.13. The movement goes along until the required profiles are acquired. Table 3.4 shows example of pattern 2 sequences (see appendix 3, A3.3, for full positioning of source and detector)

(a) First half

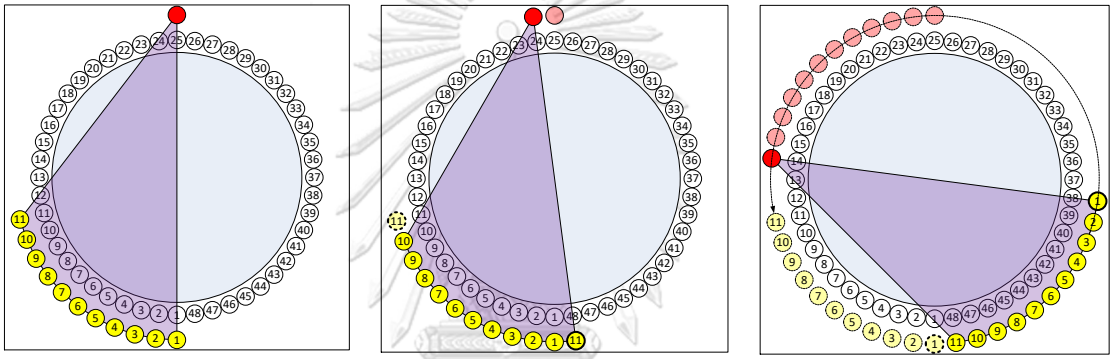

(b) Second half

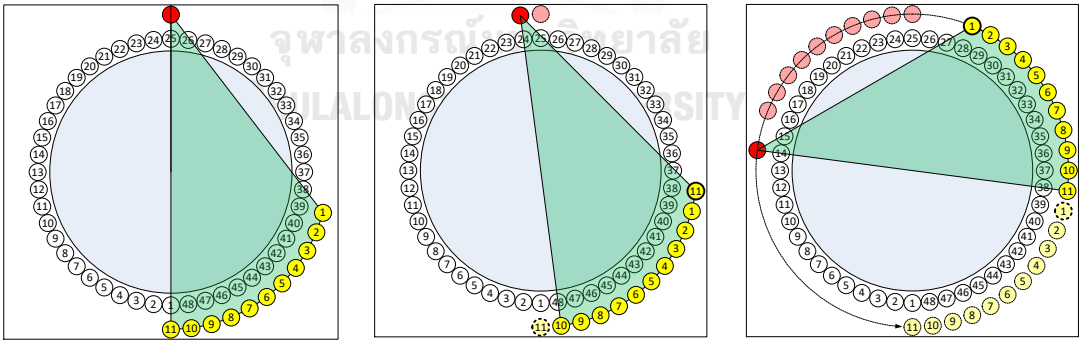

Figure 3.13 Arrangement of source and detectors in algorithm pattern 2

Table 3.4 Example of detectors and source moving sequences of Pattern 2

Step	S	D1	D2	D3	D4	D5	D6	D7	D8	D9	D10	D11
1	25	1	2	3	4	5	6	7	8	9	10	11
2	35	1	2	3	4	5	6	7	8	9	10	11
3	24	1	2	3	4	5	6	7	8	9	10	48
4	34	1	2	3	4	5	6	7	8	9	10	48
5	23	1	2	3	4	5	6	7	8	9	47	48
.	.	.	.	.	.	.	.	.	.	.	.	.
.	.	.	.	.	.	.	.	.	.	.	.	.
.	.	.	.	.	.	.	.	.	.	.	.	.
94	37	5	6	7	8	9	10	11	12	13	3	4
95	26	5	6	7	8	9	10	11	12	2	3	4
96	36	5	6	7	8	9	10	11	12	2	3	4

S : referred Radiation Source

Dx : referred Radiation Detector Number 1-11

3.6.3 One detector moved to end for double half measurement (Algorithm Pattern 3)

A first detector moves to end detector and two steps source movement. This pattern provides a movement of single detector from the first position to the end position like Pattern 2 but the source is positioned two times until two profiles are acquired (see Figure 3.14). The movement goes along until the required profiles are achieved. Table 3.5 shows example of pattern 2 sequences (see appendix 3, A3.5, for full positioning of source and detector)

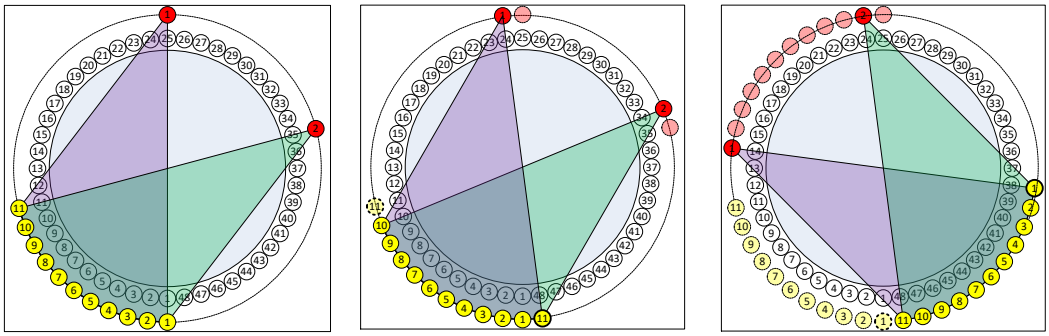

Figure 3.14 Arrangement of source and detectors in algorithm pattern 3

Table 3.5 Example of detectors and source moving sequences of Pattern 3

Step	S	D1	D2	D3	D4	D5	D6	D7	D8	D9	D10	D11
1	25	1	2	3	4	5	6	7	8	9	10	11
2	35	1	2	3	4	5	6	7	8	9	10	11
3	24	1	2	3	4	5	6	7	8	9	10	48
4	34	1	2	3	4	5	6	7	8	9	10	48
5	23	1	2	3	4	5	6	7	8	9	47	48
.	.	.	.	.	.	.	.	.	.	.	.	.
.	.	.	.	.	.	.	.	.	.	.	.	.
.	.	.	.	.	.	.	.	.	.	.	.	.
94	37	5	6	7	8	9	10	11	12	13	3	4
95	26	5	6	7	8	9	10	11	12	2	3	4
96	36	5	6	7	8	9	10	11	12	2	3	4

S : referred Radiation Source

Dx : referred Radiation Detector Number 1-11

Table 3.6 compares the scanning operation time in laboratory experiment for each algorithm pattern. The fastest scanning drew to algorithm pattern 1 since it

moves by rotation table, thus all detectors and source are moved together by rotational wheel such that the moving time is depending on only 96 steps as per source movement. Scanning operation time of algorithm pattern 3 seems to be compromised between pattern 1 and pattern 2. To extend the operation time toward the scanning operation in field work, Table 3.7 estimated the scanning time for full operation. The installation time is based on the installation that was done in conventional scanning since the equipment are the same. However, time to move radiation source and detector may vary upon the complexity of external structure. Estimated time in Table 3.7 is in terms of optimistic point of view.

Table 3.6 Comparison of scanning operation time for each pattern in laboratory work

Estimation of scanning operation for laboratory experiments			
Activities	**Pattern 1**	**Pattern 2**	**Pattern 3**
- **Detectors movement (steps per 360^{o})**	0	96 steps	48 steps
- **Source movement (steps per 360^{o})**	96 steps	96 steps	96 steps
- **Measurement time (10 sec per projection)**	960 sec	960 sec	960 sec
- **Time to move detector (5 sec per step)**	0	480 sec	240 sec
- **Time to move source (5 sec per step)**	480 sec	480 sec	480 sec
- **Total operating time (sec)**	1440	1920	1680
(minutes)	24	32	28

Table 3.7 Comparison of operating duration for each pattern

Estimation of operation time for field work			
Activities	**Pattern 1**	**Pattern 2**	**Pattern 3**
- **Equipment installation (min)**	90 min	90 min	90 min
- **Detectors movement (steps per 360^{o})**	0	96	48
- **Source movement (steps per 360^{o})**	96 steps	96 steps	96 steps
- **Measurement time (12 sec per projection)**	19.2 min	19.2 min	19.2 min
- **Time to move detector (2 min per step)**	0	192 min	96 min
- **Time to move source (2 min per step)**	192 min	192 min	192 min
- **Total operating time (min)**	301.2 min	403.2 min	397.2 min
(Hours)	5 hours	8.2 hours	6.6 hours

CHAPTER 4

RESULTS

In this chapter, the methodologies described in Chapter 3 were applied to the laboratory model. In section 4.1, the shows the calibration results. Section 4.2 shows simulation and experimental results on four different diameter metallic pipes in order to compare the different between simulation (best case) and experiments. Measurements of pipe's diameter through reconstructed image are also presented. Section 4.3 demonstrates an experiment on the packed bed structure by assume that scale was accumulated and deposited in the packed bed component. Mass of scale was varied from 100 grams, 200 grams and 400 grams in order to see the detectability of developed technique. Section 4.4, demonstration of six gaseous riser metal pipes detection. The structure was simplified from the one that has been used in distillation column to demonstrate that the technique is applicable to detect a structure. Section 4.5, experiment on broken one gaseous riser pipes to determine the detectability if some broken is occurred. Section 4.6 and 4.7 experiment on broken nozzle damaged gaseous riser. A diagram in Figure 4.1 describes overall processes of experiments. Calibration of system is mandatory depending on the source used in the experiment.

Calibration of system is required to harmonize the gain and offset of detectors as described in Chapter 3. After calibration, selection of acquisition technique is based on the external structure of the distillation column to be inspected. The corresponding pattern must be input to the software in order to specify the shuffling of data to the format which is applicable to reconstruct by software. Reconstructed image is presented in mode of positive picture, i.e. most absorbing part shall be zero gray value whereas least absorbing part shall be 256 gray value levels.

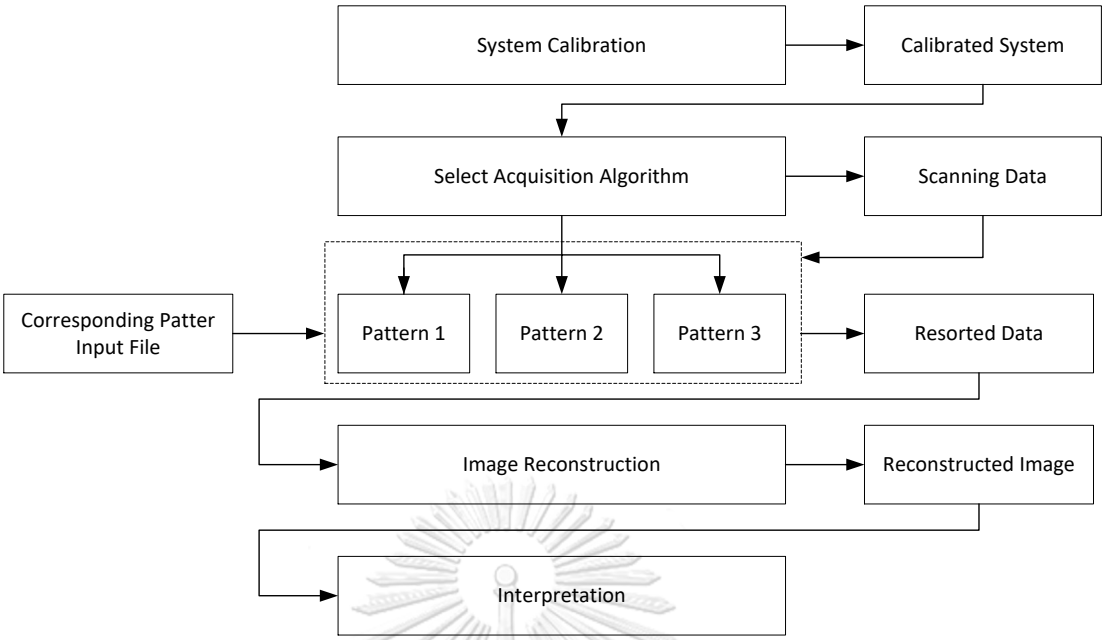

Figure 4.1 Overall processes to be used in experiment.

4.1 Calibration of measurement system

A well calibrated system always produces a good measurement. All detectors must be calibrated until a measurement of all 11 detectors is representing as the same as using single detector, this is the main idea.

4.1.1 Before calibration

The testing of detector's sensitivity would be done by first using one detector and move to the location where all detectors will be placed, see Figure 4.2 for first step calibration with one detector. After measured data at position one, move detector to position two and record measured data again. Repeat the detector movement and recording measured data until it reaches 21 positions as required.

Second step, place all detectors in their positions and measured data for first and second half set. Each set measure the profile of transmitted gamma intensity and plots both sets in one graph, see Figure 4.3 setting the second step calibration with one detector .

Figure 4.4 shows a plot of using only one detector moved in all 21 positions compared to the 11 detectors with two half sets.

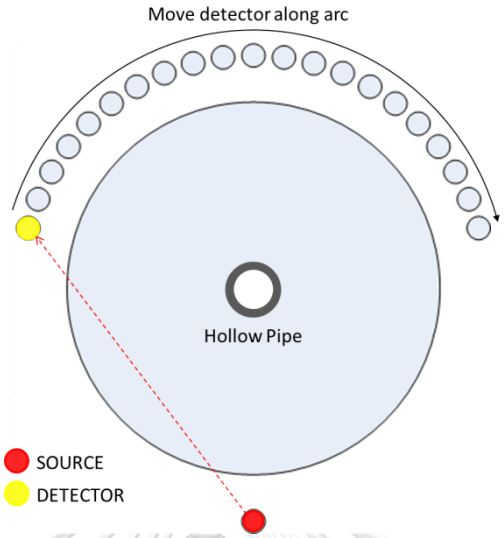

Figure 4.2 Make a profile using one detector

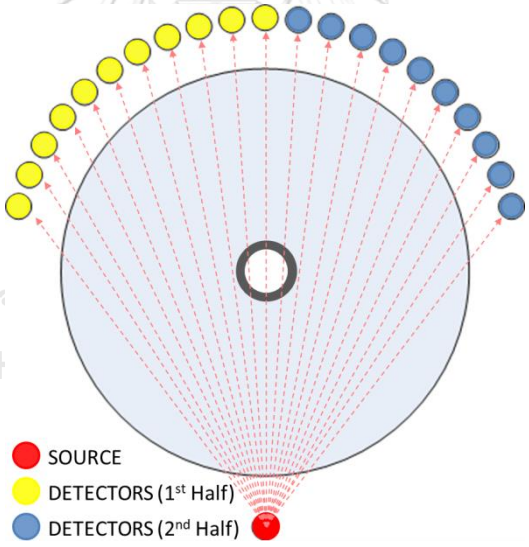

Figure 4.3 Make a profile using 11 detectors for 2 half data sets

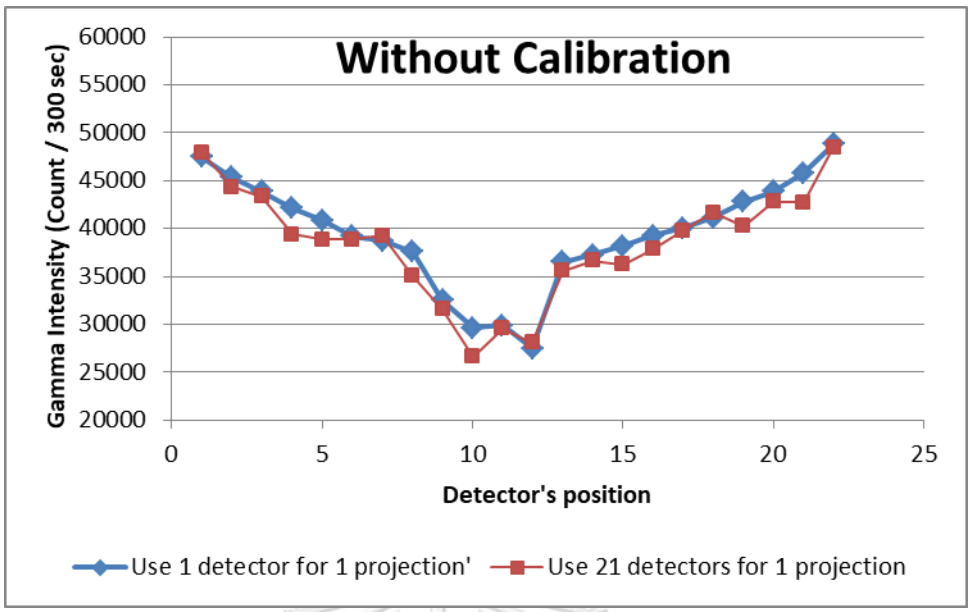

Figure 4.4 Profile comparison before calibration

4.1.2 After calibration

The system calibration experiment is quite tedious since it required several measurement and judgement on the measured data as described in 3.1.1. Detector which measured smallest count was selected as a reference detector. However, it was tested to ensure the function of detector by placing in the radiation field and notice the sensitivity if it sensed the radiation in different positions.

After calibration, all detectors were tested again as in 4.1.1 and compare the plotting as illustrated in Figure 4.5.

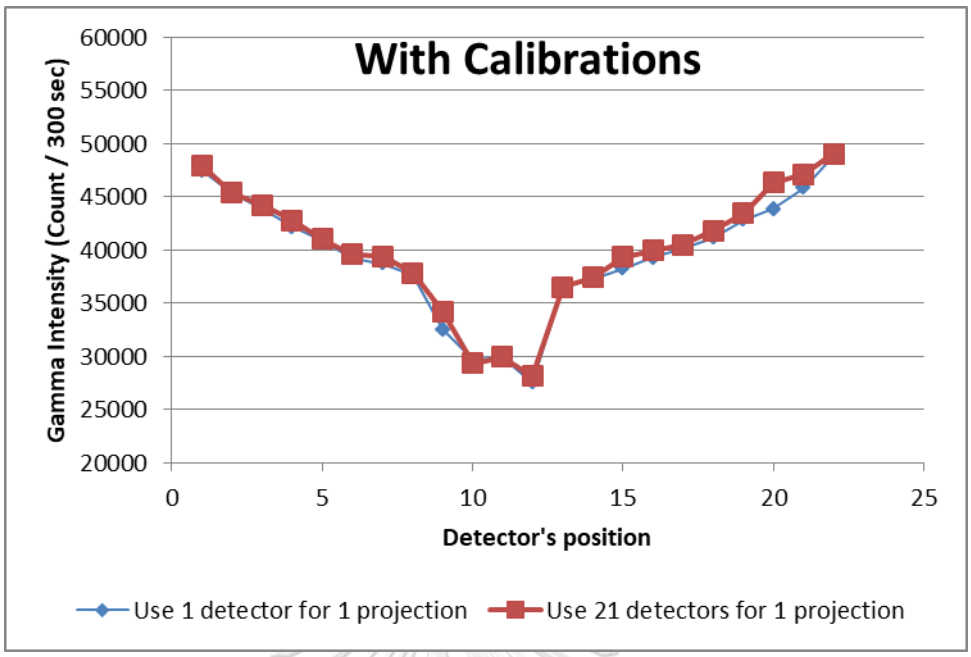

Figure 4.5 Profile comparison before calibration

The selection of acquisition algorithm depends on external structure of the column. Selected pattern was used for post processing to manage all data into format that suit for reconstruction. Reconstruction and interpretation are final process.

4.2 Experiment on sensitivity study via four metallic pipes

This experiment was done in order to compare the results of each pattern as well as comparison between simulation and experimental results. Example of MCNP input file is given in Appendix I for Projection number 1.

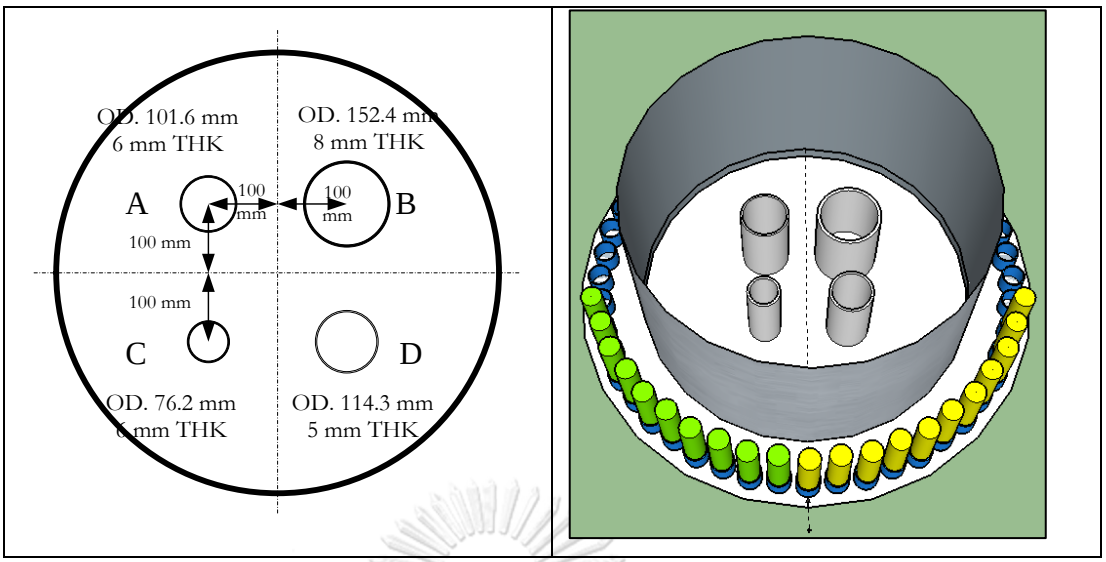

Figure 4.6 Experiment phantom of four pipes

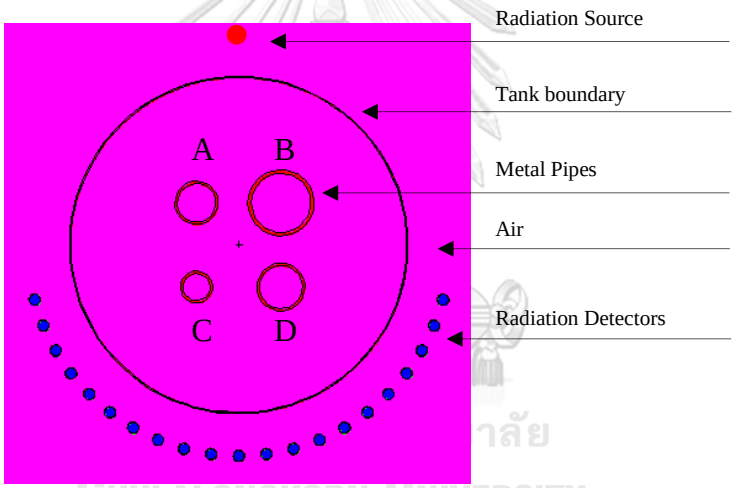

Figure 4.7 System configuration generated by MCNP computer code

As setting up in simulation in section 3.2, four different diameter metallic pipes were installed inside the top opened tank. Each pipe is located 100 mm measured from center of tank as indicated in Figure 4.6. NaI detectors were located around the tank inside PVC blocks. Three patterns were applied in data acquisition process in order to compare the different.

Reconstructed CT image from simulated data case of fine detectors, coarse detectors case and MCNPx are shown in Figure 4.8, Figure 4.10 and Figure 4.12, respectively. For experiment, reconstructed CT image using algorithm Pattern 1, Pattern 2 and Pattern 3 scanning results are illustrated in, Figure 4.14, Figure 4.15,

and Figure 4.16, respectively. Plotting of gray value profile at line pixel number 240 and line pixel number 360 of all scanning data are illustrated in Figure 4.17 and Figure 4.18, respectively. As a results, all line pixel profiles are consistent to each other which means all pattern has no significantly different in reconstructed image quality. To estimate the pipe size, pixel calibration is used by keeping “pipe a” as a reference pipe and calibration factor is used for measure other pipe’s size. Table 2, indicates an estimation of pipe’s size. The error of estimation vs true size is determined by Eq. 4.1.

$$\%error = \left| \frac{Actual\ \ Size - Measured\ \ Size}{Actual\ \ Size} \right| \times 100 \qquad \text{Eq. 4.1}$$

4.2.1 Simulation results

4.2.1.1 CT image from the simulation module with 101 detectors

This simulation performed a projection of phantom and its structure setting is shown in Figure 4.6. Instead of using 21 detectors, the best case simulation used very fine 101 small detectors (small detector) placed at same panned angle of 75 degrees. Simulation result shows in Figure 4.8 reveals that if the detector is small and fine enough back projected results became clear until thickness of pipes can be observed.

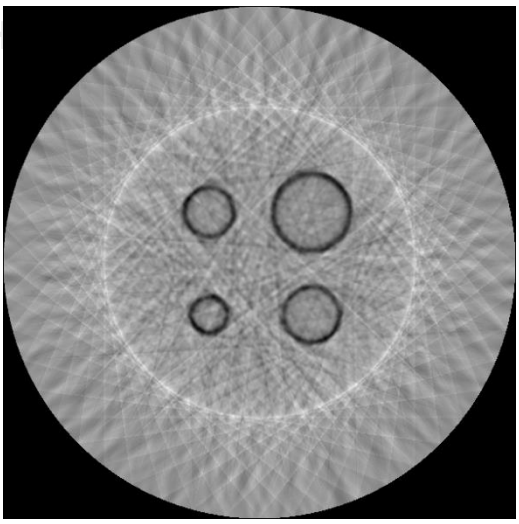

Figure 4.8 Reconstructed image from simulation data using 101 detectors

Figure 4.9 shows a plotting of normalized data of projected profile number 1 from simulation with 101 detectors using simulation module. The profile provides a satisfactory detail of pipe diameter as well as their thickness.

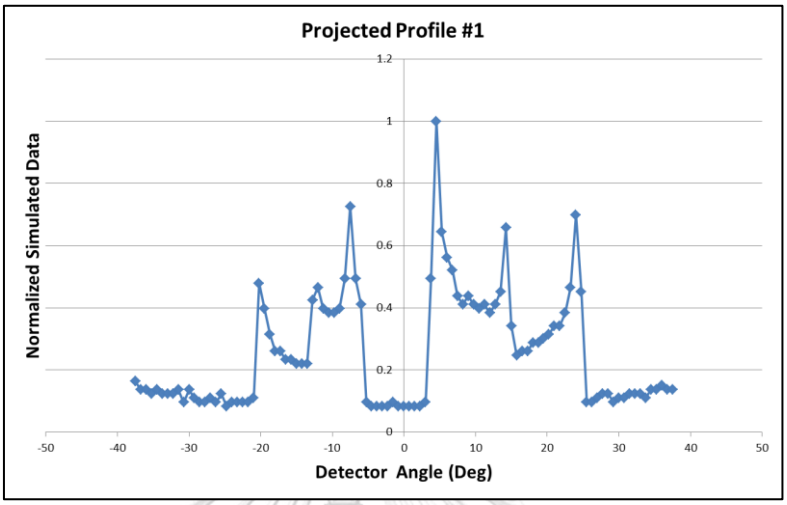

Figure 4.9 Plot of projected profile number 1 data from simulation with 101 detectors case.

4.2.1.2 CT image from the simulation module with 21 detectors

Likewise the previous section, this simulation performed a simulation using 21 detectors, and panned angle of 75 degrees. Simulation result shows in Figure 4.10 reveals that if the detector is small and fine enough back projected results became clear until thickness of pipes can be observed.

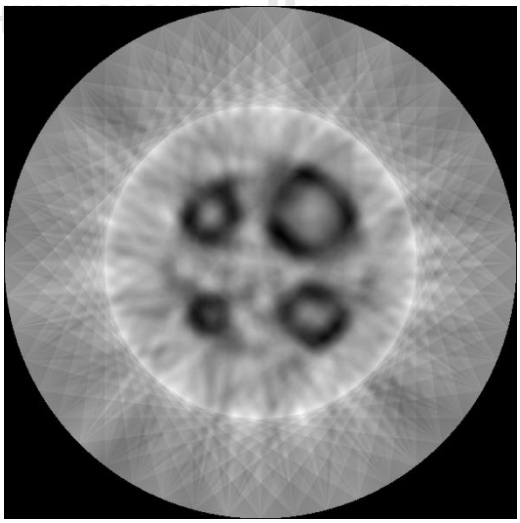

Figure 4.10 Reconstructed image from simulation data using 21 detectors

Figure 4.11 compares a plotting of normalized data of projected profile number 1 from simulation with 21 detectors and 101 detectors using simulation module.

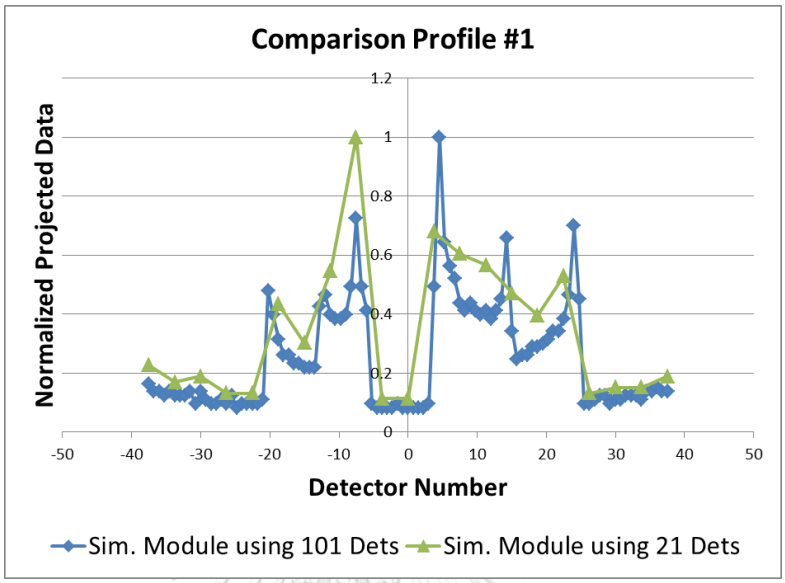

Figure 4.11 Comparison of projected profile number 1 data between simulation with 101 detectors and 21 detectors case.

4.2.1.2 CT image from the simulated data using MCNPx

Figure 4.12 shows the reconstructed image from projected data using MCNPx computer code. Plotting of projected profile number 1 compared to two previous cases is shown in Figure 4.13. Obviously, the projected result from MCNPx provided profile is similar to the projected result from simulation module considering to 21 detectors case. Comparison between the CT image from simulation using MCNPx and using simulation module are comparable with non-significantly different from each other.

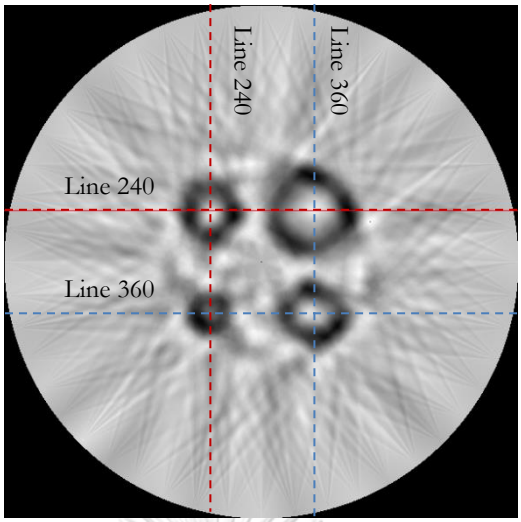

Figure 4.12 Reconstructed image from MCNPx simulation data

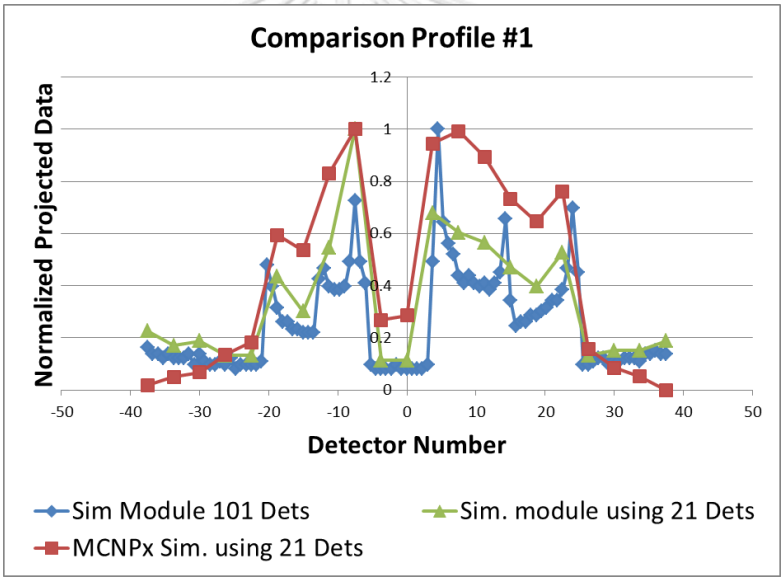

Figure 4.13 Comparison of projected profile number 1 data between simulation with 101 detectors, 21 detectors cases and 21 detectors case from MCNPx.

4.2.2 Experimental results

The developed pattern as described in Chapter 3 composed of algorithm Pattern 1, Pattern 2 and Pattern 3 are using in experiment in this section. Four metal pipes were locating at the same position as simulation cases in order to compare the different in results. Line profile plotting at pixel number 240 and number 360 of reconstructed images will be used as key comparison with the simulation case.

Reconstructed CT image of from experiment which applied algorithm Pattern 1, Pattern 2 and Pattern 3 are showed in Figure 4.14, Figure 4.15 and Figure 4.16, respectively.

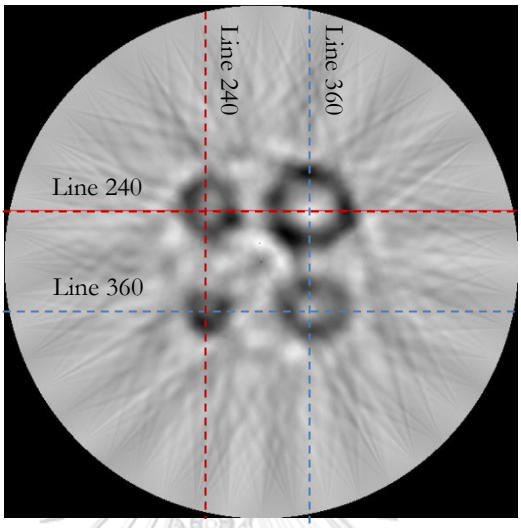

Figure 4.14 Reconstructed image from algorithm Pattern 1 data

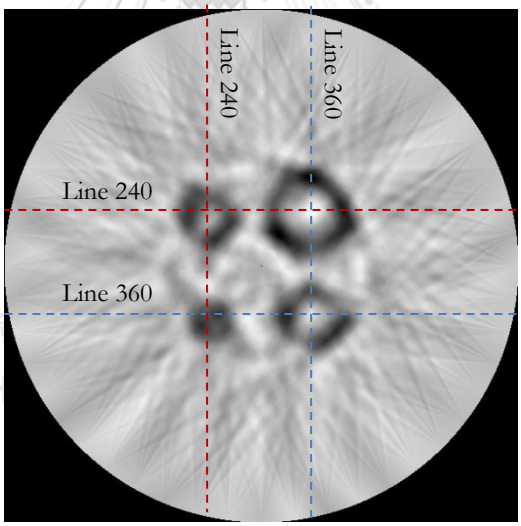

Figure 4.15 Reconstructed image from algorithm Pattern 2 data

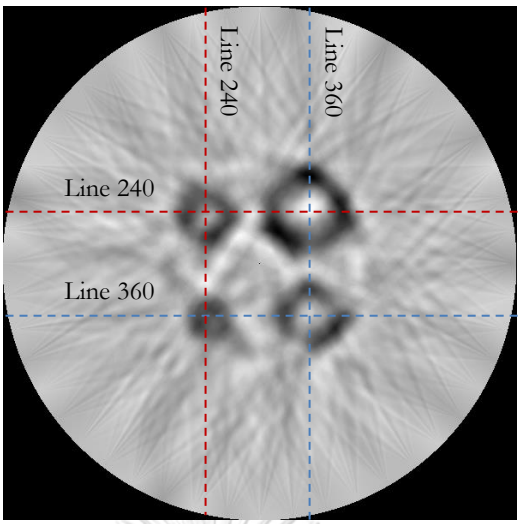

Figure 4.16 Reconstructed image from algorithm Pattern 3 data

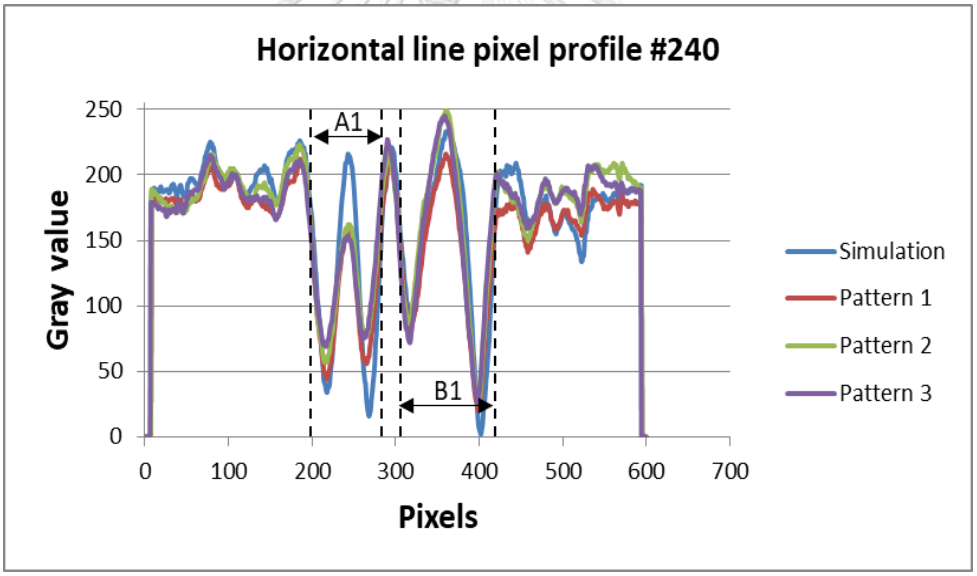

Figure 4.17 Gray value profiles comparison of horizontal line pixel number 240

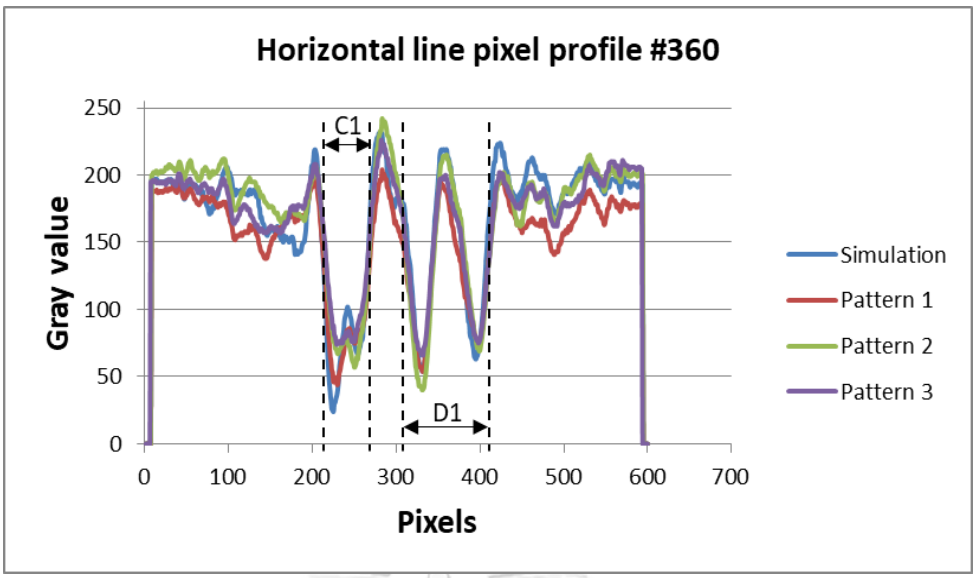

Figure 4.18 Gray value profiles comparison of horizontal line pixel number 360

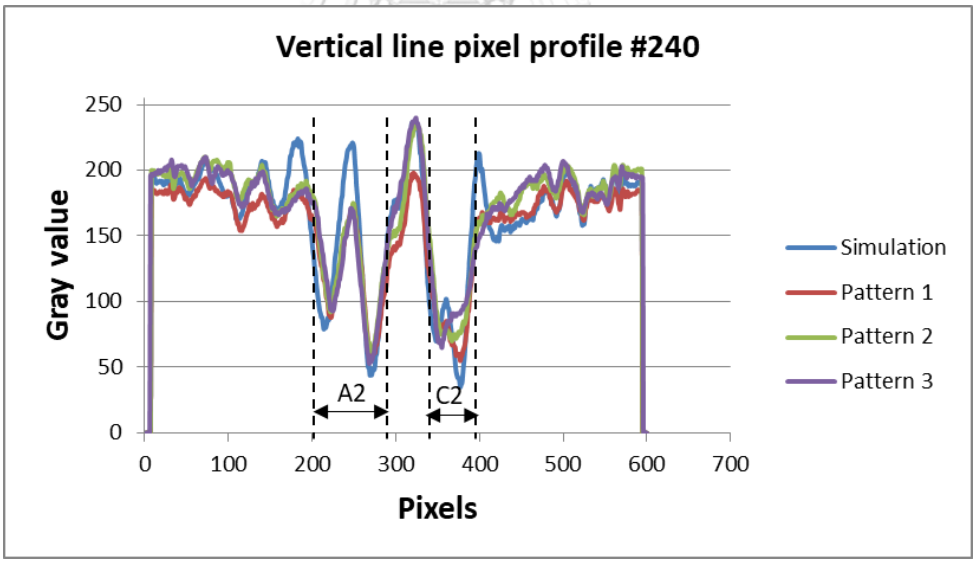

Figure 4.19 Gray value profiles comparison of vertical line pixel number 240

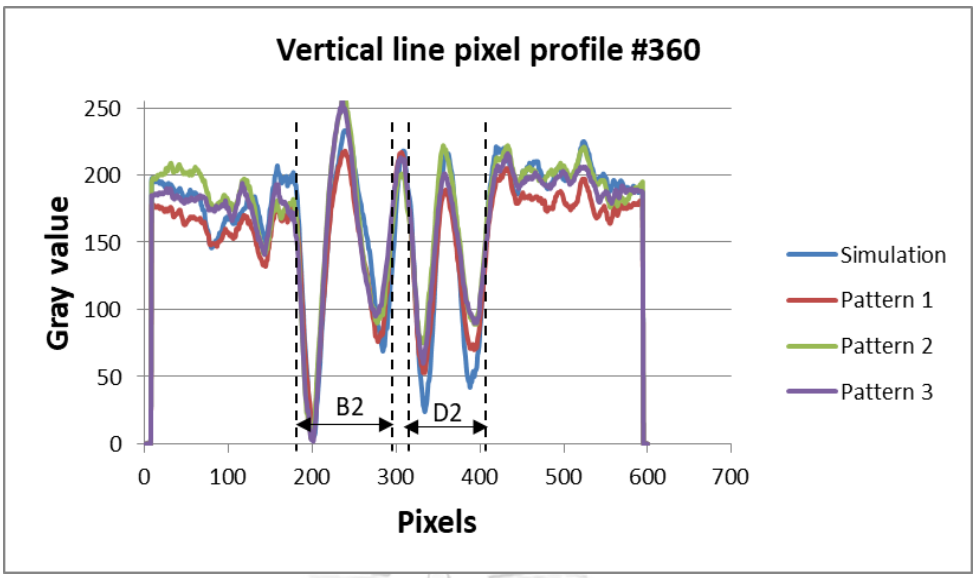

Figure 4.20 Gray value profiles comparison of vertical line pixel number 360

Marks a, b, c and d are a width represent a diameter of pipes to be estimated. In pixel calibration pipe “a” (diameter of 101.6 mm) is regarded as a reference size to be used for other sizing. Table 4.1 shows estimation of pipe diameter where Px-1 and Px-2 are pixels that read out from graph at dotted line location.

Table 4.1 Estimation of Pipe’s diameter using pixel calibration in horizontal direction

Pipe	Px-1 (pixels)	Px-2 (pixels)	Px2 – Px1 (pixels)	Estimated Size (mm)	Actual Size (mm)	error (%)
A1*	201	274	73	101.6	101.6	0
B1	303	412	109	151.7	152.4	0.5
C1	214	268	54	66.91	76.2	12.2
D1	312	413	101	125.1	114.3	9.5
A2*	209	290	81	101.6	101.6	0
B1	180	291	111	139.2	152.4	8.6

Pipe	Px-1 (pixels)	Px-2 (pixels)	Px2 – Px1 (pixels)	Estimated Size (mm)	Actual Size (mm)	error (%)
C1	339	396	57	71.5	76.2	6.2
D1	319	407	88	110.4	114.3	3.4

*Reference pipe

The results from experiment for all Patterns showed good agreement compared to the simulation. However, the percentage error in horizontal line pixel estimation of pipe C seems to be bigger than those observed in simulation. In vertical line pixel measurement, results show the biggest error occurred at pipe B. The average of pipe's size between horizontal estimation and vertical estimation are illustrated in Table 4.2 Obviously, the percentage error of measurements are compromised.

Comparison of reconstructed image between simulation result and results from experiment showed a distortion. However, the location of all pipes in reconstructed image of all algorithms is consistent to the real installation.

Table 4.2 Estimation of Pipe's diameter using pixel calibration in vertical direction

Pipe	Hor. Estimation (mm)	Ver. Estimation (mm)	Average Size (mm)	Actual Size (mm)	error (%)
A*	101.6	101.6	101.6	101.6	0
B	151.7	139.2	145.45	152.4	4.6
C	66.91	71.5	69.205	76.2	9.2
D	125.1	110.4	117.75	114.3	3.0

4.3 Experiment on fouling detection in simulated packed bed structure

The radiographic image of material represented packed bed component is illustrated in Figure 4.21. It made up of metal with a high porosity to increase a contact between two phases (gaseous and liquid) in chemical or similar process. In the production process, fouling can be occur inside the packed structure due to the solidification of liquid passed through the packed and caused a non-uniformly distribution of liquid and gaseous in the process. This fouling could be accumulated and propagated cover a whole cross-section until the distillation become malfunction and cause the product out of specification.

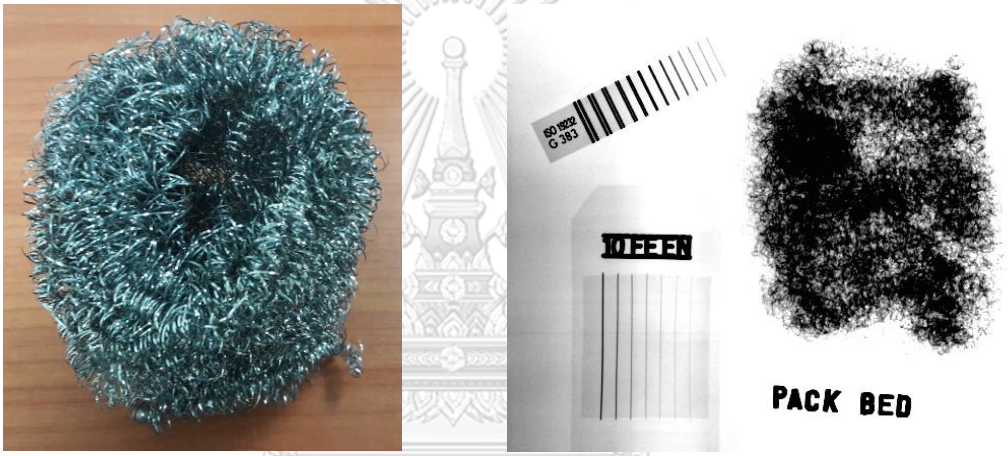

Figure 4.21 radiographic image of simulated packed bed structure

The components are randomly packed and installed into the column as shown in Figure 4.22.

Figure 4.22 Arrangement of simulated packed bed structure

The density and volume of packed bed component is approximately 35 kg/m^3 and 0.0033 m^3, respectively. The density of scale is 1442 kg/m^3, approximately, was assumed to deposit inside the porous of packed bed. In this experiment, scale content

of 10%-wt, 20%-wt and 40%-wt of total packed bed weight were investigated. Element compositions of scale were examined using X-ray Fluorescence (XRF) technique and illustrated in Table 4.3.

Table 4.3 Element composition of scale

Formula	Concentration
Fe_2O_3	2.81%
P_2O_5	0.31%
CaO	0.20%
SiO_2	0.09%
ZnO	0.05%
CuO	0.04%

4.3.1 No scale present in the packed bed.

(a) (b)

Figure 4.23 (a) Arrangement of simulated packed bed structure without scale deposited and (b) reconstructed image of structure without scale case.

In case of no scale deposit inside packed bed component, reconstructed image showed density distribution in cross-section was well established.

4.3.2 10%-wt of scale deposited in the packed bed

Content of scale deposited in this experiment was 10 %-wt (100 grams, approximately). Though it was not much clear that the location of dark spot in reconstructed image is inferred to the location where scale was depositing. However, compare to the case where no scale deposited, the darkest spot is only one position that different from the no scale case.

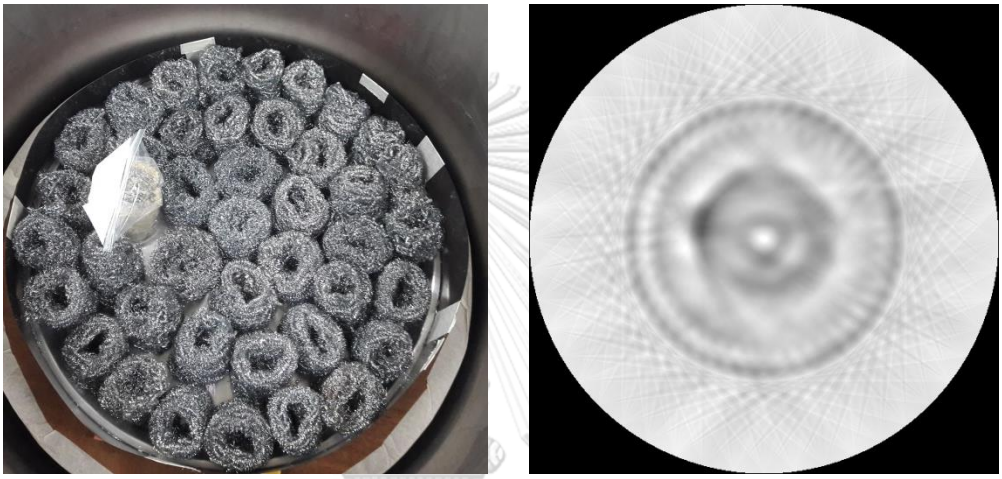

(a) (b)

Figure 4.24 (a) Arrangement of simulated packed bed structure with 10 %-wt scale deposited and (b) reconstructed image of 10 %-wt case.

4.3.3 20%-wt of scale deposited in the packed bed

Content of scale deposited in this experiment was 20 %-wt (200 grams, approximately). The darkest spot in the reconstructed image represented the location of deposited scale which is clearer compared to those presented in case of 10 %-wt deposited scale.

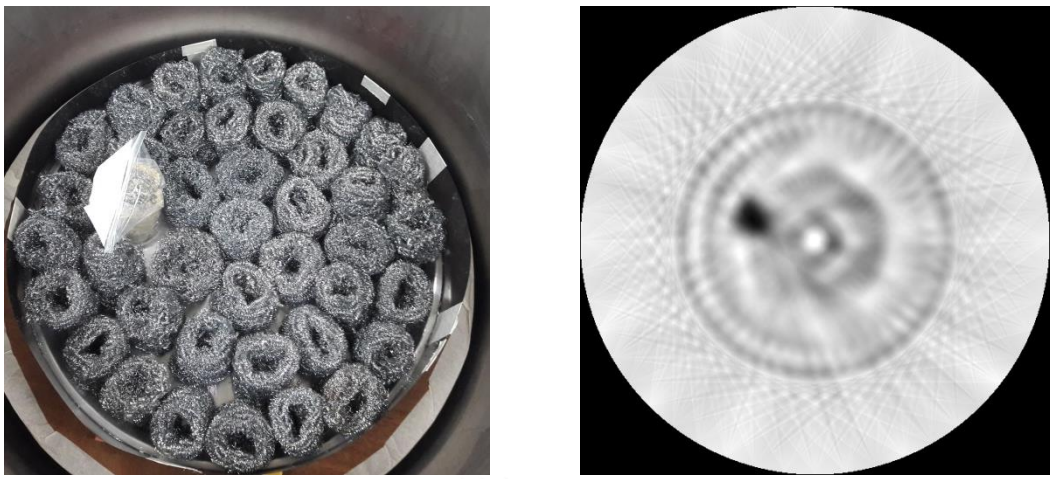

(a) (b)

Figure 4.25 (a) Arrangement of simulated packed bed structure with 20 %-wt scale deposited and (b) reconstructed image of 20 %-wt case.

4.3.4 40%-wt of scale deposited in the packed bed

Content of scale deposited in this experiment was 40 %-wt (400 grams, approximately). The darkest spot in the reconstructed image represented the location of deposited scale which is clearer compared to those presented in two cases above. The density of bigger part of scale provided darker gray value since scale doesn't contain packed bed component, thus higher density of scale itself absorbed more gamma ray compared to other area.

(a) (b)

Figure 4.26 (a) Arrangement of simulated packed bed structure with 40 %-wt scale deposited and (b) reconstructed image of 40 %-wt case.

4.4 Experiment on vertical pipes inspection

This experiment simulates the gaseous riser pipes which commonly installed inside the distillation column. Though the pipe size in this experiment are smaller than installed in real distillation column. However, the idea, methods and especially data acquisition technique, Pattern 3, developed in this dissertation was used.

4.4.1 Well installed gaseous riser pipes

Figure 4.27 Experiment phantom six riser pipes

Figure 4.28 (a) shows reconstructed image projected onto 21 detectors. The reconstructed image was clearly showed the position of six riser pipes when it was normally installed. Figure 4.28 (b) shows the comparison between pixel profile line #240 and pixel profile line #360. Though a distortion of image through the pixel profile was observed since both plotting were not completely superimposed onto each other, their trends provided good agreement to each other.

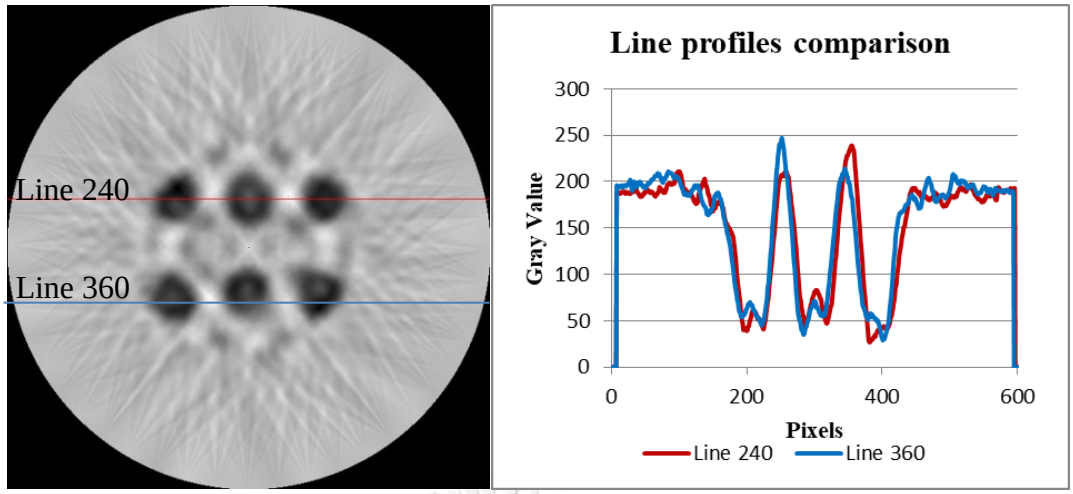

(a) (b)

Figure 4.28 (a) reconstructed image of normal installed pipes and (b) plotting profiles at pixel line #240 compared to pixel line #360.

4.4.2 One riser pipes was damaged and missed from position

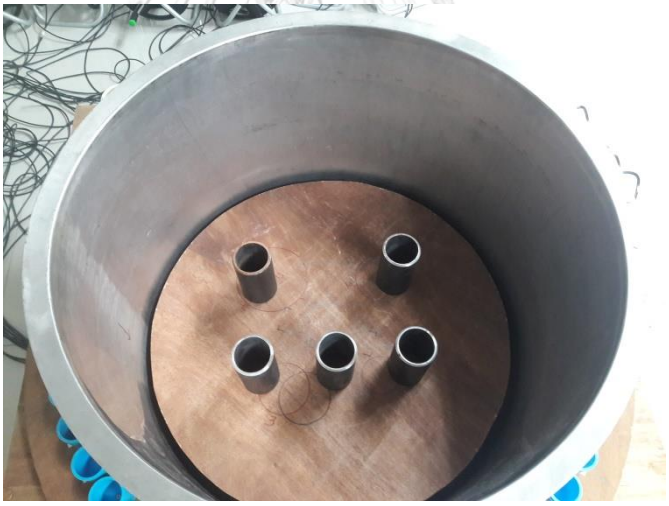

Figure 4.29 Experiment phantom broken pipe with flange

Figure 4.30 (a) shows reconstructed image of one missed pipe case. The image was clearly showed the location where pipe was missing from position. Figure 4.30 (b) shows the comparison between pixel profile line #240 and pixel profile line #360. Profiles also clearly showed that one pipe was missing from its position.

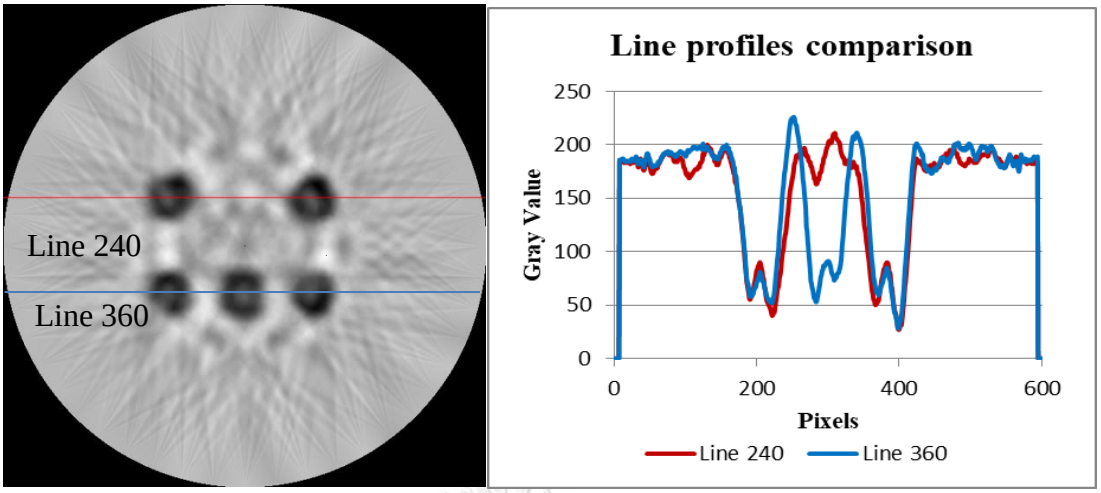

(a) (b)

Figure 4.30 (a) reconstructed image of one missed pipes and (b) plotting profiles at pixel line #240 compared to pixel line #360 of studied case 2.

4.4.3 Broken nozzle with flange

Figure 4.31 Experiment phantom broken pipe with flange

This experiment tried to determine if the pipe is broken and dropped down. The scanning result was not intended to determine the corrosion or welding of pipe. Instead, it expected to see the periphery of broken pipe. Reconstructed image shows good agreement of L-shape pipe with flange. In real situation, this case is rarely to be detected since conventional scanning could not determine the exact location or elevation to be scanned. Anyhow, this experiment demonstrate that if it is possible to

perform the scanning at the location where broken pipe is existing, it would be also possible to reconstruct a satisfactory image as well.

4.4.4 Broken nozzle drop down and damage riser pipe

This case assumed that a nozzle with pipe flange was broken and fell down to damage one of riser pipe and obstruct in between the riser pipes. Figure 4.33 (a) shows reconstructed image of case 3. The image was not clear to show the damaged nozzle pipe with flange since inside the nozzle was empty, thus gamma ray absorption in that area was low, however it clearly showed the abnormality occurred in the area of pipe riser. Figure 4.33 (b) shows the comparison between pixel profile line #240 and pixel profile line #360. Profiles also clearly showed the problem occurred at location of riser pipe in the middle of top row compared to the Figure 4.28 which normal riser pipes were installed. To be slightly bias, drawing of broken nozzle on reconstructed image is illustrated as a red shape in Figure 4.33 (a).

Figure 4.32 Experiment phantom broken pipe dropped down and damage six riser pipes

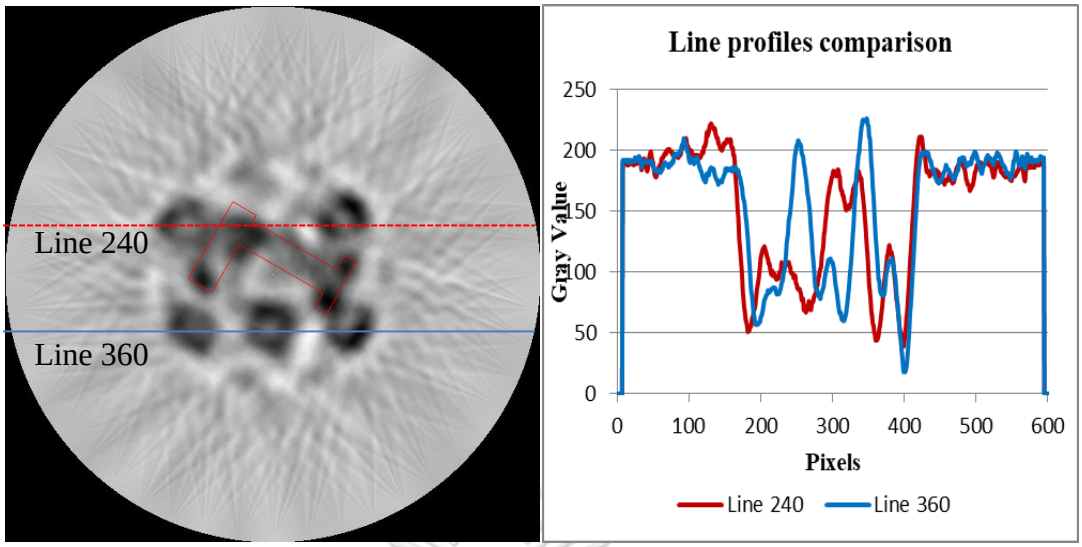

(a) (b)

Figure 4.33 (a) reconstructed image of one missed pipes and (b) plotting profiles at pixel line #240 compared to pixel line #360 of studied case 4.4.4.

4.5 Discussion

According to data acquired from developed technique, the reconstructed images showed good agreement with the phantom represent the distillation column. Simulation is an important assisting tool for scanning since it provides trends of projection profile in each single step that can be used as a guide line during a scanning. It can be regarded as the best case because the result from simulation is closed to the theory. Hence, reconstructed image also has the best quality as well. Scanning of four pipes in section 4.2 using designed patterns showed consistent result compared to the simulation. The estimation of pipe's diameter from pixel calibration provided an error at maximum of 12.2 percent by using horizontal measurement. Obviously, average value between horizontal and vertical measurement compromised the error to less than 10%. This pipe diameter estimation was not an exact value since the resolution of image was not well enough. However, at the error of 10% of smallest pipe indicated that the developed data acquisition techniques were well established to identify the integrity of pipe at diameter of 76.2 mm.

The experiment on fouling detection in section 4.3 showed that if there is a fouling in the packed bed, the density distribution would not be homogenous. To perform the investigation of fouling in packed bed, the scanning of normal packed bed

is necessary for comparison. Without prior knowledge of density distribution when packed bed is operating in normal situation, fouling detection becomes complicate job. Notice the simulated fouling in packed bed component of 10%-wt, reconstructed image showed slightly different density compared to the no fouling. The cases are different for 20%-wt and 40%-wt, reconstructed images clearly showed location of fouling. If the fouling has propagated in wide area along cross-section of column, the liquid – gas channeling could be observed. Consequently, the distillation efficiency is reduced and effects directly to the end products. At the middle of reconstructed image of all cases (including no fouling case) there was a white round circle presented in all images. This could be a reason from vertical alignment of equipment that might not be at center of elevation in vicinity of suspected location.

The experiments on data acquisition technique were extended to the inspection of pipe's structure which installed inside the vessel as indicated in section 4.4 and section 4.4.2. In many cases, pipe's structure could be damaged by malfunction of process during in services. Reconstructed image of pipe structure inspection showed a good agreement both when the pipe structure is normal and abnormal cases. The missing pipe case is normal and easy to be inspected if individual pipe is arranged in single row which can be inspected using conventional gamma scanning technique. Contradictory, if pipes are arranged in array-like, scanning result conventional gamma scanning technique becomes confusing since normal pipe could be super imposed onto the abnormal pipe that make slightly different in absorption. The developed technique is helpful to clearly identify the location of missing pipe.

The problem becomes more complicate if it caused by another broken pipe which has fallen down and damages the structure. It is interesting to investigate that if the broken nozzle has another shape, this developed technique is still valid or not. Scanning results and reconstructed image of L-shape pipe with flange, as indicated in section 4.4.3, showed that it is possible to inspect the pipe in horizontal installation. In section 4.4.4, broken L-shape nozzle was assumed to drop down and broke another pipe structure. It was obviously showed that missing pipe from location could be

observed but not for L-shape pipe. Without prior knowledge of L-shape pipe, it was not possible to identify the foreign object that damages the structure.

CHAPTER 5

CONCLUSION

5.1 Discussion

The main objective of this dissertation is to develop the data acquisition technique for computed tomography of the simplified distillation column model as used in the petroleum and petrochemical plants. Computed tomography technique was selected because its advantages in data interpretation by cross-section image. The technique is based on gamma ray transmission technique which generated from gamma radiation source (Cs-137) passed through and absorbed in the medium and reaches to the radiation detector at the end. In this case, fan beam algorithm was selected to reduce scanning time. The number of detector directly affected to the resolution of image, i.e. high resolution required many detectors and that means high cost of measurement system. In this dissertation, number of detectors was limited to 11 detectors. Thus, data acquisition technique is required in order to obtain satisfied image resolution.

The data acquisition technique was designed in terms of scanning patterns based on complexity of environment nearby scanning location. Design of scanning pattern 1 aimed to perform the scanning as straight forward operation as fan beam algorithm, i.e. detectors are attached together as an line array and simultaneously rotate with radiation source in simple way as stated in fan beam algorithm. The difficulty to apply pattern 1 in scanning is the external structure could obstruct the operation until rotation of detectors and source is not possible. Thus, this technique is suit for scanning of object when it is standing in the structure and the area nearby must not obstruct the rotation.

On the other hands, if the external structure is an issue to perform scanning, design of scanning pattern 2 and pattern 3 might solve this problem. Pattern 2 was developed to avoid the difficulty of rotational system. An algorithm allowed the movement of radiation detectors from the location where it is available, for instant,

the detector can be moved at the top of column or plat form above using ropes or sling and move it from beginning position to the assigned position. In such a case, scanning position could be performed at any elevation.

The pattern 3 algorithm was modified from pattern 2 for shorten the operation time. In pattern 2, detectors and source moved together in each single step whereas in pattern 3 one movement of detector can be used to two position of source. Shorten the operation time in pattern 3 is trade off to the data re-shuffling and positioning of source that could confuse the operator. This scanning technique was not limited to the column diameter that used in this dissertation, for larger column diameter the technique is still valid but need more steps than specified in this paper, i.e. combination of 21 detectors per one projection might not be enough and must be increased in odd number such as 23, 25, 27, etc. Pattern to be used in detectors data re-shuffling must be properly designate to the reconstruction software.

The flexibilities of developed data acquisition technique is useful to be applied in real operation in petrochemical and petroleum plant because it allows the operator to perform scanning in any location of suspicious, provided that the equipment is able to access to those location without complicate rotation mechanical installation. The results from developed technique also shows the advantages compared to conventional scanning which provided only the results in terms of x-y graph while this developed technique provides the result in terms of image at location of interest. By these advantages, the process engineer can explicitly understand the phenomena that are happening inside the column and solve problems in the proper way.

5.2 Recommendations and Future Research

5.2.1 Following recommendations propose the further development to increase the capability of this technique

5.2.2 A study of PVC effects to the detectors, since the radiation source used in this dissertation was Cs-137 and use PVC as a detector holder. PVC also absorbed low energy as well scattered low energy photon. If the cut off energy was not properly

adjusted, noise generated in Compton scattering region would interfere the measurement.

5.2.3 Improvement by using aluminum as a detector holder might be more suitable.

5.2.4 The scanning in this dissertation was only single layer, i.e. at a certain elevation. It is possible to extend the capability of technique by perform a scanning in multi-layer (varied elevation) and reconstruct an image in terms of 3 dimension viewing. This extending multi-layer scanning technique provides more information compare to single layer.

5.2.5 The resolution of image can be improved by reducing the detectors size and increase number of detectors, for example, using PIN photo diode array

5.2.6 In this dissertation, all operating condition was assumed to be operating under the steady-state condition. It is possible to extend the technique to study the dynamic system using multi-radiation gamma-ray energy source technique and select the measured data from energy bin.

REFERENCES

1. Fahim, M.A., T.A. Al-Sahhaf, and A.S. Elkilani, *Fundamentals of Petroleum Refining.* 2010: p. 496.
2. MIX, P.E., *Introduction to Nondestructive Testing.* 2005: p. 672.
3. Cember, H., *Introduction to health physics*. 3rd ed. 1996, New York: McGraw-Hill, Health Professions Division. xviii, 733 p.
4. Knoll and F. Glenn, *Radiation detection and measurement*. 3rd ed. 2000, New York: Wiley. xiv, 802 p.
5. Tavernier, S., *Experimental Techniques in Nuclear and Particle Physics.* 2010: p. 306.
6. Kak, A.C., *Principles of computerized tomographic imaging*. Classics in applied mathematics. 2001, Philadelphia: Society for Industrial and Applied Mathematics. xiv, 327 p.
7. Rafael C. Gonzalez and R.E. Woods, *Digital Image Processing.* 2010. **Third Edition**: p. 976.
8. Charlton, J.S. and E.A. Edmonds, *Radioisotope Techniques for Problem-Solving in Industrial Process Plants.* 1994: p. 320.
9. Thereska, J. and J.H. Jin, *Manual on Quality Control and ccreditation in Radioisotope Applications.* 2004: p. 100.
10. (LANL), L.A.N.L., *MCNP - A General Monte Carlo N-Particle Transport Code, Version 5.* 2003. **VOL 1 - VOL 3**.
11. Kim, J., et al., *Monte Carlo Simulation for Design of Industrial Gamma-ray Transmission Tomography.* Progress in Nuclear Science and Technology, 2011.
12. Kim, J., et al., *Industrial Gamma-Ray Tomographic Scan Method for Large Scale Industrial Plants.* Journal of Nuclear Instrument and Methods in Physics Research, 2011.
13. Kim, J., *Development of gamma-ray tomographic system for industrial plant inspection.* 2011: p. 127.
14. Green, C.W., et al., *Novel application of X-ray computed tomography: Determination of gas/liquid contact area and liquid holdup in structured packing.* Industrial & Engineering Chemistry Research, 2007. **46**(17): p. 5734-5753.
15. Wang, Z.C., et al., *Porosity distribution in random packed columns by gamma ray tomography.* Chemical Engineering and Processing, 2001. **40**(3): p. 209-219.
16. Toye, D., et al., *Local measurements of void fraction and liquid holdup in packed columns using X-ray computed tomography.* Chemical Engineering and Processing, 1998. **37**(6): p. 511-520.
17. Leroy, C. and P.-G. Rancoita, *Principles of radiation interaction in matter and detection*. 2004, Hackensack, NJ: World Scientific. xv, 698 p.
18. Rainoon, M. and S. Srisatit, *Analysis of factors affecting tomographic image quality from profile data collected by imaging plate.* 2010: p. 107.
19. Ratanapirojkajee, N. and S. Srisatit, *Development of a data acquisition system for neutron computed tomography using neutron imaging scope.* 2001: p. 101.

20. Saengchantr, D. and S. Srisatit, *A Study of Data Acquisition Techniques for Image Back Projection Algorithm used in Cross-sectional Inspection of Distillation Process column Through a Laboratory Model.* Proceeding of 15th Asia Pacific Conference for Non-Destructive Testing, 2017(2018-03).
21. Sukrod, K. and S. Srisatit, *Development of a profile data acquisition system for neutron computed tomography for the Thai Research Reactor TRR-1/M1*. 2009: p. 86.
22. Swapan, K.B., *Trouble Shooting of Column Operation using Gamma Scanning Technique.* National Seminar & Exhibition on Non-Destructive Evaluation (NDE), 2011: p. 323-325.
23. Tuntananukul, K. and S. Srisatit, *Development of a profile data acquisition system for computed tomography using line CIS.* 2004: p. 77.
24. Yin, F.H., et al., *Liquid holdup distribution in packed columns: gamma ray tomography and CFD simulation.* Chemical Engineering and Processing, 2002. **41**(5): p. 473-483.

APPENDIX

APPENDIX I

MCNP INPUT FOR FOUR PIPES OBJECT (PROJECTION NO. 1)

```
TITLE CARD HERE
c ********************************************************************
c * This code was generated by software ColumnGen by D.Saengchantr
c * @copyright for Thailand Institute of Nuclear Technology
c * DATE & TIME : 24-Aug-17 11:55:21 PM
c * FILENAME : CT-FILE001.i
c ********************************************************************
c
c ********************     CELL CARDS START HERE     **************
c
c ********************          SOURCE CELL          **************
   10    6   -1.47    -10          imp:p=1  $ Source inner container
   11    1   -7.90     10 -11      imp:p=1  $ Source outter container
c ********************  COLUMN VESSELS CELL  ************************
   102   1   -7.90   -801  800     imp:p=1  $  Vessel SUS 7.9 g/cm3
c
c TODO::internal structure will be placed here
c
c ***************************  INSULATION
   103   12 -0.0735 -811 810 #102        imp:p=1
c ******************* CELL CARDS FOR 4 PIPES
   201   7   -1.205E-3  -850     imp:p=1 $ water block 1
   202   1   -7.90   850  -851   imp:p=1 $ water block 1
   203   7   -1.205E-3  -852     imp:p=1 $ water block 1
   204   1   -7.90   852  -853   imp:p=1 $ water block 1
   205   7   -1.205E-3  -854     imp:p=1 $ water block 1
   206   1   -7.90   854  -855   imp:p=1 $ water block 1
   207   7   -1.205E-3  -856     imp:p=1 $ water block 1
   208   1   -7.90   856  -857   imp:p=1 $ water block 1
c ******************  1 inch. NaI Detector CELL *********************
   300   0   -203  fill=3 u=4  imp:p=1  $ u=3 is detector; put in u4
   301   2   -3.6  -200            u=3  imp:p=1  $ NaI
   302   4   -2.7  201 -202       u=3  imp:p=1  $ Aluminium Container
   320   7   -1.205E-3 #301 #302     u=3  imp:p=1  $ dry air
   351   like 300 but trcl=1   u=0 $ Det #1
   352   like 300 but trcl=2   u=0 $ Det #2
   353   like 300 but trcl=3   u=0 $ Det #3
   354   like 300 but trcl=4   u=0 $ Det #4
   355   like 300 but trcl=5   u=0 $ Det #5
   356   like 300 but trcl=6   u=0 $ Det #6
   357   like 300 but trcl=7   u=0 $ Det #7
   358   like 300 but trcl=8   u=0 $ Det #8
   359   like 300 but trcl=9   u=0 $ Det #9
   360   like 300 but trcl=10   u=0 $ Det #10
   361   like 300 but trcl=11   u=0 $ Det #11
   362   like 300 but trcl=12   u=0 $ Det #12
   363   like 300 but trcl=13   u=0 $ Det #13
   364   like 300 but trcl=14   u=0 $ Det #14
   365   like 300 but trcl=15   u=0 $ Det #15
```

```
   366   like 300 but trcl=16   u=0 $ Det #16
   367   like 300 but trcl=17   u=0 $ Det #17
   368   like 300 but trcl=18   u=0 $ Det #18
   369   like 300 but trcl=19   u=0 $ Det #19
   370   like 300 but trcl=20   u=0 $ Det #20
   371   like 300 but trcl=21   u=0 $ Det #21
c ****************  TERMINATION OF CELL *********************
   800   7   -1.205E-3 -999  #10  #11  #102  #103
c TODO :: excluding cell of internal structure can be put here
                       #351 #352 #353 #354 #355
                       #356 #357 #358 #359 #360
                       #361 #362 #363 #364 #365
                       #366 #367 #368 #369 #370
                       #371
c ****************** EXCLUDE CELLS
                       #201 #202 #203 #204 #205
                       #206 #207 #208
                       imp:p=1            $ dry air
   900   0   999       imp:p=0            $ out of region of interest

c **************     SURFACE CARDS START HERE     *****************
c **************          SOURCE SURFACE          *****************
   10    RCC    0.00   -50.10   -0.35  0  0  0.70  0.30
   11    RCC    0.00   -50.10   -0.50  0  0  1.0  0.375
c **************  1 inch. NaI Detector SURFACE * ******************
   200   RCC  0.0     0.0   -1.27   0.0   0.0   2.54   1.27
   201   RCC  0.0     0.0   -1.27   0.0   0.0   20.32  1.27
   202   RCC  0.0     0.0   -1.37   0.0   0.0   20.52  1.37
   203   RCC  0.0     0.0   -1.4    0.0   0.0   20.53  1.40
c ***************** Vessel shell 3 cm thickness ******************
   800   RCC   0.0   0.0  -25.0 0.0 0.0 50.0  39.80 $ vessel inside
   801   RCC   0.0   0.0  -25.0 0.0 0.0 50.0  40.00 $ vessel outside
c ******************Insulation thickness ************************
   810   RCC   0.0   0.0 -25.0  0.0 0.0 50.0  40.00 $ vessel inside
   811   RCC   0.0   0.0 -25.0  0.0 0.0 50.0  40.10 $ vessel outside
c ****************** Internal Structure ***************************
c ****************** SURFACE CARDS FOR 4 PIPES
   850   RCC   -10.0    -10.0   -25.0   0.0   0.0   50.0  7.025
   851   RCC   -10.0    -10.0   -25.0   0.0   0.0   50.0  7.825
   852   RCC   10.0     -10.0   -25.0   0.0   0.0   50.0  4.54
   853   RCC   10.0     -10.0   -25.0   0.0   0.0   50.0  5.14
   854   RCC   -10.0     10.0   -25.0   0.0   0.0   50.0  5.075
   855   RCC   -10.0     10.0   -25.0   0.0   0.0   50.0  5.675
   856   RCC   10.0      10.0   -25.0   0.0   0.0   50.0  3.21
   857   RCC   10.0      10.0   -25.0   0.0   0.0   50.0  3.81
c  *************** Sphere  *********************************
   999   SO  100.0                  $ simulation bound

c *****************        physics card       **********************
   MODE P           $ photon
c *****************       Transformation      **********************
 *TR1 48.39 12.97 0.0  0.0  90  90  90  0  90  90  90  0  1
 *TR2 46.29 19.17 0.0  0.0  90  90  90  0  90  90  90  0  1
 *TR3 43.39 25.05 0.0  0.0  90  90  90  0  90  90  90  0  1
 *TR4 39.75 30.50 0.0  0.0  90  90  90  0  90  90  90  0  1
 *TR5 35.43 35.43 0.0  0.0  90  90  90  0  90  90  90  0  1
 *TR6 30.50 39.75 0.0  0.0  90  90  90  0  90  90  90  0  1
 *TR7 25.05 43.39 0.0  0.0  90  90  90  0  90  90  90  0  1
```

```
 *TR8 19.17 46.29 0.0  0.0  90  90  90  0  90  90  90  0  1
 *TR9 12.97 48.39 0.0  0.0  90  90  90  0  90  90  90  0  1
 *TR10 6.54 49.67 0.0  0.0  90  90  90  0  90  90  90  0  1
 *TR11 0.00 50.10 0.0  0.0  90  90  90  0  90  90  90  0  1
 *TR12 -6.54 49.67 0.0  0.0  90  90  90  0  90  90  90  0  1
 *TR13 -12.97 48.39 0.0  0.0  90  90  90  0  90  90  90  0  1
 *TR14 -19.17 46.29 0.0  0.0  90  90  90  0  90  90  90  0  1
 *TR15 -25.05 43.39 0.0  0.0  90  90  90  0  90  90  90  0  1
 *TR16 -30.50 39.75 0.0  0.0  90  90  90  0  90  90  90  0  1
 *TR17 -35.43 35.43 0.0  0.0  90  90  90  0  90  90  90  0  1
 *TR18 -39.75 30.50 0.0  0.0  90  90  90  0  90  90  90  0  1
 *TR19 -43.39 25.05 0.0  0.0  90  90  90  0  90  90  90  0  1
 *TR20 -46.29 19.17 0.0  0.0  90  90  90  0  90  90  90  0  1
 *TR21 -48.39 12.97 0.0  0.0  90  90  90  0  90  90  90  0  1
c ****************  Source Definition  ***********************
c FOR Co-60 if use uncomment following lines until sp5
   SDEF ERG=0.662  POS= 0.00 -50.10 0 AXS=0 0 1   RAD=D1 EXT=D2
$
   SI1  H   0   0.3
   SP1     -21    1
   SI2  H  -0.35  0.35
   SP2     -21    0
c ***********************    MATERIAL CARD    **********************
M1   26000 -0.71          $ stainless steel
     24000 -0.17
     28000 -0.12
M2   11000  1             $ NaI
     53000  1
M3    6000  1             $ ch2 polyprophylene
      1000  2
M4   13000  1             $ aluminum
M6   55000  1             $ Cesium 137
      6000  1
M7    6000 -0.000124      $ air dry(near sea level)
      7000 -0.755268      $ density 1.205E-3
      8000 -0.231781
     18000 -0.012827
      9000 -0.759818      $ d=2.25
M9    1000 -0.111898      $ water
      8000 -0.888102
M10  82000 1               $ lead
M11   6000 -0.005         $MAT11
     26000 -0.995
M12   5000 -0.018579      $ fiber glass density = 0.073543
     8000 -0.478631
      11000 -0.059171
      12000 -0.018037
      13000 -0.021107
      14000 -0.302924
      16000 -0.000399
      20000 -0.099757
      26000 -0.001395
c ***********************    TALLY CARD    ************************
  F8:p
          (301<351)
          (301<352)
          (301<353)
          (301<354)
```

```
         (301<355)
         (301<356)
         (301<357)
         (301<358)
         (301<359)
         (301<360)
         (301<361)
         (301<362)
         (301<363)
         (301<364)
         (301<365)
         (301<366)
         (301<367)
         (301<368)
         (301<369)
         (301<370)
         (301<371)
E8 1e-6  0.05  1  1.5        $ 0 to 1MeV 0.01 MeV step
FT8  GEB 0 0.08922  -0.15373
PRDMP  J J 1 J J
NPS    1E8
```

APPENDIX II

SOFTWARE "SIMPLIFIED" USER'S MANUAL

The "Simplified" software is data acquisition software which integrated necessary modules together. It composed of 4 main modules i.e. Acquisition Module, Post Processing Module, Image Reconstruction Module and Simulation Module. Software was designed to interface with radiation counter Ludlum model 4612 (version 2005) with baud rate of 19200 bps, no parity, 8 data bits, 1 stop bit. Connection between computer and radiation counter was originally designed for RS-232 communication, however, the RS-232 communication port is very rare equip with computer, nowadays. Thus, USB to RS-232 converter cable can be used instead of original communication port. Diagram in Figure A.1 illustrates the connection between computer and radiation counter which connected to detectors.

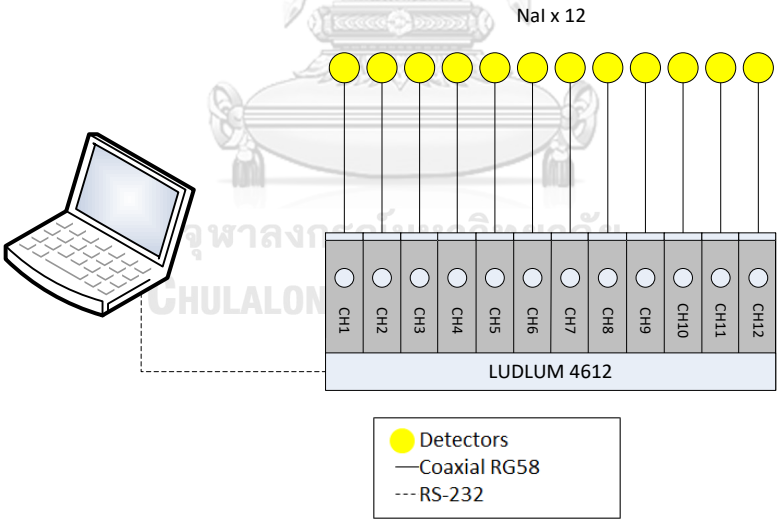

Figure A.1 System arrangement, connection of LUDLUM 4612 to detectors and computer

1. Acquisition Module

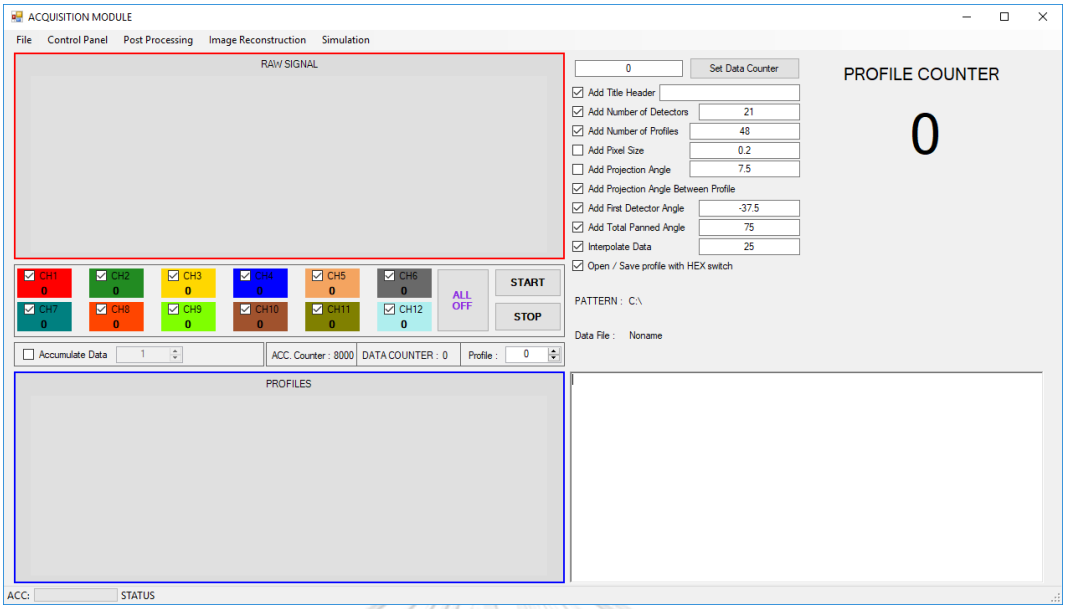

Figure A.2 Acquisition Page (Main Page)

The data acquisition module is used for interfacing with the radiation counter. Two important line graphs are accommodated in the windows i.e. “Raw Signal” which display the counting data simultaneously read from each detector and “Profiles” which display single instance combination plot of all data detector in single line. User can select the display in “Raw Signal” graph by using check boxes at each “CH” (channels)

- “Accumulate Data” checkbox allows user to measure the data in accumulation mode. For example, if the timer at radiation counter was setting to give the counting data every one second and if the accumulation data is setting to 10, the data will make a summation of all data in 10 second interval and plot once.
- “Data Counter” will display the number of data set that acquired from radiation counter.
- “Profile” up down number is the number for graph display at the required number of profile.
- “Set Start Counter” is input for providing the starting number of data set.
- “Add Title Header” is input text box to save the provided the title of projection.

- “Add Number of Detectors” is input text box to save the provided the number of detectors used in the projection.
- “Add Number of Profiles” is input text box to save the provided the number of profiles that used in the projection.
- “Add Pixel Size” is input text box to assign the pixel size for calculation (not effect much).
- “Add Projection Angle” is input text box to specify the angle step size.
- “Add Projection Angle Between Profile” is the input text box to add the value of angle between data set of profile.
- “Add First Detector Angle” is input text box to specify the angle of first angle (mostly place from right hand side of fan cone)
- “Add Total Panned Angle” is input text box to specify the panned angle of fan beam (less than or equal to 90 degree)
- “Interpolate Data” is input text box to specify the number of point interval to be interpolated. Since data acquired from projection is coarse, hence interpolation is required to increase the number of data between detectors.
- “Open /Save profile with HEX switch” is checkbox to specify the using of header switch which automatically store all above parameter status.

2. Control Panel

The control panel is a communication setting that used for setting the value of each channel. The value of “High Voltage”, “LLD” and “ULD” of each channel are available to be changed by user. Users are also requested to learn their communication port that connects to the radiation counter. The available communication ports are displayed in dropdown list. The “Output Time” is the time interval between data to data or in the other words it is the sampling duration. If connection is success, all information are read from the radiation counter and display in corresponding channels.

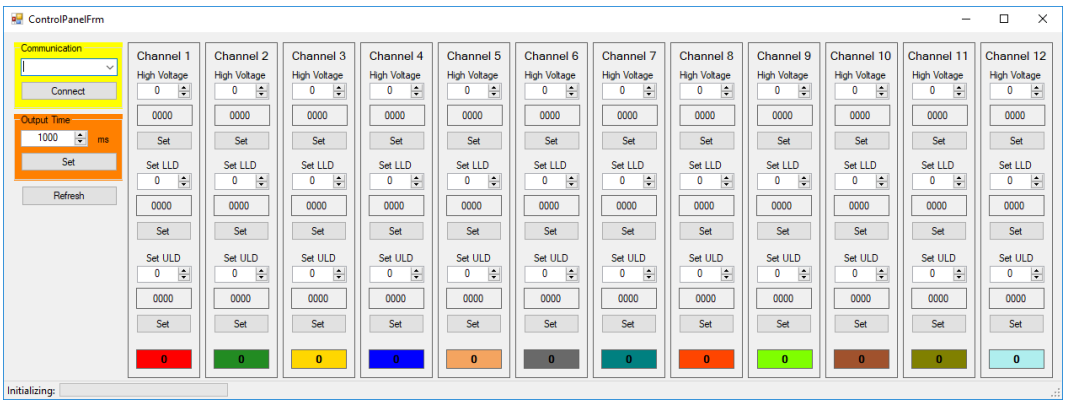

Figure A.3 Control Panel Page

3. Post Processing Module

This function is used for reshuffle all information to the pattern that allows for reconstruction. The pattern must be loaded into the software using “Load Pattern” command as well as loading raw data. If all files are loaded and meet requirement, “Process” function will be available then process it. After finish processing, save the output using “Save Output” function.

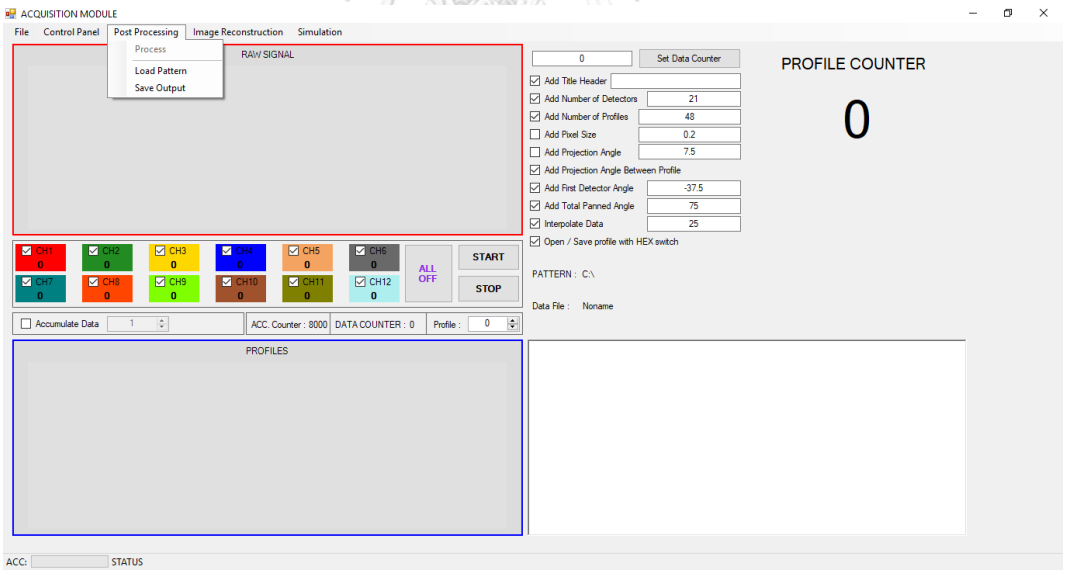

Figure A.4 Post Processing Menu

4. Image Reconstruction Module

This module is function for computing all acquired data and reconstruct the image using fan beam filtered back projection algorithm. The data saved in the

right format is loaded to the module from File->Open Projections. All checkbox switches are automatically activated from “Hex Switch Header”.

“Reconstruction” button is to start the calculation. The image will be displayed in grayscale with 256 gray value levels. Each pixel value is observable just move mouse over the position to be observed then gray value is displayed at the “Value of Pixel” as well as its reconstructed value or “Mu” (note that, this mu value is not true value of linear attenuation coefficient but it is a value from reconstruction). Reconstructed image can be saved using File->Save Reconstructed Image.

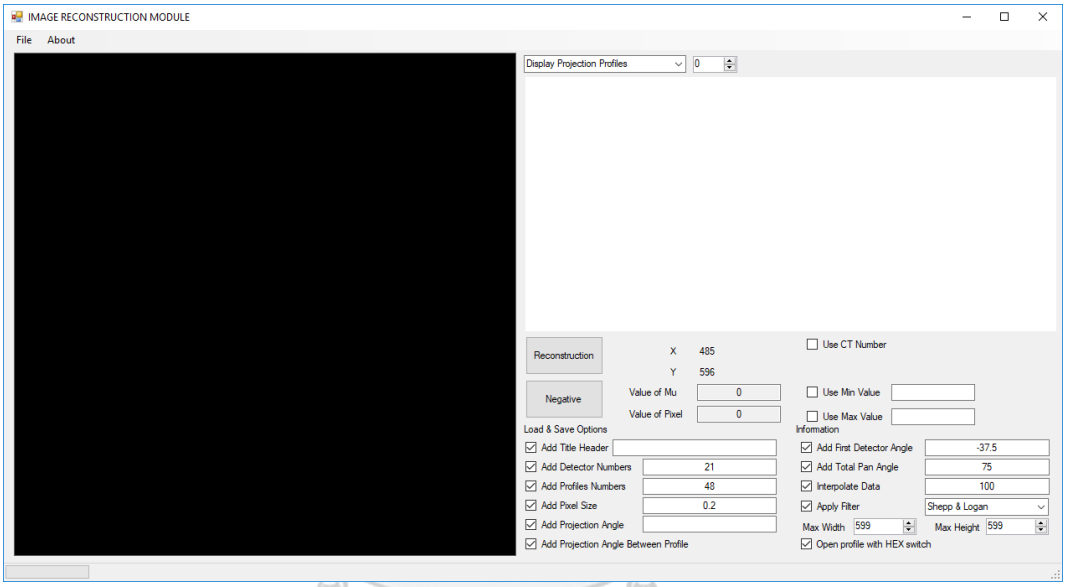

Figure A.5 Image Reconstruction Page

5. Simulation Module

The simulation module is designed to help the user for their prior knowledge before perform scanning. The user can load the image (bmp gray image format) into the simulator by click the display area and browse to file. “Fan Profile” simulate the fan projection onto the displaying image then “Save Profiles”.

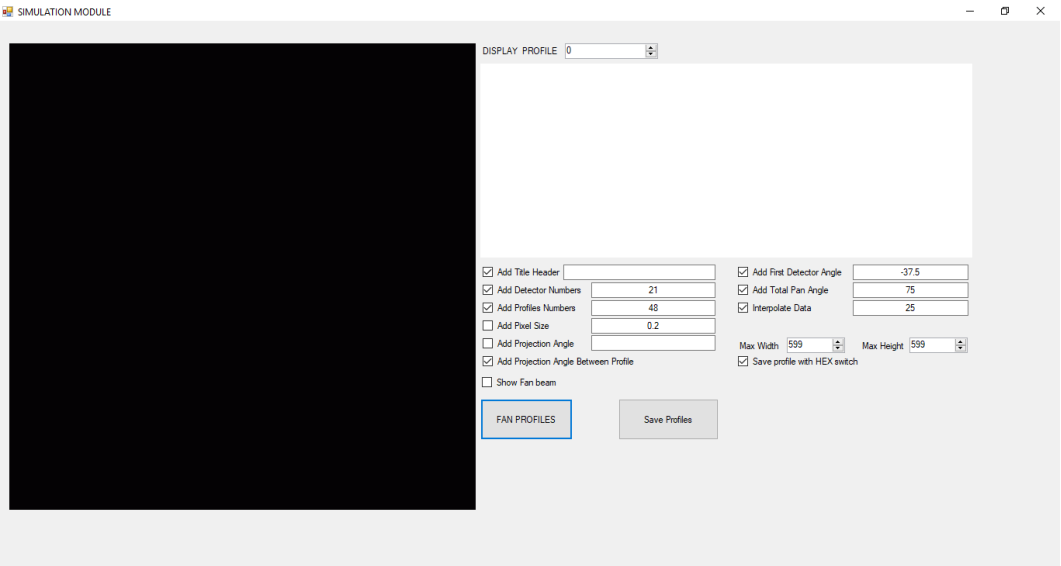

Figure A.6 Simulation Page

APPENDIX III

FULL TABLE OF SHUFFLING ALGORITHMS

A3.1 Full step positioning sequences of detectors and source in algorithm pattern 1

Step	S	D1	D2	D3	D4	D5	D6	D7	D8	D9	D10	D11
1	25	1	2	3	4	5	6	7	8	9	10	11
2	24	48	1	2	3	4	5	6	7	8	9	10
3	23	47	48	1	2	3	4	5	6	7	8	9
4	22	46	47	48	1	2	3	4	5	6	7	8
5	21	45	46	47	48	1	2	3	4	5	6	7
6	20	44	45	46	47	48	1	2	3	4	5	6
7	19	43	44	45	46	47	48	1	2	3	4	5
8	18	42	43	44	45	46	47	48	1	2	3	4
9	17	41	42	43	44	45	46	47	48	1	2	3
10	16	40	41	42	43	44	45	46	47	48	1	2
11	15	39	40	41	42	43	44	45	46	47	48	1
12	14	38	39	40	41	42	43	44	45	46	47	48
13	13	37	38	39	40	41	42	43	44	45	46	47
14	12	36	37	38	39	40	41	42	43	44	45	46
15	11	35	36	37	38	39	40	41	42	43	44	45
16	10	34	35	36	37	38	39	40	41	42	43	44
17	9	33	34	35	36	37	38	39	40	41	42	43
18	8	32	33	34	35	36	37	38	39	40	41	42
19	7	31	32	33	34	35	36	37	38	39	40	41
20	6	30	31	32	33	34	35	36	37	38	39	40
21	5	29	30	31	32	33	34	35	36	37	38	39
22	4	28	29	30	31	32	33	34	35	36	37	38
23	3	27	28	29	30	31	32	33	34	35	36	37
24	2	26	27	28	29	30	31	32	33	34	35	36
25	1	25	26	27	28	29	30	31	32	33	34	35
26	48	24	25	26	27	28	29	30	31	32	33	34
27	47	23	24	25	26	27	28	29	30	31	32	33
28	46	22	23	24	25	26	27	28	29	30	31	32
29	45	21	22	23	24	25	26	27	28	29	30	31
30	44	20	21	22	23	24	25	26	27	28	29	30
31	43	19	20	21	22	23	24	25	26	27	28	29
32	42	18	19	20	21	22	23	24	25	26	27	28
33	41	17	18	19	20	21	22	23	24	25	26	27
34	40	16	17	18	19	20	21	22	23	24	25	26
35	39	15	16	17	18	19	20	21	22	23	24	25
36	38	14	15	16	17	18	19	20	21	22	23	24
37	37	13	14	15	16	17	18	19	20	21	22	23
38	36	12	13	14	15	16	17	18	19	20	21	22
39	35	11	12	13	14	15	16	17	18	19	20	21
40	34	10	11	12	13	14	15	16	17	18	19	20
41	33	9	10	11	12	13	14	15	16	17	18	19

Step	S	D1	D2	D3	D4	D5	D6	D7	D8	D9	D10	D11
42	32	8	9	10	11	12	13	14	15	16	17	18
43	31	7	8	9	10	11	12	13	14	15	16	17
44	30	6	7	8	9	10	11	12	13	14	15	16
45	29	5	6	7	8	9	10	11	12	13	14	15
46	28	4	5	6	7	8	9	10	11	12	13	14
47	27	3	4	5	6	7	8	9	10	11	12	13
48	26	2	3	4	5	6	7	8	9	10	11	12
49	25	39	40	41	42	43	44	45	46	47	48	1
50	24	38	39	40	41	42	43	44	45	46	47	48
51	23	37	38	39	40	41	42	43	44	45	46	47
52	22	36	37	38	39	40	41	42	43	44	45	46
53	21	35	36	37	38	39	40	41	42	43	44	45
54	20	34	35	36	37	38	39	40	41	42	43	44
55	19	33	34	35	36	37	38	39	40	41	42	43
56	18	32	33	34	35	36	37	38	39	40	41	42
57	17	31	32	33	34	35	36	37	38	39	40	41
58	16	30	31	32	33	34	35	36	37	38	39	40
59	15	29	30	31	32	33	34	35	36	37	38	39
60	14	28	29	30	31	32	33	34	35	36	37	38
61	13	27	28	29	30	31	32	33	34	35	36	37
62	12	26	27	28	29	30	31	32	33	34	35	36
63	11	25	26	27	28	29	30	31	32	33	34	35
64	10	24	25	26	27	28	29	30	31	32	33	34
65	9	23	24	25	26	27	28	29	30	31	32	33
66	8	22	23	24	25	26	27	28	29	30	31	32
67	7	21	22	23	24	25	26	27	28	29	30	31
68	6	20	21	22	23	24	25	26	27	28	29	30
69	5	19	20	21	22	23	24	25	26	27	28	29
70	4	18	19	20	21	22	23	24	25	26	27	28
71	3	17	18	19	20	21	22	23	24	25	26	27
72	2	16	17	18	19	20	21	22	23	24	25	26
73	1	15	16	17	18	19	20	21	22	23	24	25
74	48	14	15	16	17	18	19	20	21	22	23	24
75	47	13	14	15	16	17	18	19	20	21	22	23
76	46	12	13	14	15	16	17	18	19	20	21	22
77	45	11	12	13	14	15	16	17	18	19	20	21
78	44	10	11	12	13	14	15	16	17	18	19	20
79	43	9	10	11	12	13	14	15	16	17	18	19
80	42	8	9	10	11	12	13	14	15	16	17	18
81	41	7	8	9	10	11	12	13	14	15	16	17
82	40	6	7	8	9	10	11	12	13	14	15	16
83	39	5	6	7	8	9	10	11	12	13	14	15
84	38	4	5	6	7	8	9	10	11	12	13	14

Step	S	D1	D2	D3	D4	D5	D6	D7	D8	D9	D10	D11
85	37	3	4	5	6	7	8	9	10	11	12	13
86	36	2	3	4	5	6	7	8	9	10	11	12
87	35	1	2	3	4	5	6	7	8	9	10	11
88	34	48	1	2	3	4	5	6	7	8	9	10
89	33	47	48	1	2	3	4	5	6	7	8	9
90	32	46	47	48	1	2	3	4	5	6	7	8
91	31	45	46	47	48	1	2	3	4	5	6	7
92	30	44	45	46	47	48	1	2	3	4	5	6
93	29	43	44	45	46	47	48	1	2	3	4	5
94	28	42	43	44	45	46	47	48	1	2	3	4
95	27	41	42	43	44	45	46	47	48	1	2	3
96	26	40	41	42	43	44	45	46	47	48	1	2

A3.2 Data rearrangement by array's position of Algorithm Pattern 1

Steps				D1	to	D21					
1	587	586	585	584	583	582	581	580	579	578	11
	10	9	8	7	6	5	4	3	2	1	
2	599	598	597	596	595	594	593	592	591	590	23
	22	21	20	19	18	17	16	15	14	13	
3	611	610	609	608	607	606	605	604	603	602	35
	34	33	32	31	30	29	28	27	26	25	
4	623	622	621	620	619	618	617	616	615	614	47
	46	45	44	43	42	41	40	39	38	37	
5	635	634	633	632	631	630	629	628	627	626	59
	58	57	56	55	54	53	52	51	50	49	
6	647	646	645	644	643	642	641	640	639	638	71
	70	69	68	67	66	65	64	63	62	61	
7	659	658	657	656	655	654	653	652	651	650	83
	82	81	80	79	78	77	76	75	74	73	
8	671	670	669	668	667	666	665	664	663	662	95
	94	93	92	91	90	89	88	87	86	85	
9	683	682	681	680	679	678	677	676	675	674	107
	106	105	104	103	102	101	100	99	98	97	
10	695	694	693	692	691	690	689	688	687	686	119
	118	117	116	115	114	113	112	111	110	109	
11	707	706	705	704	703	702	701	700	699	698	131
	130	129	128	127	126	125	124	123	122	121	
12	719	718	717	716	715	714	713	712	711	710	143
	142	141	140	139	138	137	136	135	134	133	
13	731	730	729	728	727	726	725	724	723	722	155
	154	153	152	151	150	149	148	147	146	145	
14	743	742	741	740	739	738	737	736	735	734	167

Steps				D1	to	D21					
	166	165	164	163	162	161	160	159	158	157	
15	755	754	753	752	751	750	749	748	747	746	179
	178	177	176	175	174	173	172	171	170	169	
16	767	766	765	764	763	762	761	760	759	758	191
	190	189	188	187	186	185	184	183	182	181	
17	779	778	777	776	775	774	773	772	771	770	203
	202	201	200	199	198	197	196	195	194	193	
18	791	790	789	788	787	786	785	784	783	782	215
	214	213	212	211	210	209	208	207	206	205	
19	803	802	801	800	799	798	797	796	795	794	227
	226	225	224	223	222	221	220	219	218	217	
20	815	814	813	812	811	810	809	808	807	806	239
	238	237	236	235	234	233	232	231	230	229	
21	827	826	825	824	823	822	821	820	819	818	251
	250	249	248	247	246	245	244	243	242	241	
22	839	838	837	836	835	834	833	832	831	830	263
	262	261	260	259	258	257	256	255	254	253	
23	851	850	849	848	847	846	845	844	843	842	275
	274	273	272	271	270	269	268	267	266	265	
24	863	862	861	860	859	858	857	856	855	854	287
	286	285	284	283	282	281	280	279	278	277	
25	875	874	873	872	871	870	869	868	867	866	299
	298	297	296	295	294	293	292	291	290	289	
26	887	886	885	884	883	882	881	880	879	878	311
	310	309	308	307	306	305	304	303	302	301	
27	899	898	897	896	895	894	893	892	891	890	323
	322	321	320	319	318	317	316	315	314	313	
28	911	910	909	908	907	906	905	904	903	902	335
	334	333	332	331	330	329	328	327	326	325	
29	923	922	921	920	919	918	917	916	915	914	347
	346	345	344	343	342	341	340	339	338	337	
30	935	934	933	932	931	930	929	928	927	926	359
	358	357	356	355	354	353	352	351	350	349	
31	947	946	945	944	943	942	941	940	939	938	371
	370	369	368	367	366	365	364	363	362	361	
32	959	958	957	956	955	954	953	952	951	950	383
	382	381	380	379	378	377	376	375	374	373	
33	971	970	969	968	967	966	965	964	963	962	395
	394	393	392	391	390	389	388	387	386	385	
34	983	982	981	980	979	978	977	976	975	974	407
	406	405	404	403	402	401	400	399	398	397	
35	995	994	993	992	991	990	989	988	987	986	419
	418	417	416	415	414	413	412	411	410	409	

Steps				D1	to	D21					
36	1007	1006	1005	1004	1003	1002	1001	1000	999	998	431
	430	429	428	427	426	425	424	423	422	421	
37	1019	1018	1017	1016	1015	1014	1013	1012	1011	1010	443
	442	441	440	439	438	437	436	435	434	433	
38	1031	1030	1029	1028	1027	1026	1025	1024	1023	1022	455
	454	453	452	451	450	449	448	447	446	445	
39	1043	1042	1041	1040	1039	1038	1037	1036	1035	1034	467
	466	465	464	463	462	461	460	459	458	457	
40	1055	1054	1053	1052	1051	1050	1049	1048	1047	1046	479
	478	477	476	475	474	473	472	471	470	469	
41	1067	1066	1065	1064	1063	1062	1061	1060	1059	1058	491
	490	489	488	487	486	485	484	483	482	481	
42	1079	1078	1077	1076	1075	1074	1073	1072	1071	1070	503
	502	501	500	499	498	497	496	495	494	493	
43	1091	1090	1089	1088	1087	1086	1085	1084	1083	1082	515
	514	513	512	511	510	509	508	507	506	505	
44	1103	1102	1101	1100	1099	1098	1097	1096	1095	1094	527
	526	525	524	523	522	521	520	519	518	517	
45	1115	1114	1113	1112	1111	1110	1109	1108	1107	1106	539
	538	537	536	535	534	533	532	531	530	529	
46	1127	1126	1125	1124	1123	1122	1121	1120	1119	1118	551
	550	549	548	547	546	545	544	543	542	541	
47	1139	1138	1137	1136	1135	1134	1133	1132	1131	1130	563
	562	561	560	559	558	557	556	555	554	553	
48	1151	1150	1149	1148	1147	1146	1145	1144	1143	1142	575
	574	573	572	571	570	569	568	567	566	565	

A3.3 Full step positioning sequences of detectors and source in algorithm pattern 2

Steps	S	D1	D2	D3	D4	D5	D6	D7	D8	D9	D10	D11
1	25	1	2	3	4	5	6	7	8	9	10	11
2	24	1	2	3	4	5	6	7	8	9	10	48
3	23	1	2	3	4	5	6	7	8	9	47	48
4	22	1	2	3	4	5	6	7	8	46	47	48

Steps	S	D1	D2	D3	D4	D5	D6	D7	D8	D9	D10	D11
5	21	1	2	3	4	5	6	7	45	46	47	48
6	20	1	2	3	4	5	6	44	45	46	47	48
7	19	1	2	3	4	5	43	44	45	46	47	48
8	18	1	2	3	4	42	43	44	45	46	47	48
9	17	1	2	3	41	42	43	44	45	46	47	48
10	16	1	2	40	41	42	43	44	45	46	47	48
11	15	1	39	40	41	42	43	44	45	46	47	48
12	14	38	39	40	41	42	43	44	45	46	47	48
13	13	38	39	40	41	42	43	44	45	46	47	37
14	12	38	39	40	41	42	43	44	45	46	36	37
15	11	38	39	40	41	42	43	44	45	35	36	37
16	10	38	39	40	41	42	43	44	34	35	36	37
17	9	38	39	40	41	42	43	33	34	35	36	37
18	8	38	39	40	41	42	32	33	34	35	36	37
19	7	38	39	40	41	31	32	33	34	35	36	37
20	6	38	39	40	30	31	32	33	34	35	36	37
21	5	38	39	29	30	31	32	33	34	35	36	37
22	4	38	28	29	30	31	32	33	34	35	36	37
23	3	27	28	29	30	31	32	33	34	35	36	37
24	2	27	28	29	30	31	32	33	34	35	36	26
25	1	27	28	29	30	31	32	33	34	35	25	26
26	48	27	28	29	30	31	32	33	34	24	25	26
27	47	27	28	29	30	31	32	33	23	24	25	26
28	46	27	28	29	30	31	32	22	23	24	25	26
29	45	27	28	29	30	31	21	22	23	24	25	26
30	44	27	28	29	30	20	21	22	23	24	25	26
31	43	27	28	29	19	20	21	22	23	24	25	26
32	42	27	28	18	19	20	21	22	23	24	25	26
33	41	27	17	18	19	20	21	22	23	24	25	26
34	40	16	17	18	19	20	21	22	23	24	25	26
35	39	16	17	18	19	20	21	22	23	24	25	15
36	38	16	17	18	19	20	21	22	23	24	14	15
37	37	16	17	18	19	20	21	22	23	13	14	15
38	36	16	17	18	19	20	21	22	12	13	14	15
39	35	16	17	18	19	20	21	11	12	13	14	15
40	34	16	17	18	19	20	10	11	12	13	14	15
41	33	16	17	18	19	9	10	11	12	13	14	15
42	32	16	17	18	8	9	10	11	12	13	14	15
43	31	16	17	7	8	9	10	11	12	13	14	15
44	30	16	6	7	8	9	10	11	12	13	14	15
45	29	5	6	7	8	9	10	11	12	13	14	15
46	28	5	6	7	8	9	10	11	12	13	14	4
47	27	5	6	7	8	9	10	11	12	13	3	4

Steps	S	D1	D2	D3	D4	D5	D6	D7	D8	D9	D10	D11
48	26	5	6	7	8	9	10	11	12	2	3	4
49	25	39	40	41	42	43	44	45	46	47	48	1
50	24	39	40	41	42	43	44	45	46	47	48	38
51	23	39	40	41	42	43	44	45	46	47	37	38
52	22	39	40	41	42	43	44	45	46	36	37	38
53	21	39	40	41	42	43	44	45	35	36	37	38
54	20	39	40	41	42	43	44	34	35	36	37	38
55	19	39	40	41	42	43	33	34	35	36	37	38
56	18	39	40	41	42	32	33	34	35	36	37	38
57	17	39	40	41	31	32	33	34	35	36	37	38
58	16	39	40	30	31	32	33	34	35	36	37	38
59	15	39	29	30	31	32	33	34	35	36	37	38
60	14	28	29	30	31	32	33	34	35	36	37	38
61	13	28	29	30	31	32	33	34	35	36	37	27
62	12	28	29	30	31	32	33	34	35	36	26	27
63	11	28	29	30	31	32	33	34	35	25	26	27
64	10	28	29	30	31	32	33	34	24	25	26	27
65	9	28	29	30	31	32	33	23	24	25	26	27
66	8	28	29	30	31	32	22	23	24	25	26	27
67	7	28	29	30	31	21	22	23	24	25	26	27
68	6	28	29	30	20	21	22	23	24	25	26	27
69	5	28	29	19	20	21	22	23	24	25	26	27
70	4	28	18	19	20	21	22	23	24	25	26	27
71	3	17	18	19	20	21	22	23	24	25	26	27
72	2	17	18	19	20	21	22	23	24	25	26	16
73	1	17	18	19	20	21	22	23	24	25	15	16
74	48	17	18	19	20	21	22	23	24	14	15	16
75	47	17	18	19	20	21	22	23	13	14	15	16
76	46	17	18	19	20	21	22	12	13	14	15	16
77	45	17	18	19	20	21	11	12	13	14	15	16
78	44	17	18	19	20	10	11	12	13	14	15	16
79	43	17	18	19	9	10	11	12	13	14	15	16
80	42	17	18	8	9	10	11	12	13	14	15	16
81	41	17	7	8	9	10	11	12	13	14	15	16
82	40	6	7	8	9	10	11	12	13	14	15	16
83	39	6	7	8	9	10	11	12	13	14	15	5
84	38	6	7	8	9	10	11	12	13	14	4	5
85	37	6	7	8	9	10	11	12	13	3	4	5
86	36	6	7	8	9	10	11	12	2	3	4	5
87	35	6	7	8	9	10	11	1	2	3	4	5
88	34	6	7	8	9	10	48	1	2	3	4	5
89	33	6	7	8	9	47	48	1	2	3	4	5
90	32	6	7	8	46	47	48	1	2	3	4	5

Steps	S	D1	D2	D3	D4	D5	D6	D7	D8	D9	D10	D11
91	31	6	7	45	46	47	48	1	2	3	4	5
92	30	6	44	45	46	47	48	1	2	3	4	5
93	29	43	44	45	46	47	48	1	2	3	4	5
94	28	43	44	45	46	47	48	1	2	3	4	42
95	27	43	44	45	46	47	48	1	2	3	41	42
96	26	43	44	45	46	47	48	1	2	40	41	42

A3.4 Data rearrangement by array's position of Algorithm Pattern 2

Steps				D1	to	D21					
1	587	586	585	584	583	582	581	580	579	578	11
	10	9	8	7	6	5	4	3	2	1	
2	598	597	596	595	594	593	592	591	590	589	22
	21	20	19	18	17	16	15	14	13	23	
3	609	608	607	606	605	604	603	602	601	611	33
	32	31	30	29	28	27	26	25	35	34	
4	620	619	618	617	616	615	614	613	623	622	44
	43	42	41	40	39	38	37	47	46	45	
5	631	630	629	628	627	626	625	635	634	633	55
	54	53	52	51	50	49	59	58	57	56	
6	642	641	640	639	638	637	647	646	645	644	66
	65	64	63	62	61	71	70	69	68	67	
7	653	652	651	650	649	659	658	657	656	655	77
	76	75	74	73	83	82	81	80	79	78	
8	664	663	662	661	671	670	669	668	667	666	88
	87	86	85	95	94	93	92	91	90	89	
9	675	674	673	683	682	681	680	679	678	677	99
	98	97	107	106	105	104	103	102	101	100	
10	686	685	695	694	693	692	691	690	689	688	110
	109	119	118	117	116	115	114	113	112	111	
11	697	707	706	705	704	703	702	701	700	699	121
	131	130	129	128	127	126	125	124	123	122	
12	719	718	717	716	715	714	713	712	711	710	143
	142	141	140	139	138	137	136	135	134	133	
13	730	729	728	727	726	725	724	723	722	721	154
	153	152	151	150	149	148	147	146	145	155	
14	741	740	739	738	737	736	735	734	733	743	165
	164	163	162	161	160	159	158	157	167	166	
15	752	751	750	749	748	747	746	745	755	754	176
	175	174	173	172	171	170	169	179	178	177	
16	763	762	761	760	759	758	757	767	766	765	187
	186	185	184	183	182	181	191	190	189	188	
17	774	773	772	771	770	769	779	778	777	776	198

Steps				D1	to	D21					
	197	196	195	194	193	203	202	201	200	199	
18	785	784	783	782	781	791	790	789	788	787	209
	208	207	206	205	215	214	213	212	211	210	
19	796	795	794	793	803	802	801	800	799	798	220
	219	218	217	227	226	225	224	223	222	221	
20	807	806	805	815	814	813	812	811	810	809	231
	230	229	239	238	237	236	235	234	233	232	
21	818	817	827	826	825	824	823	822	821	820	242
	241	251	250	249	248	247	246	245	244	243	
22	829	839	838	837	836	835	834	833	832	831	253
	263	262	261	260	259	258	257	256	255	254	
23	851	850	849	848	847	846	845	844	843	842	275
	274	273	272	271	270	269	268	267	266	265	
24	862	861	860	859	858	857	856	855	854	853	286
	285	284	283	282	281	280	279	278	277	287	
25	873	872	871	870	869	868	867	866	865	875	297
	296	295	294	293	292	291	290	289	299	298	
26	884	883	882	881	880	879	878	877	887	886	308
	307	306	305	304	303	302	301	311	310	309	
27	895	894	893	892	891	890	889	899	898	897	319
	318	317	316	315	314	313	323	322	321	320	
28	906	905	904	903	902	901	911	910	909	908	330
	329	328	327	326	325	335	334	333	332	331	
29	917	916	915	914	913	923	922	921	920	919	341
	340	339	338	337	347	346	345	344	343	342	
30	928	927	926	925	935	934	933	932	931	930	352
	351	350	349	359	358	357	356	355	354	353	
31	939	938	937	947	946	945	944	943	942	941	363
	362	361	371	370	369	368	367	366	365	364	
32	950	949	959	958	957	956	955	954	953	952	374
	373	383	382	381	380	379	378	377	376	375	
33	961	971	970	969	968	967	966	965	964	963	385
	395	394	393	392	391	390	389	388	387	386	
34	983	982	981	980	979	978	977	976	975	974	407
	406	405	404	403	402	401	400	399	398	397	
35	994	993	992	991	990	989	988	987	986	985	418
	417	416	415	414	413	412	411	410	409	419	
36	1005	1004	1003	1002	1001	1000	999	998	997	1007	429
	428	427	426	425	424	423	422	421	431	430	
37	1016	1015	1014	1013	1012	1011	1010	1009	1019	1018	440
	439	438	437	436	435	434	433	443	442	441	
38	1027	1026	1025	1024	1023	1022	1021	1031	1030	1029	451
	450	449	448	447	446	445	455	454	453	452	

Steps				D1	to	D21					
39	1038	1037	1036	1035	1034	1033	1043	1042	1041	1040	462
	461	460	459	458	457	467	466	465	464	463	
40	1049	1048	1047	1046	1045	1055	1054	1053	1052	1051	473
	472	471	470	469	479	478	477	476	475	474	
41	1060	1059	1058	1057	1067	1066	1065	1064	1063	1062	484
	483	482	481	491	490	489	488	487	486	485	
42	1071	1070	1069	1079	1078	1077	1076	1075	1074	1073	495
	494	493	503	502	501	500	499	498	497	496	
43	1082	1081	1091	1090	1089	1088	1087	1086	1085	1084	506
	505	515	514	513	512	511	510	509	508	507	
44	1093	1103	1102	1101	1100	1099	1098	1097	1096	1095	517
	527	526	525	524	523	522	521	520	519	518	
45	1115	1114	1113	1112	1111	1110	1109	1108	1107	1106	539
	538	537	536	535	534	533	532	531	530	529	
46	1126	1125	1124	1123	1122	1121	1120	1119	1118	1117	550
	549	548	547	546	545	544	543	542	541	551	
47	1137	1136	1135	1134	1133	1132	1131	1130	1129	1139	561
	560	559	558	557	556	555	554	553	563	562	
48	1148	1147	1146	1145	1144	1143	1142	1141	1151	1150	572
	571	570	569	568	567	566	565	575	574	573	

A3.5 Full step positioning sequences of detectors and source in algorithm pattern 2

Step	S	D1	D2	D3	D4	D5	D6	D7	D8	D9	D10	D11
1	25	1	2	3	4	5	6	7	8	9	10	11
2	35	1	2	3	4	5	6	7	8	9	10	11
3	24	1	2	3	4	5	6	7	8	9	10	48
4	34	1	2	3	4	5	6	7	8	9	10	48
5	23	1	2	3	4	5	6	7	8	9	47	48
6	33	1	2	3	4	5	6	7	8	9	47	48
7	22	1	2	3	4	5	6	7	8	46	47	48
8	32	1	2	3	4	5	6	7	8	46	47	48
9	21	1	2	3	4	5	6	7	45	46	47	48
10	31	1	2	3	4	5	6	7	45	46	47	48
11	20	1	2	3	4	5	6	44	45	46	47	48
12	30	1	2	3	4	5	6	44	45	46	47	48
13	19	1	2	3	4	5	43	44	45	46	47	48
14	29	1	2	3	4	5	43	44	45	46	47	48
15	18	1	2	3	4	42	43	44	45	46	47	48
16	28	1	2	3	4	42	43	44	45	46	47	48
17	17	1	2	3	41	42	43	44	45	46	47	48
18	27	1	2	3	41	42	43	44	45	46	47	48

Step	S	D1	D2	D3	D4	D5	D6	D7	D8	D9	D10	D11
19	16	1	2	40	41	42	43	44	45	46	47	48
20	26	1	2	40	41	42	43	44	45	46	47	48
21	15	1	39	40	41	42	43	44	45	46	47	48
22	25	1	39	40	41	42	43	44	45	46	47	48
23	14	38	39	40	41	42	43	44	45	46	47	48
24	24	38	39	40	41	42	43	44	45	46	47	48
25	13	38	39	40	41	42	43	44	45	46	47	37
26	23	38	39	40	41	42	43	44	45	46	47	37
27	12	38	39	40	41	42	43	44	45	46	36	37
28	22	38	39	40	41	42	43	44	45	46	36	37
29	11	38	39	40	41	42	43	44	45	35	36	37
30	21	38	39	40	41	42	43	44	45	35	36	37
31	10	38	39	40	41	42	43	44	34	35	36	37
32	20	38	39	40	41	42	43	44	34	35	36	37
33	9	38	39	40	41	42	43	33	34	35	36	37
34	19	38	39	40	41	42	43	33	34	35	36	37
35	8	38	39	40	41	42	32	33	34	35	36	37
36	18	38	39	40	41	42	32	33	34	35	36	37
37	7	38	39	40	41	31	32	33	34	35	36	37
38	17	38	39	40	41	31	32	33	34	35	36	37
39	6	38	39	40	30	31	32	33	34	35	36	37
40	16	38	39	40	30	31	32	33	34	35	36	37
41	5	38	39	29	30	31	32	33	34	35	36	37
42	15	38	39	29	30	31	32	33	34	35	36	37
43	4	38	28	29	30	31	32	33	34	35	36	37
44	14	38	28	29	30	31	32	33	34	35	36	37
45	3	27	28	29	30	31	32	33	34	35	36	37
46	13	27	28	29	30	31	32	33	34	35	36	37
47	2	27	28	29	30	31	32	33	34	35	36	26
48	12	27	28	29	30	31	32	33	34	35	36	26
49	1	27	28	29	30	31	32	33	34	35	25	26
50	11	27	28	29	30	31	32	33	34	35	25	26
51	48	27	28	29	30	31	32	33	34	24	25	26
52	10	27	28	29	30	31	32	33	34	24	25	26
53	47	27	28	29	30	31	32	33	23	24	25	26
54	9	27	28	29	30	31	32	33	23	24	25	26
55	46	27	28	29	30	31	32	22	23	24	25	26
56	8	27	28	29	30	31	32	22	23	24	25	26
57	45	27	28	29	30	31	21	22	23	24	25	26
58	7	27	28	29	30	31	21	22	23	24	25	26
59	44	27	28	29	30	20	21	22	23	24	25	26
60	6	27	28	29	30	20	21	22	23	24	25	26
61	43	27	28	29	19	20	21	22	23	24	25	26

Step	S	D1	D2	D3	D4	D5	D6	D7	D8	D9	D10	D11
62	5	27	28	29	19	20	21	22	23	24	25	26
63	42	27	28	18	19	20	21	22	23	24	25	26
64	4	27	28	18	19	20	21	22	23	24	25	26
65	41	27	17	18	19	20	21	22	23	24	25	26
66	3	27	17	18	19	20	21	22	23	24	25	26
67	40	16	17	18	19	20	21	22	23	24	25	26
68	2	16	17	18	19	20	21	22	23	24	25	26
69	39	16	17	18	19	20	21	22	23	24	25	15
70	1	16	17	18	19	20	21	22	23	24	25	15
71	38	16	17	18	19	20	21	22	23	24	14	15
72	48	16	17	18	19	20	21	22	23	24	14	15
73	37	16	17	18	19	20	21	22	23	13	14	15
74	47	16	17	18	19	20	21	22	23	13	14	15
75	36	16	17	18	19	20	21	22	12	13	14	15
76	46	16	17	18	19	20	21	22	12	13	14	15
77	35	16	17	18	19	20	21	11	12	13	14	15
78	45	16	17	18	19	20	21	11	12	13	14	15
79	34	16	17	18	19	20	10	11	12	13	14	15
80	44	16	17	18	19	20	10	11	12	13	14	15
81	33	16	17	18	19	9	10	11	12	13	14	15
82	43	16	17	18	19	9	10	11	12	13	14	15
83	32	16	17	18	8	9	10	11	12	13	14	15
84	42	16	17	18	8	9	10	11	12	13	14	15
85	31	16	17	7	8	9	10	11	12	13	14	15
86	41	16	17	7	8	9	10	11	12	13	14	15
87	30	16	6	7	8	9	10	11	12	13	14	15
88	40	16	6	7	8	9	10	11	12	13	14	15
89	29	5	6	7	8	9	10	11	12	13	14	15
90	39	5	6	7	8	9	10	11	12	13	14	15
91	28	5	6	7	8	9	10	11	12	13	14	4
92	38	5	6	7	8	9	10	11	12	13	14	4
93	27	5	6	7	8	9	10	11	12	13	3	4
94	37	5	6	7	8	9	10	11	12	13	3	4
95	26	5	6	7	8	9	10	11	12	2	3	4
96	36	5	6	7	8	9	10	11	12	2	3	4

A3.6 Data rearrangement by array's position of Algorithm Pattern 2

Steps				D1	to	D21					
1	930	929	928	927	926	925	935	934	933	932	11
	10	9	8	7	6	5	4	3	2	1	
2	907	906	905	904	903	902	901	911	910	909	1136

Steps				D1	to	D21					
	1135	1134	1133	1132	1131	1130	1129	1139	1138	1137	
3	884	883	882	881	880	879	878	877	887	886	1113
	1112	1111	1110	1109	1108	1107	1106	1105	1115	1114	
4	861	860	859	858	857	856	855	854	853	863	1090
	1089	1088	1087	1086	1085	1084	1083	1082	1081	1091	
5	838	837	836	835	834	833	832	831	830	829	1067
	1066	1065	1064	1063	1062	1061	1060	1059	1058	1057	
6	815	814	813	812	811	810	809	808	807	806	1033
	1043	1042	1041	1040	1039	1038	1037	1036	1035	1034	
7	781	791	790	789	788	787	786	785	784	783	1010
	1009	1019	1018	1017	1016	1015	1014	1013	1012	1011	
8	758	757	767	766	765	764	763	762	761	760	987
	986	985	995	994	993	992	991	990	989	988	
9	735	734	733	743	742	741	740	739	738	737	964
	963	962	961	971	970	969	968	967	966	965	
10	712	711	710	709	719	718	717	716	715	714	941
	940	939	938	937	947	946	945	944	943	942	
11	689	688	687	686	685	695	694	693	692	691	918
	917	916	915	914	913	923	922	921	920	919	
12	666	665	664	663	662	661	671	670	669	668	895
	894	893	892	891	890	889	899	898	897	896	
13	643	642	641	640	639	638	637	647	646	645	872
	871	870	869	868	867	866	865	875	874	873	
14	620	619	618	617	616	615	614	613	623	622	849
	848	847	846	845	844	843	842	841	851	850	
15	597	596	595	594	593	592	591	590	589	599	826
	825	824	823	822	821	820	819	818	817	827	
16	574	573	572	571	570	569	568	567	566	565	803
	802	801	800	799	798	797	796	795	794	793	
17	551	550	549	548	547	546	545	544	543	542	769
	779	778	777	776	775	774	773	772	771	770	
18	517	527	526	525	524	523	522	521	520	519	746
	745	755	754	753	752	751	750	749	748	747	
19	494	493	503	502	501	500	499	498	497	496	723
	722	721	731	730	729	728	727	726	725	724	
20	471	470	469	479	478	477	476	475	474	473	700
	699	698	697	707	706	705	704	703	702	701	
21	448	447	446	445	455	454	453	452	451	450	677
	676	675	674	673	683	682	681	680	679	678	
22	425	424	423	422	421	431	430	429	428	427	654
	653	652	651	650	649	659	658	657	656	655	
23	402	401	400	399	398	397	407	406	405	404	631
	630	629	628	627	626	625	635	634	633	632	

Steps				D1	to	D21					
24	379	378	377	376	375	374	373	383	382	381	608
	607	606	605	604	603	602	601	611	610	609	
25	356	355	354	353	352	351	350	349	359	358	585
	584	583	582	581	580	579	578	577	587	586	
26	333	332	331	330	329	328	327	326	325	335	562
	561	560	559	558	557	556	555	554	553	563	
27	310	309	308	307	306	305	304	303	302	301	539
	538	537	536	535	534	533	532	531	530	529	
28	287	286	285	284	283	282	281	280	279	278	505
	515	514	513	512	511	510	509	508	507	506	
29	253	263	262	261	260	259	258	257	256	255	482
	481	491	490	489	488	487	486	485	484	483	
30	230	229	239	238	237	236	235	234	233	232	459
	458	457	467	466	465	464	463	462	461	460	
31	207	206	205	215	214	213	212	211	210	209	436
	435	434	433	443	442	441	440	439	438	437	
32	184	183	182	181	191	190	189	188	187	186	413
	412	411	410	409	419	418	417	416	415	414	
33	161	160	159	158	157	167	166	165	164	163	390
	389	388	387	386	385	395	394	393	392	391	
34	138	137	136	135	134	133	143	142	141	140	367
	366	365	364	363	362	361	371	370	369	368	
35	115	114	113	112	111	110	109	119	118	117	344
	343	342	341	340	339	338	337	347	346	345	
36	92	91	90	89	88	87	86	85	95	94	321
	320	319	318	317	316	315	314	313	323	322	
37	69	68	67	66	65	64	63	62	61	71	298
	297	296	295	294	293	292	291	290	289	299	
38	46	45	44	43	42	41	40	39	38	37	275
	274	273	272	271	270	269	268	267	266	265	
39	23	22	21	20	19	18	17	16	15	14	241
	251	250	249	248	247	246	245	244	243	242	
40	1148	1147	1146	1145	1144	1143	1142	1141	1151	1150	218
	217	227	226	225	224	223	222	221	220	219	
41	1125	1124	1123	1122	1121	1120	1119	1118	1117	1127	195
	194	193	203	202	201	200	199	198	197	196	
42	1102	1101	1100	1099	1098	1097	1096	1095	1094	1093	172
	171	170	169	179	178	177	176	175	174	173	
43	1079	1078	1077	1076	1075	1074	1073	1072	1071	1070	149
	148	147	146	145	155	154	153	152	151	150	
44	1045	1055	1054	1053	1052	1051	1050	1049	1048	1047	126
	125	124	123	122	121	131	130	129	128	127	
45	1022	1021	1031	1030	1029	1028	1027	1026	1025	1024	103

Steps				D1	to	D21				
	102	101	100	99	98	97	107	106	105	104	
46	999	998	997	1007	1006	1005	1004	1003	1002	1001	80
	79	78	77	76	75	74	73	83	82	81	
47	976	975	974	973	983	982	981	980	979	978	57
	56	55	54	53	52	51	50	49	59	58	
48	953	952	951	950	949	959	958	957	956	955	34
	33	32	31	30	29	28	27	26	25	35	

APPENDIX IV

EXAMPLE INPUT FILE FOR RECONSTRUCTION

Following data are fold in multi-column format.

1CF	10544	22705	8580
Scanning of	5896	18586	17413
Four Pipes use	5851	18685	18648
with Pattern 1	13523	18583	18653
21	16249	18407	21760
48	5820	16046	37.5
-37.5	4817	5798	22049
75	5816	5699	18914
25	8642	8293	18960
0.0	8307	5983	18537
21327	8426	8426	18388
18708	17971	8460	8866
18946	18617	3295	11226
18676	19347	7846	5699
16386	22475	8673	8293
9553	15.0	8361	5981
10852	22863	8636	5890
5754	18646	16086	6652
8447	18891	18580	5855
14053	18618	18554	7988
16103	18435	21569	8401
4072	11137	30.0	8458
4906	5798	22813	8314
5998	5936	18697	18237
8273	8519	18702	18593
8193	13567	18590	18624
6832	15724	18197	21757
17862	8670	16183	45.0
18816	4098	8383	21711
18690	5676	5747	18813
22372	8557	8293	18655
7.5	8547	8634	18499
21813	8605	5928	17897
18667	17044	8483	10862
18702	18822	3878	11014
18606	19100	8109	15820
17133	22452	8409	8408
8377	22.5	8558	5689

5768	4910	17437	18583
4234	8452	18598	21997
5855	8147	18596	97.5
7775	13617	18999	22223
8601	18627	22057	18623
8481	18533	82.5	18894
7910	18583	22613	18636
18749	22253	18565	18371
18760	67.5	18655	9080
18639	22858	18586	5993
21362	18597	17046	5699
52.5	18693	11108	8474
23043	18574	11074	13867
18726	16052	8415	15762
18863	10858	9313	5822
18687	11043	6184	6026
17618	15155	15914	5879
11071	8293	8325	6060
11054	8500	5589	8635
16100	6063	6031	17144
13557	8442	5707	18636
5928	3928	9546	18574
5768	5931	17812	18711
8503	8013	18566	21117
3295	6948	18750	105.0
7793	16642	18659	22733
8543	18614	21532	18732
8490	18755	90.0	18713
5997	18655	21864	18700
18641	21749	18607	18514
18533	75.0	18880	16203
18779	22435	18594	6009
21943	18812	18012	5905
60.0	18878	10427	5782
22000	18761	8393	13463
18800	17499	6085	9895
18877	11009	8490	6161
18611	11086	13463	7252
17171	7274	16066	5703
10991	9171	5855	8529
11178	8391	3490	9576
16166	14956	5894	16038
8065	7127	5369	18630
6002	5182	8518	18549
6033	5927	17702	18629
8469	5191	18693	21815
3295	5688	18811	112.5

21978	18666	11215	7011
18719	17635	7663	5768
19170	10321	5923	8296
18618	11288	3223	8609
18765	8221	5962	5709
10324	8293	4434	9384
5971	3223	7665	12334
5699	5529	8305	18712
8416	7003	10638	18677
13596	6242	8876	18533
6037	7802	18150	18583
6422	10411	18638	21365
7439	10116	18533	165.0
4189	14848	18602	22591
9202	18629	21564	18623
10350	19163	150.0	18850
13545	18725	22665	18664
18710	21117	18813	8479
18582	135.0	18655	11082
18799	22779	18625	10763
21622	18631	8526	4552
120.0	18655	11089	6790
21811	18546	11094	6391
18565	14968	6295	5970
19065	10759	5787	13790
18547	11100	6625	8336
18557	8323	4230	5676
8302	8349	5888	5924
10957	3643	8415	15983
5699	6108	8496	18770
8685	3405	10447	18465
7853	11172	8473	18946
5981	8056	18583	18869
7309	10607	18518	22002
6099	10094	18533	172.5
5895	16671	18854	23052
10294	18580	21805	18565
9929	18753	157.5	19078
13478	18583	22617	18732
18723	21798	18565	9989
18943	142.5	18933	10891
18839	22704	18543	8421
22026	18672	8377	5406
127.5	18873	11008	5733
23018	18676	11087	5980
18624	10509	5853	13577
19075	10972	6981	13642

5918	10071	18737	225.0
7158	18248	18865	21998
5904	18659	22049	18672
15995	18786	210.0	18709
18757	18583	22424	18750
18499	21995	18844	6805
18731	195.0	18964	8384
18866	21898	18555	8420
21568	18767	15974	7721
180.0	18892	7906	5705
22383	18550	7869	6022
18599	18049	5519	5945
18903	8366	3577	5825
18696	6143	8537	6061
16134	5897	5971	15862
9871	5260	8069	11018
5081	5783	7500	11092
5746	15967	16053	18109
3392	7231	10985	18545
6091	8639	11112	18533
15926	5898	16767	18999
13658	10958	18623	21527
8607	10963	18979	232.5
5676	18149	18583	22336
8733	18631	21785	18608
8248	19207	217.5	18837
18165	18872	21788	18350
18527	21991	18565	8248
18533	202.5	18717	8435
18784	22740	18656	8529
21660	18627	7210	7452
187.5	18922	8458	9125
23037	18468	8528	5152
18619	18356	5718	5832
18655	5688	3564	7584
18818	5932	8441	8415
17756	5711	5972	5676
8309	4527	5935	10919
6174	8415	13535	9397
6016	6498	16109	18853
5166	8646	11061	18499
6105	8415	11074	19867
16122	15370	17271	18813
11104	11060	18620	21814
8415	10885	18965	240.0
5838	17349	18583	22197
11141	18785	22199	18714

18788	8281	4730	10885
16819	8615	8343	8809
8350	7425	16230	8487
8248	3368	13640	10941
8463	8669	5812	11047
7401	15144	6293	8551
6045	6173	10525	18727
8495	8845	9579	18989
6125	6107	16038	19217
8366	5756	18535	22221
9045	8248	18533	292.5
7900	18456	19042	22092
9416	18499	22497	18796
11048	19605	277.5	18868
18522	18860	21867	18726
18499	22382	18713	16200
19207	262.5	18696	5688
19231	21896	17803	6072
22510	18734	5756	5680
247.5	18699	8125	7213
21797	16328	6012	5783
18628	8285	5876	6003
18792	8308	5398	8557
16106	8498	5187	8619
8388	4883	15916	8391
8248	3173	13445	11032
8419	5987	6306	11071
7518	16086	5676	8358
5301	13592	11115	18684
8445	8378	10575	19568
6010	6927	12838	18583
8325	8515	18499	21997
8609	8304	18533	300.0
5733	18064	18583	21406
5926	18871	22180	18896
16202	18748	285.0	18879
18417	19685	22017	18679
18603	22524	18663	18355
19403	270.0	18847	10988
18820	21554	18601	5913
22051	18749	8586	5686
255.0	18684	7193	7755
21351	18079	5968	6001
18658	7622	5999	5768
18799	8640	4005	3205
15375	8509	6038	11107
8486	5785	9681	8196

10865	18575	21586	18803
11034	18958	337.5	18711
8586	19228	21593	18694
18617	21981	18662	13605
18966	322.5	18896	10777
18788	22293	18694	11132
22086	18666	10876	6544
307.5	19061	10631	9348
21523	18574	10671	13626
18751	16237	6952	12636
18887	10704	8540	5765
18686	10643	3223	5482
17721	5913	6215	6071
8302	6018	7099	5547
4272	3223	6095	7447
4843	6019	5888	8573
7142	7063	5325	18600
6859	6272	8454	18604
5607	5380	18039	19032
4494	9905	18635	2159
5406	9327	18932	
8433	17972	18779	
10675	18676	22239	
10909	19247	345.0	
13669	18583	21583	
18560	22042	18700	
18939	330.0	18758	
18583	21962	18592	
22195	18565	10876	
315.0	18851	10984	
21978	18513	11096	
18692	13509	6826	
18779	10990	8489	
18635	10666	7034	
17153	8059	5990	
9090	8344	5765	
9665	3619	3901	
3349	5500	5999	
6153	6829	5753	
5783	6716	5688	
6053	5777	16491	
5376	3628	18535	
6155	8586	18533	
5676	18292	18777	
9997	18589	21742	
10800	19029	352.5	
16258	18794	21839	

VITA

Mr. Dhanaj Saengchantr was born in August 26, 1974 in Bangkok, Thailand. After completing his diploma in Electronics Engineering from Bangkok Technical Campus, he completed his bachelor degree from Kingmongkut University of Technology Thonburi in 1997. In July 1997, he had joined the Office of Atoms for Peace (OAP) for working as Nuclear Engineer. During his work from 1997 – 2006, he was responsible in operating of Thai Research Reactor as a reactor operator. In 2006, after the organization reengineering, he moved to Thailand Institute of Nuclear Technology and in the same year, he started his Master Degree in Nuclear Engineering at Chulalongkorn University and completed in 2009. In 2013, he started his Doctoral of Engineering at Chulalongkorn University with major of Radioisotope Application in Industries and graduated in 2018.